Appendix 3.

EXPERIMENTAL STUDIES OF A SIDE IMPACT INFLATABLE HEAD PROTECTOR

2. INTRODUCTION

This paper describes experimental studies of a side inflatable head protector used in "Saturn"cars. The main objective of the studies is to find out relationships between the pressure within the airbag, its elongation and the tension force in tethers attached to the car's body that extend the airbag longitudinally.

3. OBJECT OF STUDIES

The side protection airbag for "Saturn" (Fig. 73) is an elongated construction that consists of two flat sheets of a strong fabric impregnated with an elastic synthetic material and glued along their perimeters and in interior areas. The figure is a photogrammetry: sizes can be measured on it to scale. Four reference points on the figure are placed in the vertices of a rectangle 60 cm by 80 cm.

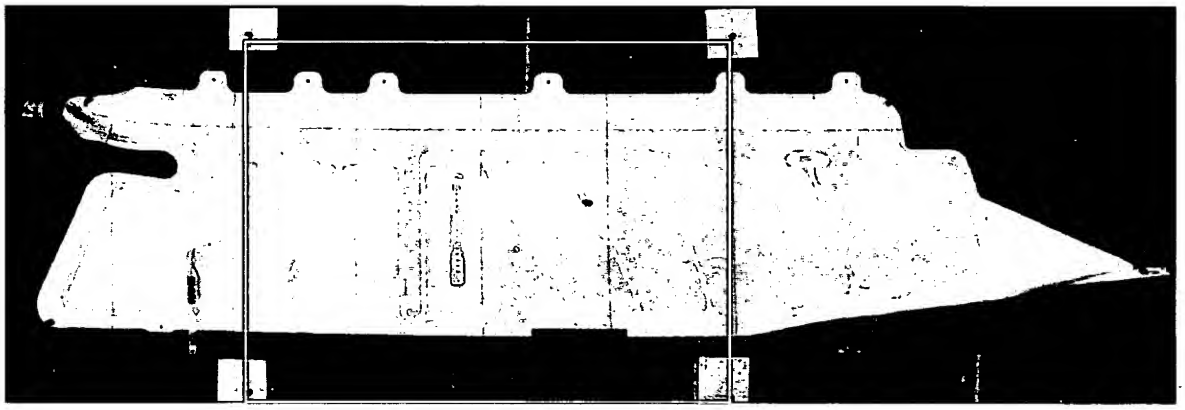

Fig. 73. A photogrammetry of the side head protector for "Saturn"

The airbag is equipped with two fixing tethers. The airbag is placed along the side wall of the car body and is attached to the body along its upper edge above the car door openings; also, it is attached to the front and back parts of the body with the tethers. The tethers are needed to create a tension in the airbag and thus reduce its deformability.

4. GOAL OF STUDIES

As the airbag is inflated, cylindrical convexities tilted to its longitudinal axis appear in its working area (Fig. 74). The length of the bag is thus reduced. As the tethers resist to it, a tension force appears in the airbag.

The tension force depends on the pressure within the airbag and on the distance between points where the tethers are attached. The goal of this study is to find out these dependences experimentally.

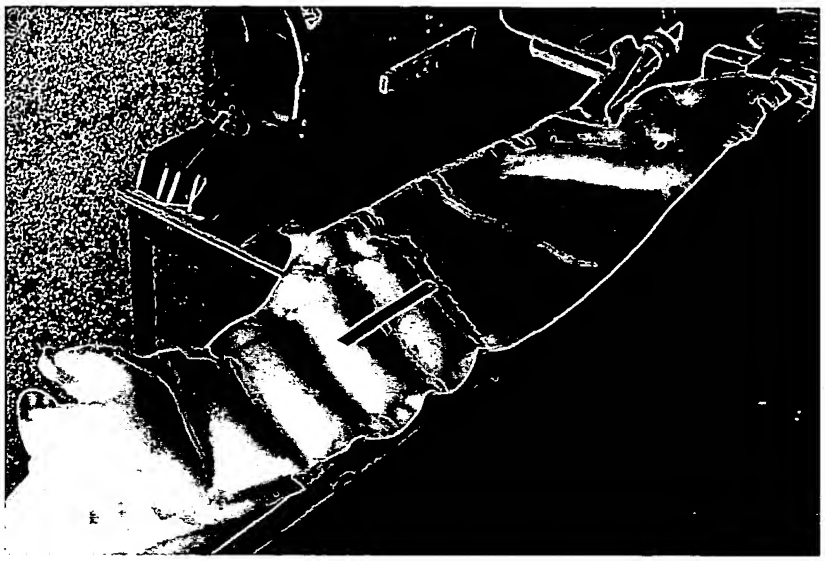

Fig. 74. The appearance of the airbag when inflated.

5. ЭКСПЕРИМЕНТАЛЬНАЯ УСТАНОВКА

The experimental bench (Fig. 75) includes a Base, a Tensioning device, an Inflating device, a Dy-namometer and a Pressure gauge.

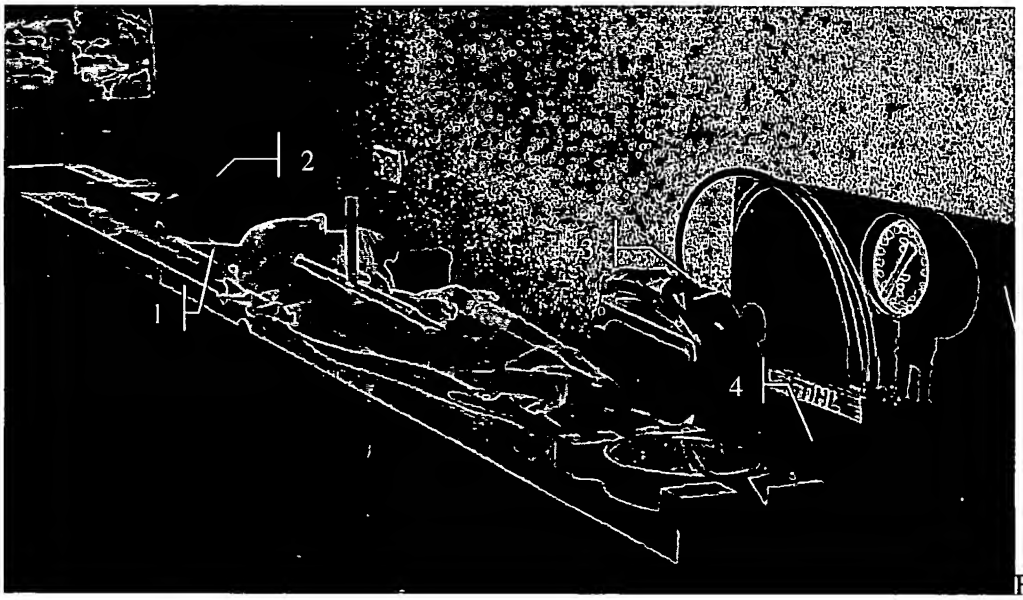

Fig. 75. The general view of the experimental bench. (1) the base, (2) the tensioning device, (3) the inflating device, (4) the dynamometer, (5) the pressure gauge

The *base* (Fig. 76) is made of a wooden plank 50 mm thick. Blocks of wood are attached to the plank using screws and glue to make a support for the tensioning device and the dynamometer.

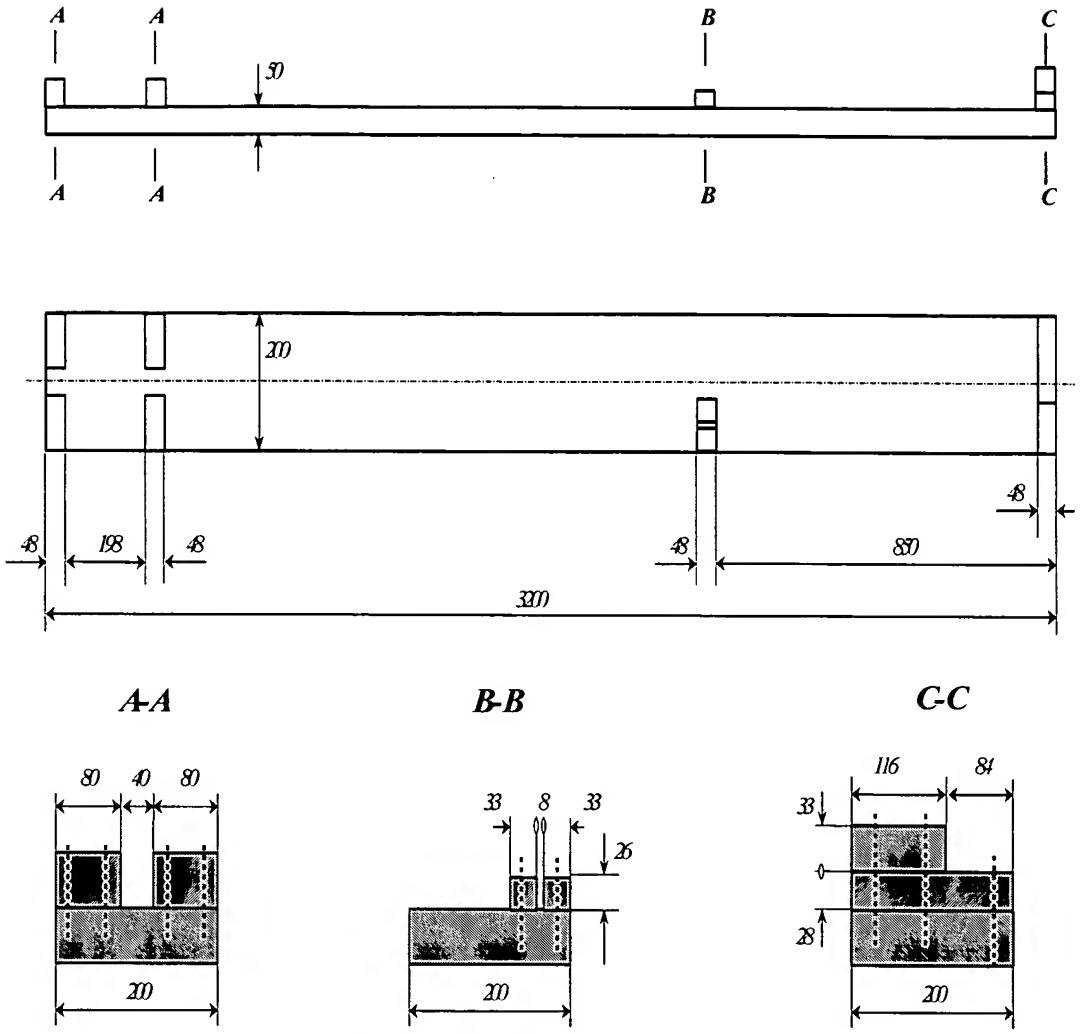

Fig. 76. The base of the experimental bench

The *tensioning device* (Fig. 77) is a bar with a rack along which moves a carriage with a pinion. The pinion is toothed with the rack and has a handle. The position of the carriage on the rack can be measured using a centimeter scale on the bar and fixed using a lock screw. The tensioning device is actually a post from a photographic enlarger "Belarus".

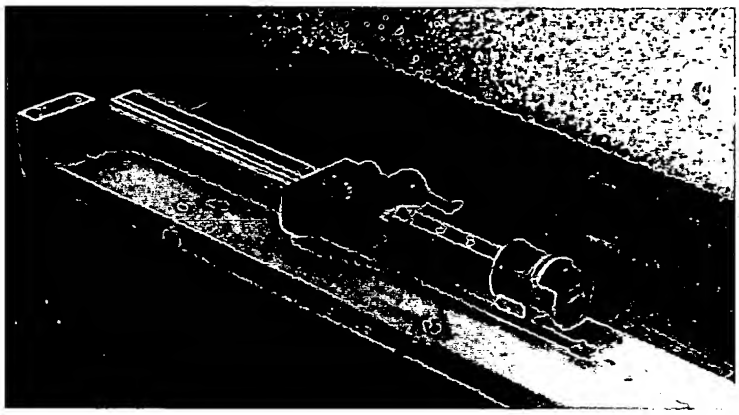

Fig. 77. The tensioning device

The *inflating device* (Fig. 78) is a pump with a valve and a pressure gauge to control the inflation. The inflating device is actually a standard foot-operated car pump.

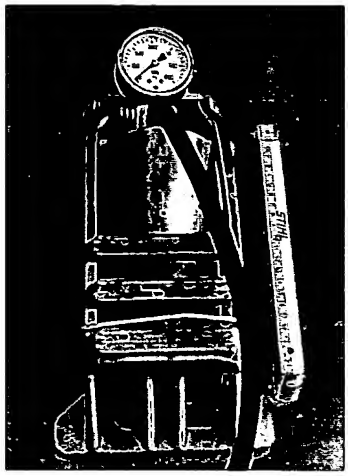

Fig. 78. The inflating device

The *dynamometer* (Fig. 79) is a pointer instrument for force measurements graduated for kilograms of force with the measurement limits 0 to 20 kgf. Its face has the diameter of about 20 cm. The dynamometer has an ear to hang a weight or to apply a force.

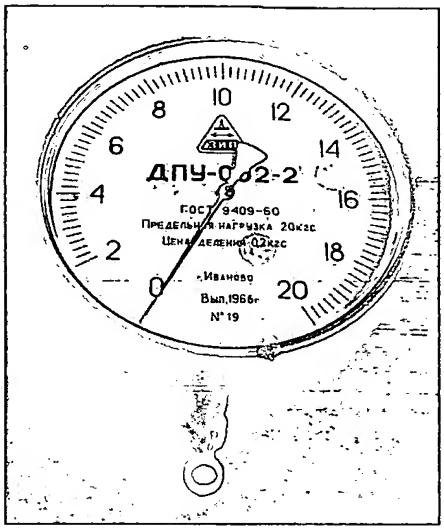

Fig. 79. The dynamometer

The *pressure gauge* (Fig. 80) is a pointer device for pressure measurements graduated for kgf/cm^2 with the measurement limits 0 to 1.6 kgf/cm^2. The diameter of its face is about 16 cm.

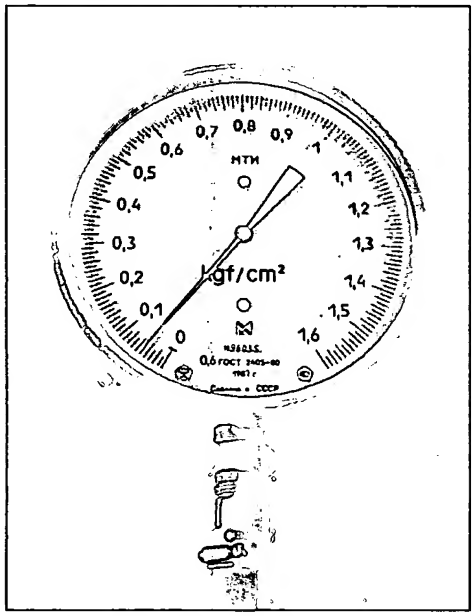

Fig. 80. The pressure gauge

One tether of the airbag is attached to the dynamometer's hook and the other one to the carriage of the tensioning device using a steel stripe with ears.

A bronze cork with a socket fabricated specially for this purpose is inserted into the air hole of the airbag. A rubber hose is connected to the socket. The other end of the hose is connected to a tee joint. The pressure gauge and the inflating device are connected to the same T-joint.

6. DETERMINING THE ELASTIC COMPLIANCE OF THE DYNAMOMETER

Components of the experimental bench are stiff, except for the dynamometer. Their compliance, comparing to that of the airbag, can be neglected a priori. The only doubt was about the dynamometer that is noticeably compliant. To measure this compliance quantitatively, two series of measurements were performed. The traction of the dynamometer and the displacement of its ear

were measured. The displacements were measured by a clock-type indicator (Fig. 81) with the measurement limits 0 to 1 mm and the scale factor 0.001 mm.

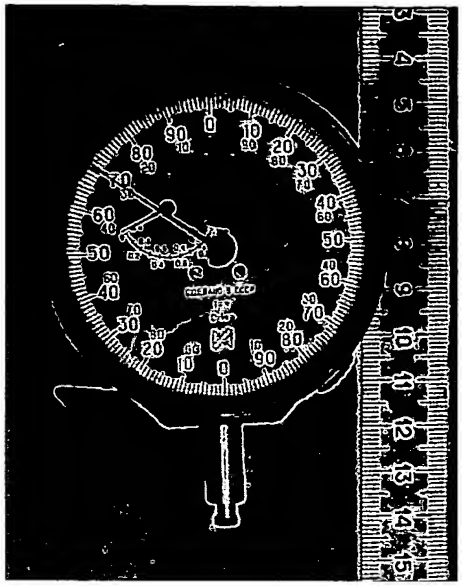

Fig. 81. A clock-type indicator

The table of the measurement results is given below.

Tab. 1. Numerical results of the dynamometer compliance investigation

First series		Second series			
F kgf	**S** mm	**F** kgf	**S** mm	**F** kgf	**S** mm
6.0	0.058	2.0	0.049	5.0	0.354
6.2	0.080	2.2	0.068	6.0	0.450
6.4	0.100	2.4	0.090	7.0	0.550
6.6	0.122	2.6	0.111	8.0	0.660
6.8	0.141	2.8	0.131		
7.0	0.160	3.0	0.150		
7.2	0.184	3.2	0.172		
7.4	0.202	3.4	0.192		
7.6	0.224	3.6	0.212		
8.0	0.269	3.8	0.230		
8.2	0.287	4.0	0.250		
8.4	0.305	4.2	0.272		
8.6	0.329	4.4	0.290		
8.8	0.349	4.6	0.310		
9.0	0.372	4.8	0.330		

On the basis of these numerical data, linear dependencies between the dynamometer traction and the position of its moving ear were built by the method of least squares. Those are shown as solid lines on Fig. 82.

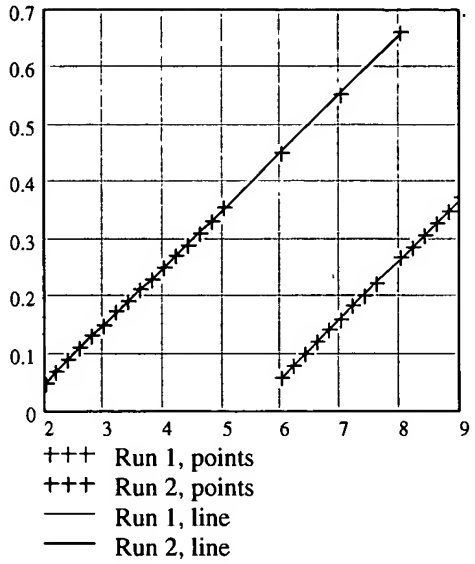

Fig. 82. Results of the dynamometer investigation

The compliance factor for the first series of measurements was 0.104 mm/kgf, and 0.101 mm/kgf for the second series. The additional displacement caused by the dynamometer compliance during measurements of the airbag with the traction of up to 19 kgf does not exceed 2 mm that is about 1 to 2% of the airbag extension. Therefore we can neglect the influence of the dynamometer compliance on the measurement results.

7. AIRBAG TESTING TECHNIQUE

The technique of testing was as follows. The airbag was fixed on the experimental bench so that the distance between the tether fixation points was a predefined small number. Then the pressure in the airbag was maximized. The tension force in the airbag was measured. Then the pressure in the airbag was reduced to the next fixed value. Again, the tension force was measured.

Notice that the airbag is not hermetical, and the pressure within falls naturally. The venting places are located in concavities of the large hollows (the A area on Fig. 73). According to rough estimates, the permeability is such that the airbag permits about 0.1 liter per second to escape at the pressure of 0.6 kgf/cm^2.

Making the pressure in the airbag lower step by step and measuring the airbag tension at each step, we were obtaining a curve of dependence between the tension force and the internal pres-sure for a fixed distance between the tether fixation points.

After that, the distance between the tether fixation points was increased by 1 to 2 cm, and an-other series of measurements was done. Such series followed one another until the distance between the fixation points became maximal.

Full sets of measurements were repeated many times in different days.

Before each series the length of the empty airbag l_0 was measured. The length of the empty air-bag means the distance between the centers of fixation holes of the airbag tethers measured at the tension force of 0.5 kgf. The empty airbag length increased noticeably after the first series of tests. After that it changed little.

8. RESULTS OF AIRBAG TESTS

Below, tables of measurement results are given. Fields of the tables contain the registration of the dynamometer that measured the tension force f in kgf. At the head of each column the regis-tration of the pressure gauge stands: pressure above ambient p in the airbag in kgf/cm^2. The left cell of each row contains the registration of the tensioning device scale x in cm.

Tab. 2. Tension f in kgf. First series of measurements 11/11/01.
Empty bag length before measurement l_0=183.9 cm

	p, kgf/cm^2									
x cm	0.02	0.04	0.06	0.08	0.10	0.12	0.14	0.16	0.18	0.20
2	0.00	0.10	0.20	0.25	0.30	0.38	0.42	0.50	0.58	0.60
4	0.05	0.17	0.23	0.33	0.42	0.55	0.65	0.72	0.90	0.95
6	0.12	0.22	0.33	0.43	0.60	0.70	0.81	0.95	1.03	1.18
8	0.15	0.30	0.45	0.62	0.93	1.00	1.15	1.30	1.42	1.58
10	0.20	0.35	0.43	0.65	0.85	1.05	1.21	1.39	1.58	1.78
12	0.20	0.40	0.88	1.10	1.40	1.70	2.00	2.23	2.50	2.70
14	0.25	0.50	1.00	1.45	1.95	2.33	2.65	3.00	3.40	3.70
15	0.30	0.65	1.30	1.90	2.45	2.90	3.30	3.80	4.20	4.50
16	0.35	0.90	1.65	2.35	2.93	3.50	4.10	4.60	5.10	5.50
17	0.40	1.15	2.05	2.90	3.65	4.26	4.90	5.55	6.10	6.50
18	0.50	1.45	2.57	3.50	4.35	5.00	5.75	6.40	6.95	7.60
19	0.62	1.80	3.00	4.10	5.10	5.87	6.70	7.60	8.20	8.80
20	0.70	2.10	3.50	4.80	5.80	6.85	7.80	8.60	9.40	10.20
21	0.90	2.58	4.20	5.50	6.70	8.00	8.80	9.70	10.80	11.60
22	1.00	2.90	4.70	6.30	7.40	8.80	10.00	11.10	12.10	13.10
23	1.35	3.40	5.40	7.10	8.60	9.90	11.10	12.50	13.70	14.70
24	1.70	3.95	6.20	8.00	9.60	11.20	12.60	14.00	15.40	16.60

Tab. 3. Tension f in kgf. Second series of measurements 11/13/01
Empty bag length before measurement l_0=186.8 cm

	p, kgf/cm^2									
x cm	0.02	0.04	0.06	0.08	0.10	0.12	0.14	0.16	0.18	0.20
10	0.20	0.40	0.60	0.80	1.10	1.25	1.40	1.60	1.80	2.00
12	0.30	0.60	1.00	1.35	1.65	1.95	2.20	2.50	2.72	3.00
14	0.40	0.80	1.30	1.90	2.30	2.70	3.00	3.40	3.75	4.10
16	0.50	1.20	1.90	2.60	3.20	3.70	4.30	5.00	5.50	6.00
18	0.85	1.60	2.86	3.70	4.60	5.40	6.20	6.70	7.50	8.00

20	1.22	2.70	4.00	5.20	6.20	7.40	8.30	9.30	10.10	11.00
22	1.80	3.60	5.30	6.80	8.30	9.50	11.00	12.00	13.30	14.30
24	2.60	5.00	7.00	9.00	11.00	12.40	14.20	15.70	17.20	18.40

Tab. 4. Tension f in kgf. Third series of measurements 11/15/01
Empty bag length before measurement l_0=186.8 cm

	p, kgf/cm^2									
x cm	0.02	0.04	0.06	0.08	0.10	0.12	0.14	0.16	0.18	0.20
10	0.10	0.25	0.50	0.70	0.90	1.05	1.25	1.40	1.62	1.80
12	0.20	0.41	0.75	1.05	1.40	1.65	2.00	2.25	2.50	2.70
14	0.28	0.65	1.15	1.60	2.15	2.55	2.90	3.30	3.65	4.00
16	0.40	1.10	1.85	2.50	3.20	3.65	4.22	4.80	5.30	5.70
18	0.70	1.70	2.70	3.60	4.30	5.20	6.00	6.70	7.30	7.90
20	1.00	2.40	3.70	5.00	6.00	7.10	8.10	9.00	9.90	10.80
22	1.50	3.30	5.10	6.70	8.00	9.40	10.60	12.00	13.00	14.00
24	2.10	4.50	6.80	8.70	10.40	12.20	13.90	15.40	16.70	18.40

Tab. 5. Tension f in kgf. Fourth series of measurements 11/20/01
Empty bag length before measurement l_0=186.8 cm

	p, kgf/cm^2									
x cm	0.02	0.04	0.06	0.08	0.10	0.12	0.14	0.16	0.18	0.20
10	0.19	0.43	0.70	0.95	1.20	1.50	1.60	1.90	2.00	2.1
12	0.30	0.70	1.00	1.30	1.65	2.00	2.20	2.50	2.70	3.10
14	0.40	0.90	1.50	2.00	2.36	2.80	3.20	3.60	4.00	4.30
16	0.50	1.20	1.90	2.50	3.10	3.70	4.40	5.00	5.40	5.80
18	0.70	1.70	2.70	3.60	4.50	5.30	6.00	6.80	7.50	8.00
20	1.00	2.40	3.90	5.10	6.20	7.10	8.20	9.10	10.00	10.90
22	1.50	3.40	5.30	6.80	8.20	9.50	10.90	11.90	13.10	14.20
24	2.00	4.60	7.00	8.90	10.70	12.40	13.90	15.50	17.00	18.30

Tab. 6. Tension f in kgf. Fifth series of measurements 11/20/01
Empty bag length before measurement l_0=186.8 cm

	p, kgf/cm^2									
x cm	0.02	0.04	0.10	0.12	0.16	0.20	0.30	0.40	0.50	0.60
12	0.20	0.50	1.40			2.70	3.6	4.30		5.90
14	0.40	0.80	2.10			3.80	5.30	6.80	7.70	8.50

16	0.60	1.20		3.60	0.45	5.30	7.50	9.70	11.00	12.00
18	0.80	1.70	4.40			9.90	10.70	13.00	14.60	

Tab. 7. Tension f in kgf. Sixth series of measurements 11/21/01
Empty bag length before measurement l_0=186.8 cm

	p, kgf/cm^2									
x cm	0.02	0.04	0.06	0.08	0.10	0.12	0.14	0.16	0.18	0.20
10	0.15	0.35	0.60	0.75	1.00	1.20	1.30	1.50	1.70	1.80
12	0.20	0.60	0.95	1.30	1.50	1.90	2.20	2.40	2.60	2.80
14	0.35	0.80	1.40	1.80	2.10	2.60	3.10	3.50	3.80	4.10
16	0.40	1.20	1.80	2.50	3.10	3.70	4.35	4.90	5.30	5.80
18	0.60	1.70	2.50	3.60	4.30	5.20	6.20	6.90	7.60	8.00
20	0.90	2.40	3.80	4.90	6.10	7.20	8.10	9.10	10.00	10.80
22	1.40	3.30	5.30	6.80	8.20	9.40	10.90	12.10	13.10	14.00
24	2.00	4.40	6.9	8.90	10.60	12.30	13.90	15.50	17.00	18.30

Tab. 8. Tension f in kgf. Seventh series of measurements at a higher pressure 11/22/01
Empty bag length before measurement l_0=186.8 cm

	p, kgf/cm^2					
x cm	0.1	0.2	0.3	0.4	0.5	0.6
10	1.1	2.0	2.8	3.5	4.1	4.6
12	1.4	2.6	3.6	4.6	5.4	6.0
14	2.1	3.9	5.4	6.7	7.7	8.6
16	3.1	5.6	7.5	9.3	10.7	12.0
18	4.2	7.6	10.2	12.5	14.5	16.2
20	5.6	9.8	13.2	16.0	18.7	20.6

Results of the first series are slightly different from those of subsequent series. This difference was apparently caused by non-elastic deformations of the airbag elements during the first series. Also, the testing technique was still under development in the course of the first series of measurements. It was noticed that the measurement of small forces can be substantially distorted due to the friction of the heavy cork and the airbag at the laboratory table. After that we decided to hang up the cork and stir the airbag from time to time to reduce the friction. The first series of measurements lasted for several hours, therefore in this case the influence of creep of the tether and the airbag material was stronger.

Nevertheless, actual readings of all measurement instruments are included in this report to illustrate the results and to facilitate the comparison.

9. MEASUREMENT RESULTS PROCESSED

Two sets of curves have been built after results of the studies. The first set was built on the basis of measurements described in Tab. 3, Tab. 4, Tab. 5 and Tab. 7, and the second set on the basis of those described in Tab. 8.

The sets of curves describe a functional dependence of the tension force in the airbag on the pressure above ambient within it and on the location of the tether attachment points.

The following experimental readings of the measuring instruments were processed:

f, - the tension of the airbag;

p, the pressure above ambient within the airbag;

x, the readings of the tensioning device scale that define the locations of the tether attachment points.

The final diagrams use the argument d instead of the argument x: the difference of the distance between the points of the tether attachment to the experimental bench and the length of the empty airbag. This investigation refers to negative values of d (the distance between the tether attachment points is less than the empty airbag length).

The distance between the tether attachment points in the experimental bench l and the tensioning device readings x are related as follows:

(2) $l = x + 160.2$ cm.

Thus,

(3) $d = x - l_0 + 160.2$ cm;

where l_0 is the empty airbag length before the test.

Results of the first measurement series listed in Tab. 2 are shown on

Fig. 83.

Most representative data are found in Tab. 3, Tab. 4, Tab. 5 and Tab. 7. These tables contain data of measurements of the airbag tension in the range of the internal pressure above ambient p 0.02 to 0.2 kgf/cm^2 and with the x value 10 to 24 cm. In essence, those are results of the same measurement series performed at different times. The results correlate pretty well: it can be seen from diagrams of Fig. 84 that describe four series of experiments.

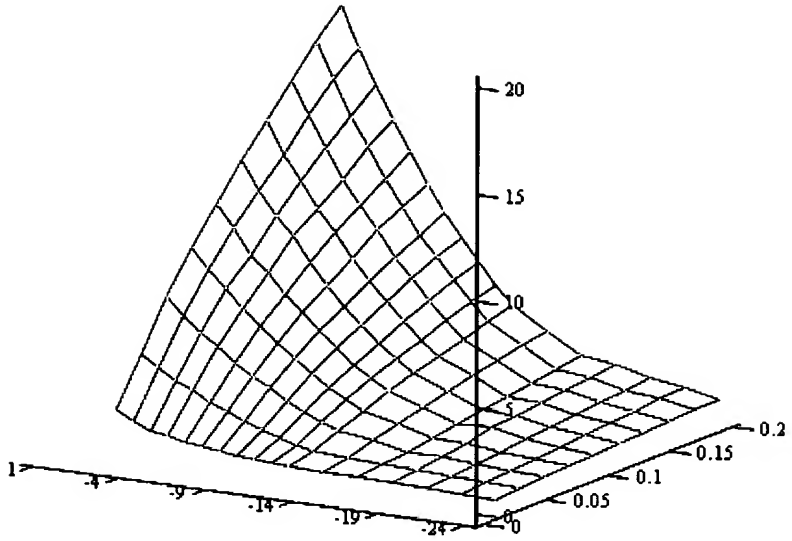

Fig. 83. Results of the first trial set of measurements

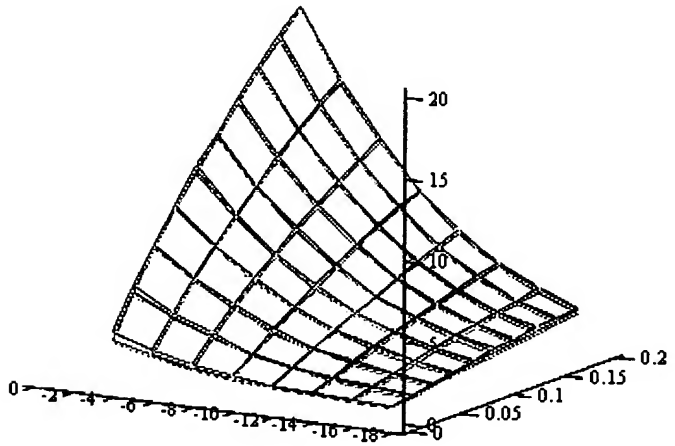

Fig. 84. A comparison between the measurement results
Grid colors: red for Tab. 3, green for Tab. 4, blue for Tab. 5, black for Tab. 7 7.

An approximation of the dependence by a surface of the fourth order gives results shown in Tab. 9.

Tab. 9. Averaged data from Tab. 3, Tab. 4, Tab. 5, Tab. 7.

	p, kgf/cm^2

x cm	0.02	0.04	0.06	0.08	0.10	0.12	0.14	0.16	0.18	0.20
10	0.179	0.383	0.586	0.795	1.011	1.231	1.446	1.640	1.794	1.882
12	0.247	0.589	0.910	1.223	1.532	1.838	2.137	2.419	2.667	2.861
14	0.305	0.837	1.325	1.784	2.225	2.653	3.067	3.461	3.826	4.143
16	0.424	1.203	1.910	2.564	3.180	3.768	4.332	4.871	5.377	5.840
18	0.654	1.741	2.724	3.625	4.465	5.258	6.012	6.729	7.409	8.043
20	1.026	2.487	3.807	5.013	6.129	7.175	8.162	9.098	9.986	10.823
22	1.549	3.455	5.178	6.750	8.200	9.551	10.820	12.019	13.155	14.230
24	2.215	4.640	6.835	8.839	10.685	12.399	14.003	15.514	16.943	18.295

By changing to variables p, d, f we obtain Tab. 10.

Tab. 10. Averaged data in variables p, d, f.

	p, kgf/cm^2									
d cm	0.02	0.04	0.06	0.08	0.10	0.12	0.14	0.16	0.18	0.20
-14	0.262	0.655	1.021	1.373	1.717	2.056	2.386	2.699	2.979	3.208
-12	0.331	0.932	1.480	1.992	2.481	2.952	3.407	3.842	4.246	4.604
-10	0.479	1.344	2.128	2.850	3.529	4.173	4.790	5.378	5.933	6.444
-8	0.750	1.942	3.019	4.006	4.923	5.786	6.605	7.384	8.122	8.813
-6	1.167	2.754	4.187	5.497	6.707	7.838	8.904	9.915	10.873	11.777
-4	1.735	3.789	5.645	7.340	8.902	10.355	11.719	13.007	14.226	15.380
-2	2.438	5.034	7.386	9.533	11.510	13.344	15.060	16.675	18.201	19.645
0	3.239	6.458	9.381	12.053	14.512	16.791	18.918	20.914	22.797	24.578

The same information is shown visually as a 3D diagram on Fig. 85.

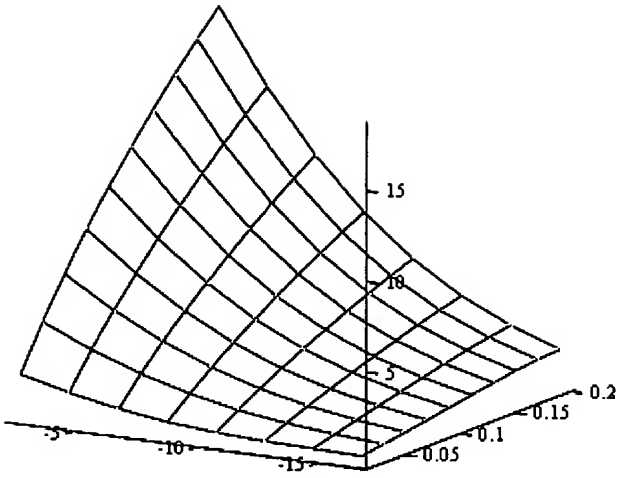

Fig. 85. Averaged data in variables p, d, f.

A set of curves shown on Fig. 86 is more convenient to use.

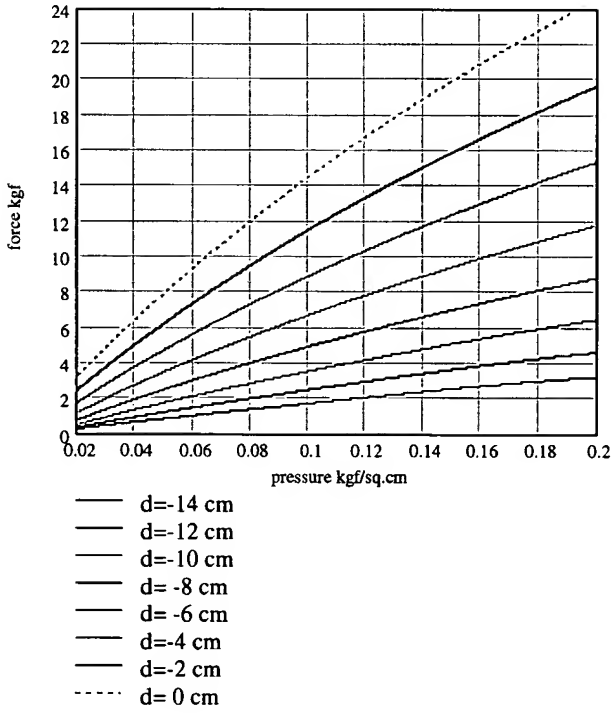

Fig. 86. A set of curves to determine the airbag tension force f

Results of the airbag test at an increased pressure are listed in Tab. 6 and Tab. 8. Systematic data are given in Tab. 8 that is used to obtain final results. Those are shown visually on Fig. 87. The same figure shows a surface that approximate the results. Tab. 11 lists ordinates of this surface.

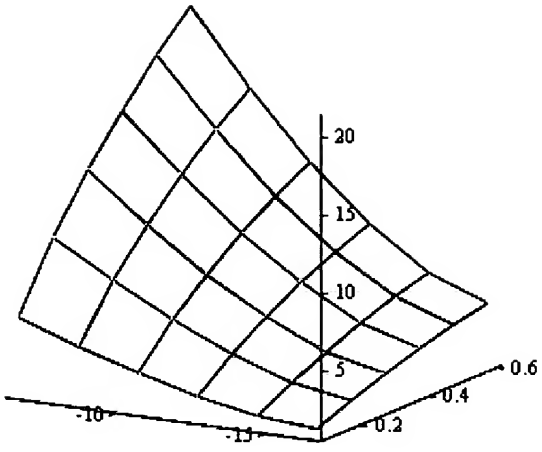

Fig. 87. Results of measurements at the increased pressure and their approximation

The surface that approximates the experimental data is shown in red. The difference is hardly noticeable. Fig. 88 shows the same function as a set of curves.

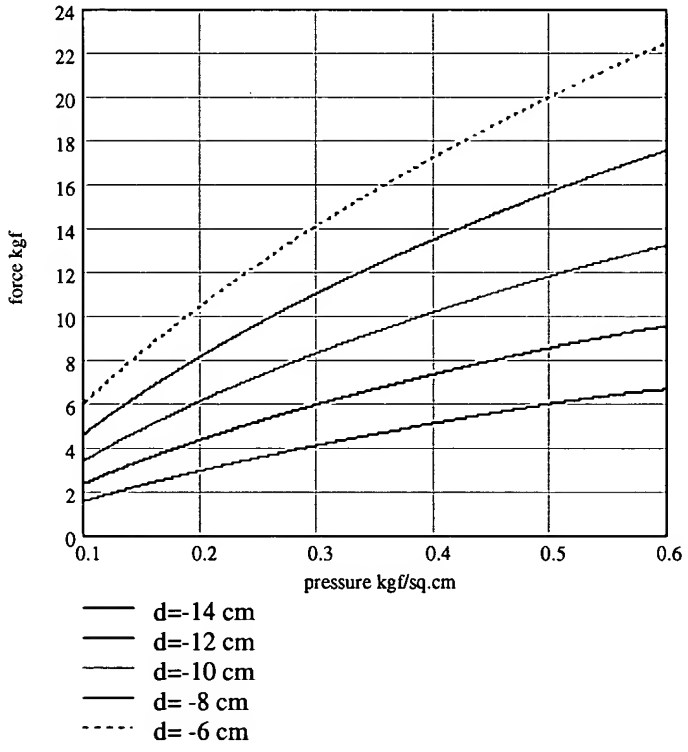

Fig. 88. A set of curves to determine the airbag tension force *f* at the increased pressure

Tab. 11. Averaged data of measurement at the increased pressure

	p, kgf/cm^2					
x cm	0.1	0.2	0.3	0.4	0.5	0.6

10	1.115	1.995	2.756	3.484	4.145	4.589
12	1.371	2.642	3.674	4.593	5.403	5.995
14	2.090	3.908	5.360	6.610	7.704	8.573
16	3.084	5.584	7.584	9.287	10.781	12.035
18	4.254	7.552	10.209	12.468	14.457	16.184
20	5.593	9.785	13.188	16.087	18.646	20.917

It is noticeable that there is a substantial difference between the approximation functions on Fig. 86 and Fig. 88. This difference was apparently caused by the airbag material creep that revealed itself when testing the airbag at different speeds.

10. AIRBAG MATERIAL CREEP

The following experiment was run to obtain tentative data about the material creep rate. The air-bag with no gas within was quickly stretched by 8 cm and maintained in this state until the stress relaxed (20 min). Then the airbag was brought back to its initial state.

Tab. 12 that describes this experiment contains a row that lists reference time t in minutes from the beginning of the experiment, a row of displacements x in cm and a row of the tension force f measured in kilograms of force.

Tab. 12. Results of the stress relaxation experiment

t min	0	0.25	0.5	0.75	1	1.25	1.5	1.75	2	22	22.25	22.5	22.75	23	23.25	23.5
x cm	0	1	2	3	4	5	6	7	8	8	7	6	5	4	3	2
f kgf	0	0.5	1.6	2.4	4.65	7.1	9.9	13.0	16.6	11.7	5.7	3.1	1.6	0.6	0.2	0.0

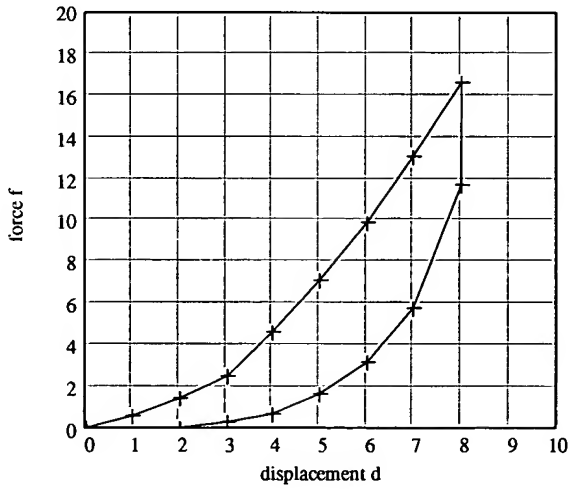

Fig. 89. A hysteresis loop observed in the airbag when loaded and unloaded

The experiment shows that the tension in the airbag material relaxes by approximately the following value:

(4) (1 - 11.7/16.6) 100% = 30%.

The relaxation time is about 20 min. This explains, apparently, the discrepancy between results of experiments where the measurements were done at different speeds.

11. CONCLUSIONS

1. This report describes qualitative and quantitative results that characterize the dependence between the tension force, the internal pressure, and the distance between the tether fixation points (at relatively low pressures).
2. It has been established that plastic deformations of the airbag material at the internal pressure up to 0.6 kgf/cm2 and the tension up to 20 kgf have little effect on its elastic response. Though, deformations caused by creeping of the material affect the parameters of interest very essentially.
3. The airbag is not hermetic and it permits the air to escape through seams where the flat sheets are connected. The venting places are located in concavities of the large hollows (the A area Fig. 73). The permeability is 0.1 liter per second at the pressure of 0.6 kgf/cm2.
4. Designers of the airbag should try to avoid large hollows with concavities at the edge.

12. REFERENCES

[13]. V.Gordeyev. Considerations to investigation of side impact inflatable head protector, Kiev, November 13, 2001

[14]. Roof Rail Airbag Modules. General Specification Interior. GM WORLDWIDE ENGINEERING STANDARDS GMW3121

[15]. Verification of Requirements for Side Impact/Roof Rail Airbag Modules. General Specification Interior. GM WORLDWIDE ENGINEERING STANDARDS GMW3118

Appendix 4.

DEFORMED SHAPE AND STRESS STATE OF SIDE HEAD PROTECTORS

Contents

11. INTRODUCTION

Side impact and roll-over airbags are similar to air mattresses attached to components of a car's body. The airbag consists essentially of two flat pieces of film glued between each other both along their contours and in intermediate areas. Areas where the sheets are connected have complicated shapes which can be seen, for instance, from the picture of a side impact airbag for the "Saturn" car shown on Fig. 11.1.

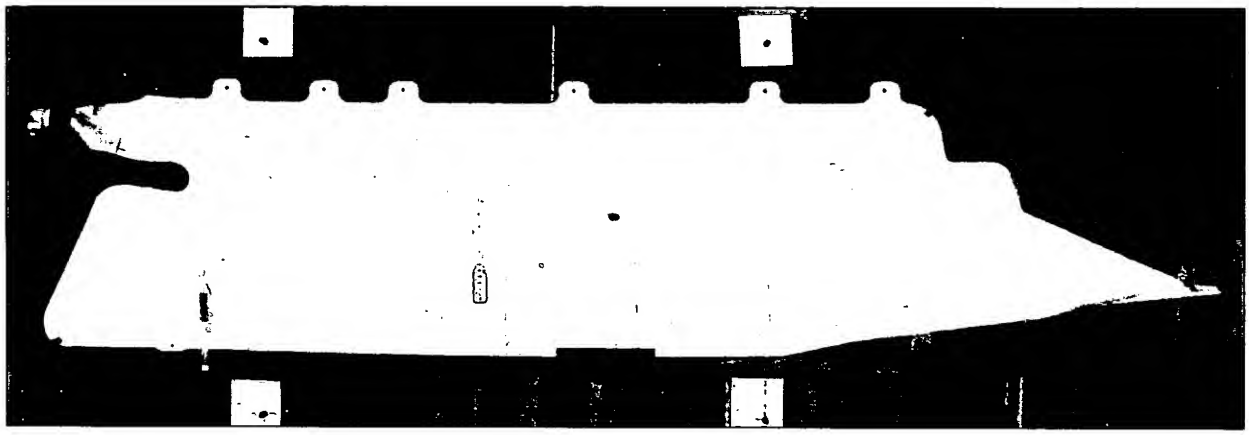

Fig. 11.1. A side impact airbag for the "Saturn" car

In convex sections of the glued areas, there is a concentration of stress that tears off the glued seam. A bigger radius of the rounded corners reduces this stress but at the same time decreases hollows filled with gas thus deteriorating the effectiveness of the airbag. So here we have a reason to formulate an optimization problem. The peeling strength of the adhesive seam may prove a determinant for the whole airbag design being an active limit for any optimizing solution.

Before discussing an optimal design, one should learn how to determine a shape and stress of studied objects.

The present work solves a number of simplified tasks where typical elements of sheets pasted together are contained. This problem is solved partly using analytical methods and partly numerically. The latter case is based on the finite elements method, and the computation was carried out using ANSYS 5.5.

12. AIRBAG WITH HOLLOWS PERPENDICULAR TO THE TENSION

The peculiarity of the side impact airbag's design is the presence of a number of cylindrical hollows (pockets) filled with gas and arranged perpendicularly or at an angle to the longitudinal axis of the airbag.

Seeing the complex configuration of the real side impact airbag, we will investigation simplified models that keep most relevant features of the real object of study.

This part deals with a simplified model where the cylindrical pockets are arranged perpendicularly to the longitudinal direction of the airbag. The purpose of this study is to find relationships between the gas pressure, the airbag material tension and its elongation.

The part contains differential equations derived, solutions thereof in the analytical form, and families of curves for a set of source data as close to the reality as possible.

12.1. Analytical model

Let's suppose that the system contains an infinite sequence of cylindrical hollows with a constant spacing, and each hollow is infinitely long. The system is built of two infinite film pieces glued with stripes $2b$ wide. Between each couple of adjacent glued stripes there is a non-glued space $2a$ wide that forms a cylindrical hollow to be filled with gas under the pressure p. The thin film that the airbag is made of has the thickness h, elasticity modulus E and Poisson ratio ν. The film is assumed to be absolutely flexible.

Fig. 12.1 shows an excision from the infinite system that has the size one along the generatrix. This excision contains two cylindrical hollows and their adjacent glued stripes of the width b. Sizes a, b and size one refer to the non-deformed state of the film. When loaded, the film stretches and the sizes change.

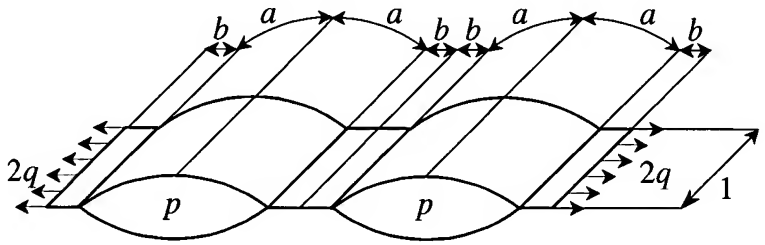

Fig. 12.1 An excision from a system with a sequence of infinite cylindrical hollows perpendicular to the longitudinal direction of the airbag

As one can see from the above-stated, the shape of the bag can be drawn by a rectilinear generatrix moving along a curvilinear guide.

The panel formed by the generatrices is in tension, and the linear distributed loading on it is $2q$.

The system is symmetric, so we can analyze only a repeatable elementary cell instead of the whole structure [19].

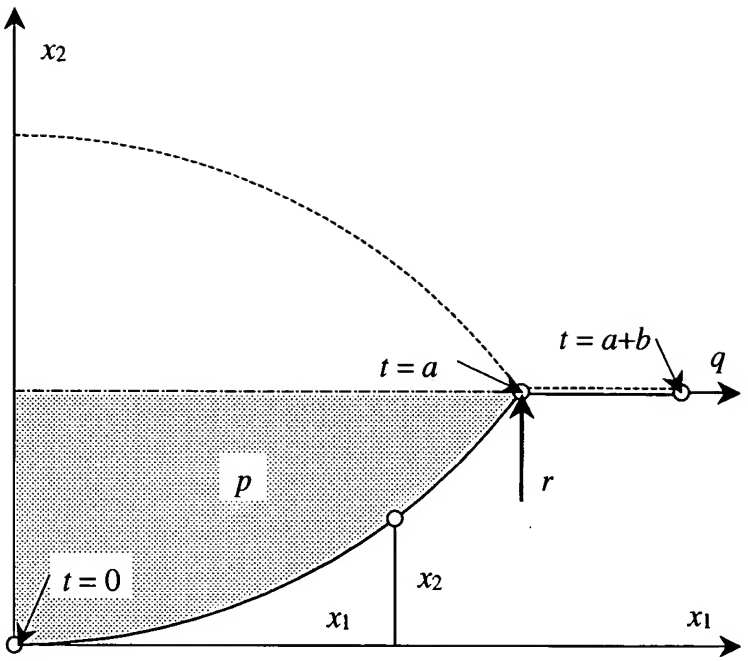

Fig. 12.2. An elementary cell for the system from Fig. 12.1

Fig. 12.2 shows fragments of the film included in the elementary cell as bold lines. Note that only one of the glued films is included in the cell, and also only the quarter of the whole gas volume that fills one hollow. The elementary cell accepts only the half of the linear force that stretches the airbag.

12.2. Mathematical formulation

Let's place the elementary cell in a Cartesian coordinate system $x_1 0 x_2$ as shown on Fig. 12.2. Then introduce the parameter t the physical meaning of which is the length of the guiding curve measured along the non-deformed surface of the film. The starting point of the measurement is the middle of the non-glued film area (Fig. 12.2).

The variation limits of the parameter are:

(12.1) $\quad 0 \le t \le a+b;$

where a is the half-width of the non-glued airbag area in the non-deformed state;

b is the half-width of the glued airbag area in the non-deformed state.

Value $t = a$ corresponds to the boundary between the non-glued and glued areas.

The airbag is a cylindrical body with a rectilinear generatrix, therefore its shape is completely defined by the fragment of the generatrix described above.

Let this line be defined parametrically using coordinates $x_1(t)$, $x_2(t)$ that depend on the parameter t.

The displacement method is used to solve the problem. New functions will be introduced during the derivation of the respective formulae. All of them will be functions of the parameter t.

As all variables are functions of one parameter t, it will be omitted below as an argument of functions. Differentiation with respect to this parameter will be denoted by a stroke.

Obviously, the curve length element in the deformed state is:

(12.2) $$ds = dt\sqrt{(x_1')^2 + (x_2')^2}\ .$$

The relative elongation of the film along the guide curve ε_1 can be described by the formula:

(12.3) $$\varepsilon_1 = \frac{ds - dt}{dt} = s' - 1;$$

where

(12.4) $$s' = \sqrt{(x_1')^2 + (x_2')^2}\ .$$

The relative elongation along the generatrix will be denoted as ε_2. Note that this is a constant that does not depend on the parameter t.

To determine the elastic potential of the system and find stresses in the film, we will need the physical relationships:

(12.5) $$\sigma_1 = \frac{E}{1-\nu^2}(\varepsilon_1 + \nu\varepsilon_2);$$

(12.6) $$\sigma_2 = \frac{E}{1-\nu^2}(\nu\varepsilon_1 + \varepsilon_2);$$

where σ_1 and σ_2 are stresses along the generatrix and the guide, respectively.

12.3. Full energy of the system

We use the variation approach to solve the problem using the displacement method. This approach gives us a good formalization of this solution stage, helps choose a consistent system of variables, formulate natural boundary conditions, pose the dual problem if necessary. Also, there is no need to compose equilibrium equations looking at figures.

Let's choose a system of functions and constants to completely define the deformed state of the system. These functions can be x_1, x_2, and the constant ε_2.

The full energy of the system W, that includes the energy of loading also, is now described by the following functional:

(12.7) $$W = \int_0^{a+b}\left[\frac{Eh}{2(1-\nu^2)}\left(\varepsilon_1^2 + 2\nu\varepsilon_1\varepsilon_2 + \varepsilon_2^2\right) - p\chi(a-t)x_1x_2'(1+\varepsilon_2)\right]dt;$$

where $\chi(z)$ is the Heviside function equal to 1 at $z \geq 0$ and 0 at $z < 0$.

The first term in the brackets is the elastic energy of the airbag material, and the second term is the energy of gas as an external loading.

One should treat the integrand as a function of independent variables x_1, x_2, x_1', x_2', t taking into account (12.3) and (12.4).

12.4. Equation derivation principle

To derive necessary equations, we use a very general technique known as Pontryaghin principle of maximum [18], [16]. This technique was developed to solve problems of optimal control, and both Hamiltonian and Lagrangian mechanics can be treated as special cases of it.

The goal of solving a problem of optimal control is to find n state variables $x_1(t),..,x_n(t)$ and r control variables $u_1(t),..,u_r(t)$ within a specific interval of variation of the argument $t_0 \leq t \leq t_1$ to minimize a given functional:

(12.8) $$x_0 = \int_{t_0}^{t_1} f_0(x_1,..,x_n,u_1,..,u_r,t)\,dt\ ;$$

on the stipulation that the state equations be satisfied:

(12.9) $$x_i' = f_i(x_1,..,x_n,u_1,..,u_r,t) \qquad (i=1,..,n).$$

The stroke denotes the differentiation with respect to t.

Let's introduce n conjugate variables $N_1(t),..,N_n(t)$ and build the Hamiltonian function:

(12.10) $$H(x_1,..,x_n,N_1,..,N_n,u_1,..,u_r,t) = -f_0 + \sum_{i=1}^{n} N_i f_i\ .$$

The Pontryaghin principle of maximum states: the optimal control that minimizes the functional (12.8) is formed by controls $u_1,..,u_r$ that maximize the Hamiltonian function for each t from the interval $t_0 \le t \le t_1$.

Also, the following differential relationships must hold:

(12.11) $$N_i' = -\frac{\partial H}{\partial x_i} \qquad (i=1,..,n);$$

(12.12) $$x_i' = \frac{\partial H}{\partial N_i} \qquad (i=1,..,n).$$

Relationships (12.11), (2.18) are canonical Euler equations for the problem being solved. The system of equations (2.18) is identical with the system of state equations (12.9).

12.5. Formulation of the problem as an optimal control problem

The problem of minimization of the functional (12.7) can be treated as an optimal control problem if we treat x_1, x_2 as state variables and x_1', x_2' as control variables. Variables x_1', x_2' are assumed to be independent from x_1, x_2. Let's denote them as u_1, u_2.

In this case the state equations are the following

(12.13) $$x_1' = u_1;$$

(12.14) $$x_2' = u_2.$$

Thus having introduced the notation of the Pontryaghin principle, we have:

(12.15) $$f_0 = \frac{Eh}{2(1-\nu^2)}\left(\varepsilon_1^2 + 2\nu\varepsilon_1\varepsilon_2 + \varepsilon_2^2\right) - p\chi(a-t)x_1u_2(1+\varepsilon_2)\ ;$$

(12.16) $$f_1 = u_1;$$

(12.17) $$f_2 = u_2;$$

Notice that

(12.18) $$\varepsilon_1 = s'\text{-}1;$$

(12.19) $$s' = \sqrt{u_1^2 + u_2^2}\ .$$

Introducing conjugate variables N_1 and N_2, we build the Hamiltonian function:

(12.20) $$H = -\frac{Eh}{2(1-\nu^2)}\left(\varepsilon_1^2 + 2\nu\varepsilon_1\varepsilon_2 + \varepsilon_2^2\right) + p\chi(a-t)x_1u_2(1+\varepsilon_2) + N_1u_1 + N_2u_2\ .$$

For our further computations we need derivatives of the Hamiltonian function with respect to all variables.

Derivatives with respect to the state variables:

$$\frac{\partial H}{\partial x_1} = p\chi(a-t)u_2(1+\varepsilon_2); \quad (12.21)$$

$$\frac{\partial H}{\partial x_2} = 0. \quad (12.22)$$

Derivatives with respect to the control variables:

$$\frac{\partial H}{\partial u_1} = -\frac{Eh}{1-\nu^2}(\varepsilon_1 + \nu\varepsilon_2)\frac{u_1}{s'} + N_1; \quad (12.23)$$

$$\frac{\partial H}{\partial u_2} = -\frac{Eh}{1-\nu^2}(\varepsilon_1 + \nu\varepsilon_2)\frac{u_2}{s'} + N_2 + p\chi(a-t)x_1(1+\varepsilon_2). \quad (12.24)$$

Derivatives with respect to the conjugate variables:

$$\frac{\partial H}{\partial N_1} = u_1; \quad (12.25)$$

$$\frac{\partial H}{\partial N_2} = u_2. \quad (12.26)$$

According to the maximum principle of Pontryaghin, the optimal control that minimizes the functional (12.15) is achieved by the controls u_1, u_2 that maximize the Hamiltonian function for each t from the interval $0 \le t \le a+b$. There are no limitations (in our particular case), so at least we should meet the conditions of stationarity of the Hamiltonian function (12.20) with respect to u_1, u_2. These conditions can be obtained by equating (12.23) and (12.24) to zero:

$$\frac{Eh}{1-\nu^2}(\varepsilon_1 + \nu\varepsilon_2)\frac{u_1}{s'} = N_1; \quad (12.27)$$

$$\frac{Eh}{1-\nu^2}(\varepsilon_1 + \nu\varepsilon_2)\frac{u_2}{s'} = N_2 + p\chi(a-t)x_1(1+\varepsilon_2) \quad (12.28)$$

These conditions are algebraic equations that establish relationships between the functions of interest.

Also, the system of differential equations (12.11), (2.18) should be fulfilled:

$$\frac{dN_1}{dt} = -p\chi(a-t)u_2(1+\varepsilon_2); \quad (12.29)$$

$$\frac{dN_2}{dt} = 0; \quad (12.30)$$

$$\frac{dx_1}{dt} = u_1; \quad (12.31)$$

$$\frac{dx_2}{dt} = u_2. \quad (12.32)$$

Besides the equations (12.27) to (12.32), four boundary conditions should hold according to the number of differential equations of first order in the system:

(12.33) $x_1(0)=0;$

(12.34) $x_2(0)=0.$

These conditions are obvious from Fig. 12.2. The same figure gives us:

(12.35) $$\frac{dx_2}{dt}\Big|_{t=0} = u_2(0) = 0.$$

If we remember that $x_1(0) = 0$, then the equation (12.24) gives us the following:

(12.36) $N_2(0) = 0.$

The fourth condition is formulated for the point $t = a+b$.

(12.37) $x_1(a+b) = a+b+\Delta;$

where Δ is the forced elongation of the elementary cell.

If we solve a problem with a given linear elongation of the airbag, then

(12.38) $$\sigma_1(a+b) = \frac{q}{h};$$

so, taking into account the fact that in the vicinity of $t = a+b$ the equality $u_1 = s'$ holds, the equation (12.27) gives:

(12.39) $N_1(a+b) = q.$

12.6. Closed analytical solution of the problem

It is intuitively obvious that in the interval $0 \le t \le a$ the integral curve is a circle, for example:

(12.40) $$x_1 = R\sin\frac{kt}{R};$$

(12.41) $$x_2 = R\left(1-\cos\frac{kt}{R}\right);$$

where R and k are arbitrary constants.

This curve fulfils the initial conditions (12.33), (12.34).

The solution for the conjugate variable is also obvious:

(12.42) $N_2 = 0.$

It satisfies both the equation (12.30) and the initial condition (12.36).

In order to meet the requirement of satisfying the equations (12.31), (12.32), we derive the following expressions for the functions u_1, u_2 at the interval $0 \le t \le a$:

(12.43) $$u_1 = k\cos\frac{kt}{R};$$

(12.44) $$u_2 = k\sin\frac{kt}{R}.$$

Now we have from the formula (12.19):

(12.45) $s' = k;$

and then from the formula (12.18):

(12.46) $\varepsilon_1 = k - 1.$

From the formula (12.27) we derive:

(12.47) $$N_1 = \frac{Eh}{1-\nu^2}(k-1+\nu\varepsilon_2)\cos\frac{kt}{R}.$$

By differentiating the expression of N_1 and substituting the result to (12.29), we have the following after some simple transformations:

(12.48) $$\frac{Eh}{1-\nu^2}(k-1+\nu\varepsilon_2) = pR(1+\varepsilon_2).$$

The physical meaning of this formula becomes clear if we transform it as follows using the formulae (12.5) and (12.46):

(12.49) $$\sigma_1 = \frac{pR(1+\varepsilon_2)}{h}.$$

From the formula (12.48) we can determine the arbitrary constant k:

(12.50) $$k = \frac{pR(1+\varepsilon_2)(1-\nu^2)}{Eh} + 1 - \nu\varepsilon_2.$$

The formula (12.47) becomes as follows:

(12.51) $$N_1 = pR(1+\varepsilon_2)\cos\frac{kt}{R}.$$

Thus we have found a partial solution of the system of differential and algebraic equations (12.27) to (12.32) that satisfies the initial conditions (12.33), (12.34), (12.36) and contains one arbitrary constant R.

The value of this arbitrary constant should be chosen using (12.37) or (12.39). Though, to do that, we need to extend the solution of the system of equations to the interval $a < t \le a+b$.

Because at $a < t \le a+b$

(12.52) $\chi(a - t) = 0;$

the equations (12.28) and (12.29) at this interval have the following form:

(12.53) $$\frac{Eh}{1-\nu^2}(\varepsilon_1 + \nu\varepsilon_2)\frac{u_2}{s'} = N_2;$$

(12.54) $$\frac{dN_1}{dt} = 0.$$

The following functions satisfy the equations (12.27), (12.53), (12.54), (12.30), (12.31), (12.32):

(12.55) $$x_1 = R\sin\alpha + k_b(t-a);$$

(12.56) $$x_2 = R(1-\cos\alpha);$$

(12.57) $$N_1 = pR(1+\varepsilon_2)\cos\alpha;$$

(12.58) $N_2 = 0;$

where

(12.59) $$\alpha = \frac{ka}{R};$$

(12.60) $$k_b = \frac{pR(1+\varepsilon_2)(1-\nu^2)}{Eh}\cos\alpha + 1 - \nu\varepsilon_2 .$$

The formulae (12.28), (12.29) yield

(12.61) $$u_1 = k_b; \qquad u_2 = 0; \qquad s' = k_b;\ \varepsilon_1 = k_b - 1;$$

and these expressions enable us to check the dependencies (12.55), (12.58) by the direct substitution to the respective equations. Also, the integral curve maintains its continuity in the vicinity of the point $t = a$.

The stresses in the airbag material can be easily found from the formulae (12.5), (12.6):

(12.62) $$\sigma_1^a = \frac{pR(1+\varepsilon_2)}{h};$$

(12.63) $$\sigma_2^a = \frac{pR(1+\varepsilon_2)}{h}\nu + E\varepsilon_2;$$

(12.64) $$\sigma_1^b = \frac{pR(1+\varepsilon_2)}{h}\cos\alpha;$$

(12.65) $$\sigma_2^a = \frac{pR(1+\varepsilon_2)}{h}\nu\cos\alpha + E\varepsilon_2;$$

where σ_1^a is the stress along the guide in the non-glued area;

σ_2^a is the stress along the generatrix in the non-glued area;

σ_1^b is the stress along the guide in the glued area;

σ_2^b is the stress along the generatrix in the glued area.

The force that tears the sheets apart on the gluing boundary can be found from the conditions of equilibrium:

(12.66) $$r = pR(1+\varepsilon_2)\sin\alpha .$$

The arbitrary constant R can be found from the equality (12.39) in the following form:

(12.67) $$q = pR(1+\varepsilon_2)\cos\alpha .$$

To calculate the elongation Δ, we can use the formulae (12.37) and (12.55):

(12.68) $$\delta = R\sin\alpha + \frac{pR(1+\varepsilon_2)(1-\nu^2)b}{Eh}\cos\alpha - a - \nu\varepsilon_2 b .$$

If the value of δ is specified, then the arbitrary constant R should be determined from the equation (12.68) and the linearly distributed tension force from the formula (12.67).

All computations above are made with the assumption that ε_2 is a given value. If the airbag is not prevented from deforming along its guide, then this value can be found from the condition of equilibrium of forces applied to the cross-section of the airbag:

(12.69) $$Sp = \sigma_2^a ah + \sigma_2^b bh;$$

where S is the area of the cross-section of the hollow filled with gas included in one elementary cell.

By expanding the formula (12.69), we obtain:

$$\frac{pR^2}{2}(\alpha - \cos\alpha\sin\alpha) = pR(a + b\cos\alpha)(1+\varepsilon_2)\nu + Eh(a+b)\varepsilon_2 . \qquad (12.70)$$

Thus, one needs to solve the system of two nonlinear equations (12.67) and (12.70), or (12.68) and (12.70), with respect to R и ε_2 in order to find these values.

12.7. Approaching the reality

In the preceding sections we have obtained an accurate solution of the problem that describes an infinitely long model No.1. In this model, the cylindrical hollows are perpendicular to the tension force applied to the airbag.

The real system is finite, and it contains a finite number of hollows filled with gas. Also, it has additional elastic parts and elastic elements that affect its behavior as a whole.

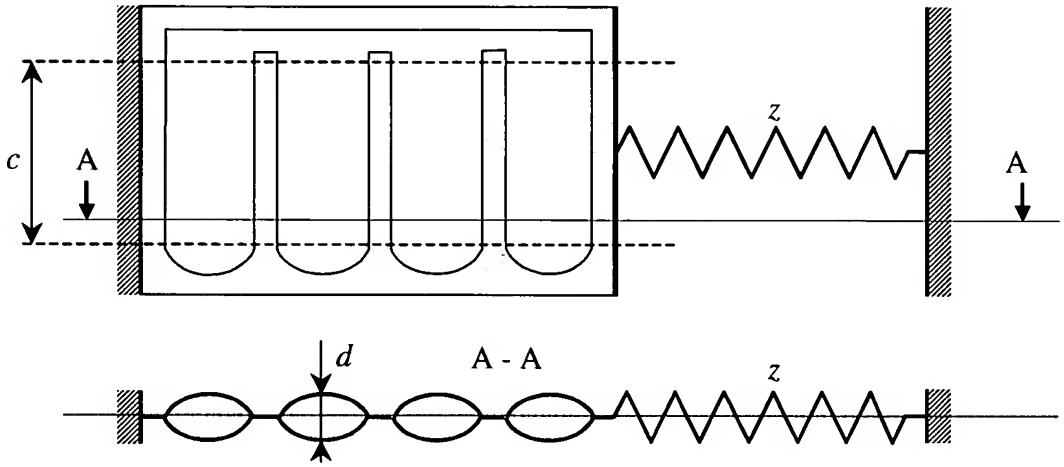

Fig. 12.3. Design model of the airbag

Fig. 12.3 shows a design model of the airbag. This model includes a working area that contains n hollows with the effective width c, and an additional elastic part of the compliance z.

Let the tension force for this airbag be Q, and the elongation be Δ. On the basis of data obtained from the investigation of the elementary cell, we can determine these values by the following formulae:

$$Q = 2qc; \qquad (12.71)$$

$$\Delta = 2\delta n + Qz. \qquad (12.72)$$

12.8. The set of computational formulae

Source data:

h is the film thickness;

E is the elasticity modulus of the film;

ν is the Poisson ratio of the film;

a is the half-width of the non-glued band (Fig. 12.1);

b is the half-width of the glued band (Fig. 12.1);

c is the effective width of the bag (Fig. 12.3);

n is the number of inflatable hollows;

p is the pressure within the bag;

Δ is the elongation of the airbag comparing to its non-deformed length under the zero internal gauge pressure.

To analyze the airbag, one needs to compose two nonlinear algebraic equations:

$$2n\left(R\sin\alpha+\frac{pRb(1+\varepsilon_2)(1-\nu^2)}{Eh}\cos\alpha-a-\nu b\varepsilon_2\right)+2zcpR(1+\varepsilon_2)\cos\alpha=\Delta; \quad (12.73)$$

$$\frac{pR^2}{2}(\alpha-\cos\alpha\sin\alpha)-pR\nu(1+\varepsilon_2)(a+b\cos\alpha)-Eh(a+b)\varepsilon_2=0; \quad (12.74)$$

where

$$\alpha=\frac{pa(1+\varepsilon_2)(1-\nu^2)}{Eh}+\frac{(1-\nu\varepsilon_2)a}{R}. \quad (12.75)$$

These equations should be solved (numerically) with respect to R and ε_2 and thus find the values. Next, using the formulae (12.62) - (12.66), (12.76), (12.77), one can find all values of interest.

$$d=2R(1-\cos\alpha); \quad (12.76)$$

$$Q=2cpR(1+\varepsilon_2)\cos\alpha; \quad (12.77)$$

where d is the thickness of the inflated hollow (Fig. 12.3);

Q is the tension force.

12.9. Behavior of a separate hollow in a stiff airbag

Peculiarities of the behavior of the structure can be revealed by analyzing a separate hollow contained in an airbag made of an infinitely stiff material (Fig. 12.1).

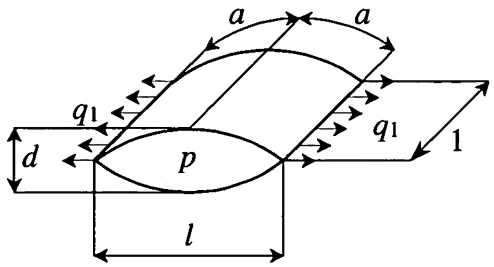

Fig. 12.4. The model of a separate hollow

Let's assume: $n = 1$; $b = 0$; $E = \infty$; $c = 1$.

Then the principal formulae will look like:

$$\alpha=\frac{a}{R}; \quad (12.78)$$

$$d=2R(1-\cos\alpha); \quad (12.79)$$

$$l=2R\sin\alpha; \quad (12.80)$$

$$\Delta=2(R\sin\alpha-a); \quad (12.81)$$

$$q_1=2pR\cos\alpha; \quad (12.82)$$

(12.83) $$r = pR\sin\alpha;$$

(12.84) $$\sigma_1^a = \frac{pR}{h};$$

(12.85) $$\sigma_2^a = \frac{pR}{2h}\left(1 - \frac{\sin 2\alpha}{2\alpha}\right).$$

The latter follows from (12.69).

These formulae contain the only arbitrary constant R that can be determined either from the equation (12.81) or from the equation (12.82) depending on the source data.

Let's introduce dimensionless values:

(12.86) $$\bar{d} = \frac{d}{2a};\ \bar{l} = \frac{l}{2a};\ \bar{\Delta} = \frac{\Delta}{2a};\ \bar{q} = \frac{q_1}{2pa};\ \bar{r} = \frac{r}{2pa};\ \bar{\sigma}_1 = \frac{\sigma_1^a h}{2pa};\ \bar{\sigma}_2^a = \frac{\sigma_2^a h}{2pa};$$

Then the formulae (12.79) - (12.85) can be written in the form:

(12.87) $$\bar{d} = \frac{1-\cos\alpha}{\alpha};$$

(12.88) $$\bar{l} = \frac{\sin\alpha}{\alpha};$$

(12.89) $$\bar{\Delta} = \frac{\sin\alpha}{\alpha} - 1;$$

(12.90) $$\bar{q} = \frac{\cos\alpha}{\alpha};$$

(12.91) $$\bar{r} = \frac{\sin\alpha}{2\alpha};$$

(12.92) $$\bar{\sigma}_1 = \frac{1}{2\alpha};$$

(12.93) $$\bar{\sigma}_2 = \frac{1}{4\alpha}\left(1 - \frac{\sin 2\alpha}{2\alpha}\right).$$

Here the arbitrary constant is the angle α.

The dependencies are shown graphically on Fig. 12.5 - Fig. 12.7. In all dependencies the argument is the dimensionless elongation $\bar{\Delta}$. The limits of variation of this elongation, provided the force $\bar{q}$ is positive (extending the airbag), can be found from the inequalities:

(12.94) $$\frac{2}{\pi} - 1 \le \bar{\Delta} < 0.$$

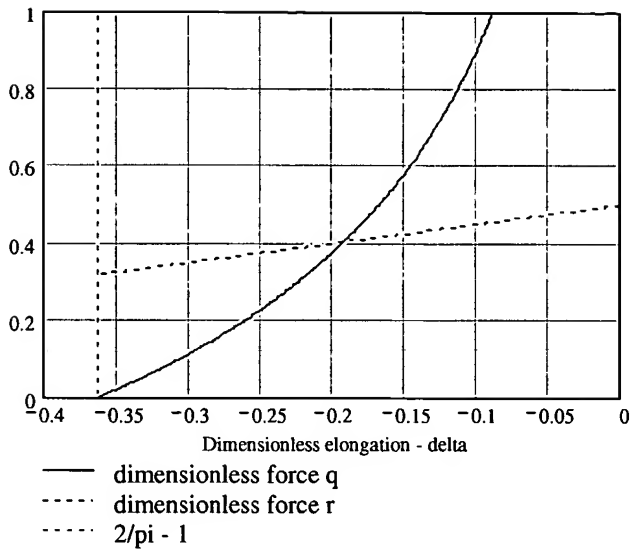

Fig. 12.5. Dependence of dimensionless forces $\bar{q}$ and $\bar{r}$ on the dimensionless elongation $\bar{\Delta}$

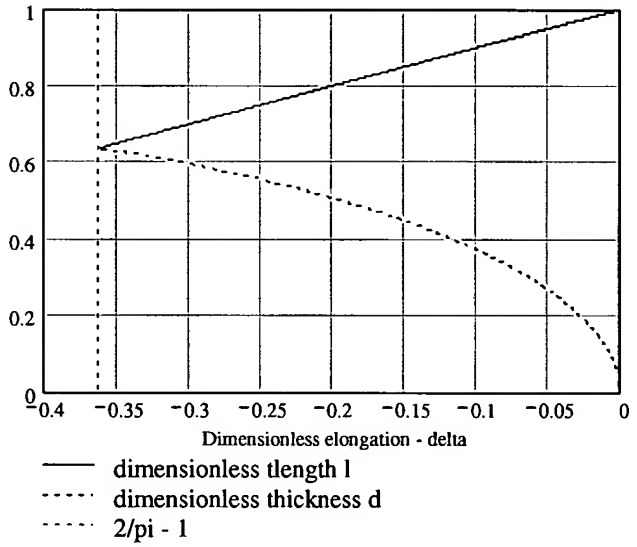

Fig. 12.6. Dependence of relative sizes of the hollow $\bar{l}$ and $\bar{d}$
on the dimensionless elongation $\bar{\Delta}$

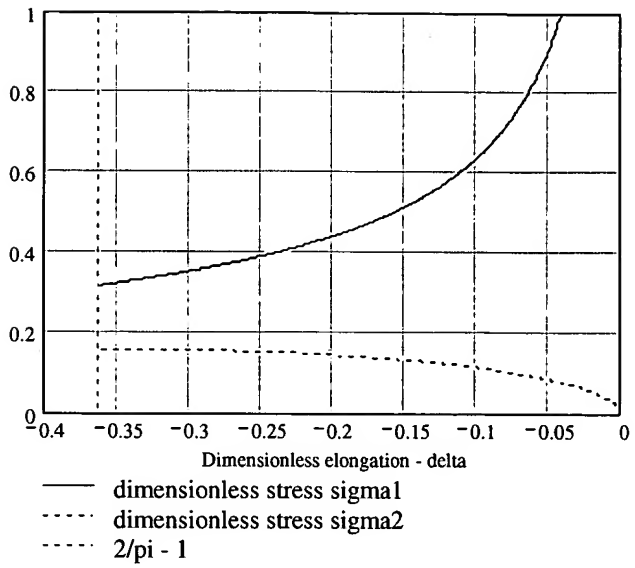

Fig. 12.7. Dependence of dimensionless stresses $\bar{\sigma}_1$ and $\bar{\sigma}_2$ on the dimensionless elongation $\bar{\Delta}$

12.10. Behavior of the real airbag

Let's take a look at a real airbag for the "Saturn" car (see Fig. 11.1and [21]). This airbag has four inclined cylindrical pockets in the driver area and another pocket of the same kind in the passenger area. The hollows are about 24 cm long and 10.9 cm wide. Glued stripes between them are about 1 cm wide. The material is a synthetic fabric with impregnation.

We assume the following source data: actual values a = 5.45 cm; b = 0.5 cm; n = 5; intuitive values c = 12 cm; h = 0.01 cm; E = 4000 kgf/cm^2; ν = 0.39; z = 0.25 cm/kgf. Using the results of Section 12.8, let's build curves of deformation of the side impact airbag. The curves are shown on Fig. 12.8. The comparison of these data with experimental results on Fig. 12.9 shows that the general behavior of the dependencies and the order of magnitude of values is described correctly by the approximate theory.

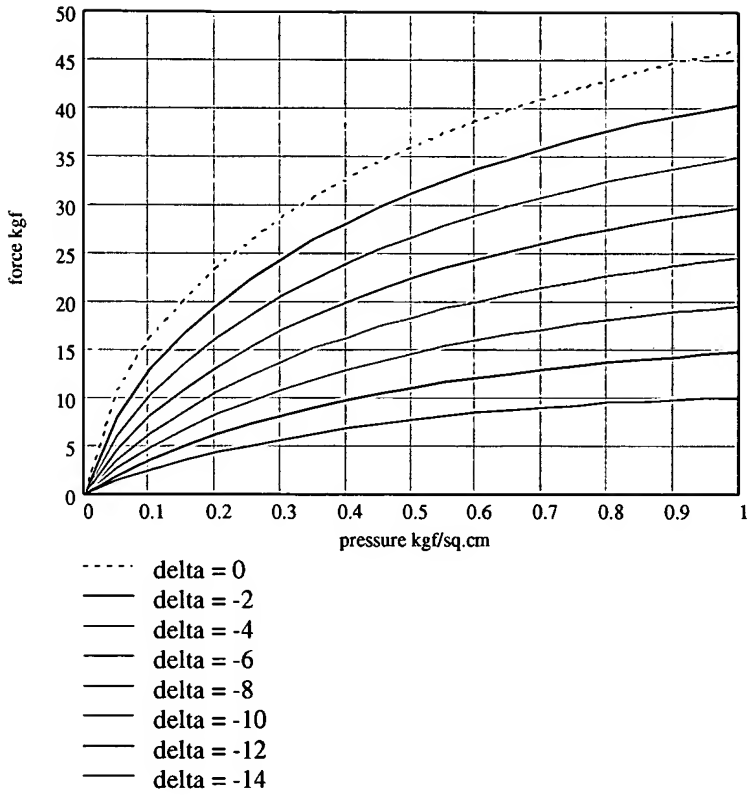

Fig. 12.8. Dependence of the longitudinal tension force on the internal pressure and elongation

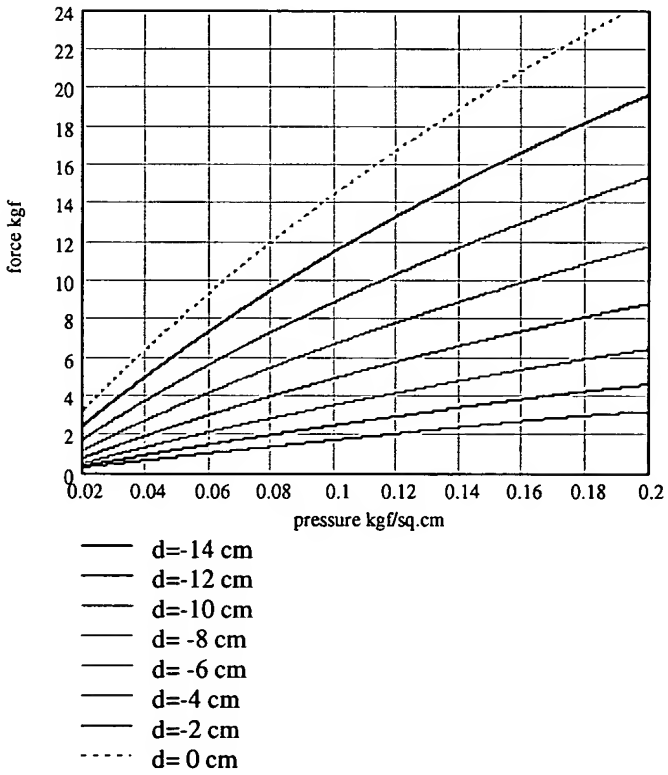

Fig. 12.9. Experimental data from the paper [21]

Theoretical results have been compared with experimental data. In spite of the model being very different from the real structure, results of the comparison can be treated as quite satisfactory.

13. AIRBAG WITH HOLLOWS AT AN ANGLE TO THE TENSION

13.1. Introduction

In this chapter we will investigation a simplified model of a side impact protector airbag that keep the essential behavior of the real object of interest.

The chapter 12 deals with a model in which there are cylindrical hollows filled with gas and perpendicular to the longitudinal axis of the airbag. The present chapter deals with a model in which the hollows are at some angle to the longitudinal direction of the airbag. As in the previous case, the goal of the study is to find out dependencies between the gas pressure, the airbag tension and its elongation.

The chapter derives differential equations, gives solutions to them in a closed form, and builds sets of curves for a non-deformable film and for the airbag model with which an experiment has been run.

13.2. Design model

As in the chapter 12, we assume the system of interest to include an infinite sequence of cylindrical hollows spaced evenly, each hollow being infinitely long. The system is built out of two infinite film pieces glued with stripes $2b$ wide. Between each couple of adjacent glued stripes there is a non-glued gap $2a$ wide that makes a cylindrical hollow filled with gas under the pressure p. Thin film that the bag is made of has the thickness h, elasticity modulus E, Poisson ratio ν. We assume the film not to be resistant to flexion.

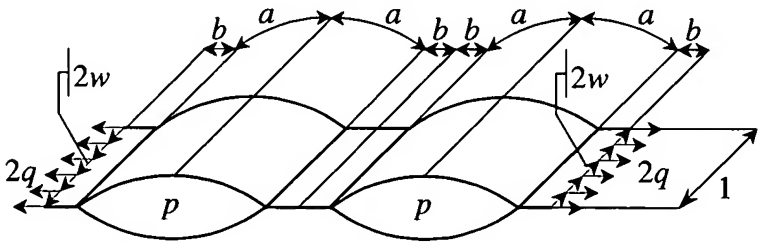

Fig. 13.1. A cut from a system having a sequence of infinitely long cylindrical hollows perpendicular to the lengthwise direction of the airbag

Fig. 12.1 shows a cut fragment of an infinite system with the length 1 along the generatrix. The cut includes two cylindrical hollows and their adjacent stripes of gluing of the width b. The sizes a, b and the unit size refer to the non-deformed state of the film. In the course of loading, the film deforms and the sizes change.

As one can see from the above said, the shape of the bag is drawn in space by a rectilinear generatrix moving along a curvilinear guide.

The cloth of the bag is tensioned at an angle to the guides, the component of the linear load perpendicular to the guide is $2q$, and the component acting along the generatrix is $2w$.

This system has certain properties of symmetry, and we can analyze only a repeatable elementary cell instead of the whole system [19].

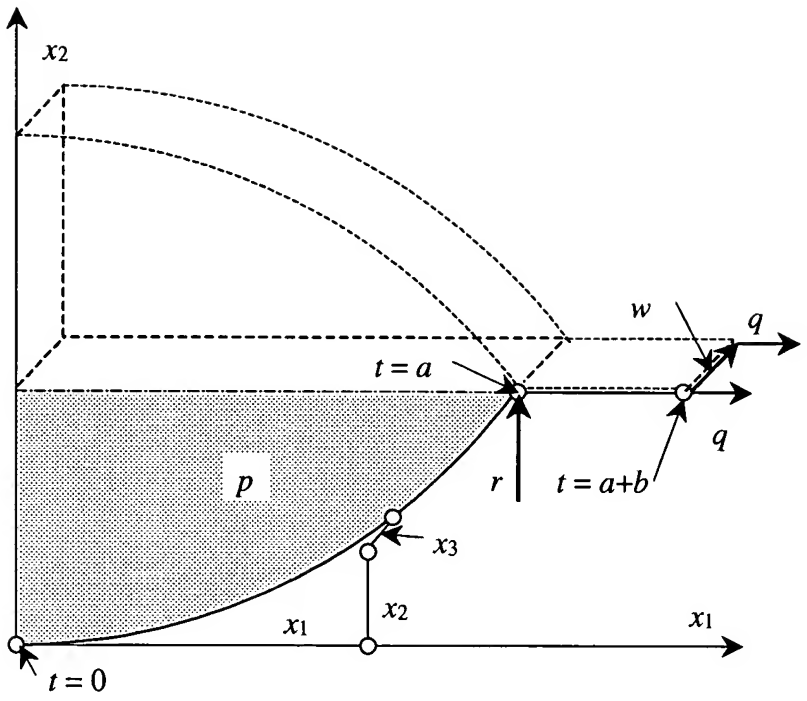

Fig. 13.2. An elementary cell of the system from Fig. 12.1

Fig. 12.2 shows film fragments belonging to the elementary cell with bold lines in cross-section. One should note that the elementary cell includes only one of the glued films and only one quarter of the gas that fills one hollow. The elementary cell accepts a half of the linear load that tensions the airbag.

13.3. Mathematical formulation

Let's refer the elementary cell to a Cartesian coordinate system $x_1 0 x_2$ as shown on Fig. 12.2. We introduce into consideration the parameter t which has the following physical meaning: it is the arc distance along the guide line measured on the non-deformed film surface. The reference point of the measurement is the middle of the non-glued area of the film (Fig. 12.2).

The parameter may change within the following limits:

(13.1) $\quad 0 \le t \le a+b;$

where a is the half-width of the non-glued airbag area in the non-deformed state;

b is the half-width of the glued airbag area in the non-deformed state.

The value $t = a$ corresponds to the boundary between the glued and non-glued areas.

As the airbag is a cylindrical body with a rectilinear generatrix, its deformed state is completely defined by the section of the guide line described above.

Let this line be specified parametrically using coordinates $x_1(t)$, $x_2(t)$, $x_3(t)$ that depend on the parameter t.

The displacement method will be used to solve the problem. During the derivation of formulae we will introduce new functions, all depending on the parameter t.

As all variables are functions of the only parameter t, its notation as an argument of the functions will be omitted. The differentiation with respect to this argument will be denoted by a stroke.

Apparently, the elementary arc length in the deformed state is described by the formula:

(13.2) $$ds = dt\sqrt{(x_1')^2 + (x_2')^2 + (x_3')^2}\ .$$

The relative elongation of the film along the guide curve ε_1 can be described by the following formula:

(13.3) $$\varepsilon_1 = \frac{ds - dt}{dt} = s' - 1;$$

where

(13.4) $$s' = \sqrt{(x_1')^2 + (x_2')^2 + (x_3')^2}\ .$$

The relative elongation along the generatrix will be denoted as ε_2. Note that this is a constant that does not depend on the parameter t.

The distortion γ in this case is described by the following formula [17]:

(13.5) $$\gamma = \frac{x_3'}{s'}.$$

To define the elastic potential energy of the system and the stresses in the film, we need physical equations:

(13.6) $$\sigma_1 = \frac{E}{1-\nu^2}(\varepsilon_1 + \nu\varepsilon_2);$$

(13.7) $$\sigma_2 = \frac{E}{1-\nu^2}(\nu\varepsilon_1 + \varepsilon_2);$$

(13.8) $$\tau = \frac{E}{2(1+\nu)}\gamma;$$

where σ_1 and σ_2 are normal stresses along the guide and the generatrix respectively.;

τ is the tangential stress.

13.4. Full energy of the system

Here we use a variation approach to the displacement method solution. This approach gives us a good formalization of this solution phase, helps choose a consistent system of variables, formulate natural boundary conditions, pose the dual problem if necessary. Also, there is no need to compose equilibrium equations looking at figures.

Let's choose a system of functions and constants to completely define the deformed state of the system. These functions can be x_1, x_2, and the constant ε_2.

The full energy of the system W, that includes the energy of loading also, is now described by the following functional:

(13.9) $$W = \int_0^{a+b}\left[\frac{Eh}{2(1-\nu^2)}(\varepsilon_1^2 + 2\nu\varepsilon_1\varepsilon_2 + \varepsilon_2^2) + \frac{Eh}{4(1+\nu)}\gamma^2 - p\chi(a-t)x_1x_2'(1+\varepsilon_2)\right]dt;$$

where $\chi(z)$ is the Heaviside function equal to 1 at $z \geq 0$ and 0 at $z < 0$.

The first term in the brackets is the elastic energy of the airbag material, and the second term is the energy of gas as an external loading.

One should treat the integrand as a function of independent variables x_1, x_2, x_1', x_2', x_3', t taking into account (12.3) and (12.4).

13.5. Equation derivation principle

To derive necessary equations, we use a very general technique known as Pontryagin principle of maximum [18], [16]. This technique was developed to solve problems of optimal control, and both Hamiltonian and Lagrangian mechanics can be treated as special cases of it.

The goal of solving a problem of optimal control is to find n state variables $x_1(t),..,x_n(t)$ and r control variables $u_1(t),..,u_r(t)$ within a specific interval of variation of the argument $t_0 \le t \le t_1$ to minimize a given functional:

(13.10) $$x_0 = \int_{t_0}^{t_1} f_0(x_1,..,x_n,u_1,..,u_r,t)\,dt\ ;$$

on the stipulation that the state equations be satisfied:

(13.11) $$x_i' = f_i(x_1,..,x_n,u_1,..,u_r,t) \qquad (i=1,..,n).$$

The stroke denotes the differentiation with respect to t.

Let's introduce n conjugate variables $N_1(t),..,N_n(t)$ and build the Hamiltonian function:

(13.12) $$H(x_1,..,x_n,N_1,..,N_n,u_1,..,u_r,t) = -f_0 + \sum_{i=1}^{n} N_i f_i\ .$$

The Pontryaghin principle of maximum states: the optimal control that minimizes the functional (12.8) is formed by controls $u_1,..,u_r$ that maximize the Hamiltonian function for each t from the interval $t_0 \le t \le t_1$.

Also, the following differential relationships must hold:

(13.13) $$N_i' = -\frac{\partial H}{\partial x_i} \qquad (i=1,..,n);$$

(13.14) $$x_i' = \frac{\partial H}{\partial N_i} \qquad (i=1,..,n).$$

Relationships (12.11), (2.18) are canonical Euler equations for the problem being solved. The system of equations (2.18) is identical with the system of state equations (12.9).

13.6. Formulation of the problem as an optimal control problem

The problem of minimization of the functional (12.7) can be treated as an optimal control problem if we treat x_1, x_2, x_3 as state variables and x_1', x_2', x_3' as control variables. Variables x_1', x_2', x_3' are assumed to be independent from x_1, x_2, x_3. Let's denote them as u_1, u_2, u_3.

In this case the state equations are the following

(13.15) $$x_1' = u_1;$$

(13.16) $$x_2' = u_2;$$

(13.17) $$x_3' = u_3.$$

Thus having introduced the notation of the Pontryagin principle, we have:

(13.18) $$f_0 = \frac{Eh}{2(1-\nu^2)}\left(\varepsilon_1^2 + 2\nu\varepsilon_1\varepsilon_2 + \varepsilon_2^2\right) + \frac{Eh}{4(1+\nu)}\gamma^2 - p\chi(a-t)x_1u_2(1+\varepsilon_2)\,;$$

(13.19) $$f_1 = u_1;$$

(13.20) $$f_2 = u_2;$$

(13.21) $f_3 = u_3$.

One should note that

(13.22) $\varepsilon_1 = s'-1;$

(13.23) $\gamma = \frac{u_3}{s'}.$

(13.24) $s' = \sqrt{u_1^2 + u_2^2 + u_3^2}\ ;$

Introducing conjugate variables N_1, N_2 and N_3,, we build the Hamiltonian function:

(13.25)

$$H = -\frac{Eh}{2(1-\nu^2)}\left(\varepsilon_1^2 + 2\nu\varepsilon_1\varepsilon_2 + \varepsilon_2^2\right) + \frac{Eh}{4(1+\nu)}\gamma^2 + p\chi(a-t)x_1u_2(1+\varepsilon_2) + N_1u_1 + N_2u_2 + N_3u_3.$$

For our further computations we need derivatives of the Hamiltonian function with respect to all variables.

Derivatives with respect to the state variables:

(13.26) $$\frac{\partial H}{\partial x_1} = p\chi(a-t)u_2(1+\varepsilon_2);$$

(13.27) $$\frac{\partial H}{\partial x_2} = 0;$$

(13.28) $$\frac{\partial H}{\partial x_3} = 0.$$

Derivatives with respect to the control variables:

(13.29) $$\frac{\partial H}{\partial u_1} = -\frac{Eh}{1-\nu^2}(\varepsilon_1 + \nu\varepsilon_2)\frac{u_1}{s'} + \frac{Eh\gamma u_1u_3}{2(1+\nu)(s')^3} + N_1;$$

(13.30) $$\frac{\partial H}{\partial u_2} = -\frac{Eh}{1-\nu^2}(\varepsilon_1 + \nu\varepsilon_2)\frac{u_2}{s'} + \frac{Eh\gamma u_2u_3}{2(1+\nu)(s')^3} + N_2 + p\chi(a-t)x_1(1+\varepsilon_2);$$

(13.31) $$\frac{\partial H}{\partial u_3} = -\frac{Eh}{1-\nu^2}(\varepsilon_1 + \nu\varepsilon_2)\frac{u_3}{s'} + \frac{Eh\gamma u_3u_3}{2(1+\nu)(s')^3} + N_3 - \frac{Eh\gamma}{2(1+\nu)s'}.$$

Derivatives with respect to the conjugate variables:

(13.32) $$\frac{\partial H}{\partial N_1} = u_1;$$

(13.33) $$\frac{\partial H}{\partial N_2} = u_2;$$

(13.34) $$\frac{\partial H}{\partial N_3} = u_3.$$

According to the maximum principle of Pontryaghin, the optimal control that minimizes the functional (12.15) is achieved by the controls u_1, u_2, u_3 that maximize the Hamiltonian function for

each t from the interval $0 \le t \le a+b$. There are no limitations in our particular case, so at least we should meet the conditions of stationarity of the Hamiltonian function (12.20) with respect to u_1, u_2, u_3.. These conditions can be obtained by equating (12.23), (12.24) and (13.31) to zero:

(13.35) $$\frac{Eh}{1+\nu}\left(\frac{s'-1+\nu\varepsilon_2}{1-\nu}-\frac{u_3^2}{2(s')^3}\right)\frac{u_1}{s'}=N_1;$$

(13.36) $$\frac{Eh}{1+\nu}\left(\frac{s'-1+\nu\varepsilon_2}{1-\nu}-\frac{u_3^2}{2(s')^3}\right)\frac{u_2}{s'}=N_2+p\chi(a-t)x_1(1+\varepsilon_2);$$

(13.37) $$\frac{Eh}{1+\nu}\left(\frac{s'-1+\nu\varepsilon_2}{1-\nu}-\frac{u_3^2}{2(s')^3}\right)\frac{u_3}{s'}=N_3-\frac{Ehu_3}{2(1+\nu)(s')^2}.$$

These conditions are algebraic equations that establish relationships between the functions of interest.

Also, the system of differential equations (12.11), (2.18) should be fulfilled:

(13.38) $$\frac{dN_1}{dt}=-p\chi(a-t)u_2(1+\varepsilon_2);$$

(13.39) $$\frac{dN_2}{dt}=0$$

(13.40) $$\frac{dN_3}{dt}=0;$$

(13.41) $$\frac{dx_1}{dt}=u_1;$$

(13.42) $$\frac{dx_2}{dt}=u_2;$$

(13.43) $$\frac{dx_3}{dt}=u_3.$$

Ideally, we should have determined u_1, u_2, u_3 from the equations (12.27) - (13.37) and substituted those to the differential equations (12.27) - (12.32). Then these equations would contain only six unknown functions.

Besides the equations (12.27) - (12.32), we should meet six boundary conditions according to the number of equations of first order in the system.

Conditions at the beginning of the integration interval are obvious from Fig. 12.2:

(13.44) $x_1(0)=0;$

(13.45) $x_2(0)=0;$

(13.46) $x_3(0)=0.$

Conditions at the end of the integration interval are defined by the requirement that the elongation of the elementary cell in a skewed direction (at the angle φ as can be seen on Fig. 13.3) be equal to a given value of δ. The angle φ is also known. It can be measured on the airbag directly.

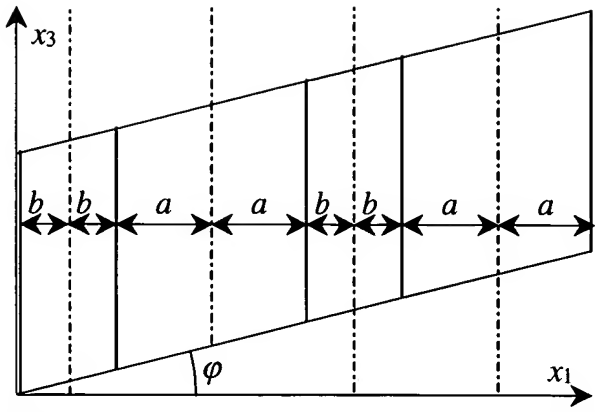

Fig. 13.3. A skewed cut from the system having a sequence of infinitely long cylindrical hollows

The manifold of final states [16] is described by the following formula in this case:

(13.47) $$G = \sqrt{x_1^2 + x_4^2} - (a+b)\sqrt{1+\tan^2\varphi} - \delta = 0;$$

where

(13.48) $$x_4 = (a+b)(1+\varepsilon_2)\tan\varphi + x_3.$$

Three more boundary conditions are the transversality conditions [16]:

(13.49) $$N_i - q\frac{\partial G}{\partial x_i} = 0 \qquad (t = a+b;\ i = 1,2,3).$$

They look as follows:

(13.50) $$N_1 - \frac{qx_1}{\sqrt{x_1^2 + x_4^2}} = 0 \qquad (t = a+b);$$

(13.51) $$N_2 = 0 \qquad (t = a+b);$$

(13.52) $$N_3 - \frac{qx_4}{\sqrt{x_1^2 + x_4^2}} = 0 \qquad (t = a+b);$$

where q is a new unknown constant. To determine the latter, we add the equation (13.47) to the system (13.50) - (13.52), in the following form:

(13.53) $$\sqrt{x_1^2 + x_4^2} - (a+b)\sqrt{1+\tan^2\varphi} - \Delta = 0 \qquad (t = a+b).$$

13.7. Closed solution of the problem

The analytical closed solution has been guessed. It is given in the table that follows, with undetermined constants R, k, k_1, ζ, ζ_1, T.

	$0 \le t \le a$	$a < t \le b$
(13.54)	$x_1 = R\sin\frac{kt}{R}$	$x_1 = R\sin\frac{ka}{R} + k_1(t-a)$
(13.55)	$x_2 = R\left(1-\cos\frac{kt}{R}\right)$	$x_2 = R\left(1-\cos\frac{ka}{R}\right)$
(13.56	$x_3 = \zeta t$	$x_3 = \zeta a + \zeta_1(t-a)$

)		
(13.57)	$N_1 = pR\cos\frac{kt}{R}(1+\varepsilon_2)$	$N_1 = pR\cos\frac{ka}{R}(1+\varepsilon_2)$
(13.58)	$N_2 = 0$	$N_2 = 0$
(13.59)	$N_3 = T$	$N_3 = T$

The auxiliary functions follow:

	$0 \le t \le a$	$a < t \le b$
(13.60)	$u_1 = k\cos\frac{kt}{R}$	$u_1 = k_1$
(13.61)	$u_2 = k\sin\frac{kt}{R}$	$u_2 = 0$
(13.62)	$u_3 = \zeta$	$u_3 = \zeta_1$
(13.63)	$s' = \sqrt{k^2+\zeta^2}$	$s' = \sqrt{k_1^2+\zeta_1}$
(13.64)	$\varepsilon_1 = \sqrt{k^2+\zeta^2} - 1$	$\varepsilon_1 = \sqrt{k_1^2+\zeta_1} - 1$
(13.65)	$\gamma = \frac{\zeta}{\sqrt{k^2+\zeta^2}}$	$\gamma = \frac{\zeta_1}{\sqrt{k_1^2+\zeta_1}}$
(13.66)	$\sigma_1 = \frac{E}{1-\nu^2}\left(\sqrt{k^2+\zeta^2} - 1 + \nu\varepsilon_2\right)$	$\sigma_1 = \frac{E}{1-\nu^2}\left(\sqrt{k_1^2+\zeta_1} - 1 + \nu\varepsilon_2\right)$
(13.67)	$\sigma_2 = \frac{E}{1-\nu^2}\left[\nu\left(\sqrt{k^2+\zeta^2} - 1\right) + \varepsilon_2\right]$	$\sigma_2 = \frac{E}{1-\nu^2}\left[\nu\left(\sqrt{k_1^2+\zeta_1} - 1\right) + \varepsilon_2\right]$
(13.68)	$\tau = \frac{E\zeta}{2(1+\nu)\sqrt{k^2+\zeta^2}}$	$\tau = \frac{E\zeta_1}{2(1+\nu)\sqrt{k_1^2+\zeta_1}}$

A direct substitution makes it sure that the differential equations (12.29) - (12.32) hold. Also, the initial conditions (13.44) - (12.34) and the condition (13.51) hold. Besides, the integral curves are continuous in the vicinity of the point $t = a$.

To comply with the constraint equations (12.27) - (13.37) and boundary conditions (13.50), (13.52), (13.53), we should choose the constants R, k, k_1, ζ, ζ_1, T, q correctly.

A system of algebraic equations to determine these constants follows:

(13.69) $$\rho h\frac{k}{\sqrt{k^2+\zeta^2}} = pR(1+\varepsilon_2);$$

(13.70) $$\rho_1 h\frac{k_1}{\sqrt{k_1^2+\zeta_1^2}} = pR(1+\varepsilon_2)\cos\alpha;$$

(13.71) $$\rho h\frac{\zeta}{\sqrt{k^2+\zeta^2}} = T - \frac{Eh\zeta}{2(1+\nu)(k^2+\zeta^2)};$$

(13.72) $$\rho_1 h\frac{\zeta_1}{\sqrt{k_1^2+\zeta_1^2}} = T - \frac{Eh\zeta_1}{2(1+\nu)(k_1^2+\zeta_1^2)};$$

(13.73) $$pR(1+\varepsilon_2)\cos\alpha = \frac{q}{D}(R\sin\alpha + k_1 b);$$

(13.74) $$T = \frac{q}{D}[(a+b)(1+\varepsilon_2)\tan\varphi + a\zeta + b\zeta_1];$$

(13.75) $$D = (a+b)\sqrt{1+\tan^2\varphi} + \delta.$$

Here the following notation has been introduced to reduce the length of the expressions:

(13.76) $$\rho = \frac{E}{1+\nu}\left(\frac{\sqrt{k^2+\zeta^2}-1+\nu\varepsilon_2}{1-\nu} - \frac{\zeta^2}{2\left(\sqrt{k^2+\zeta^2}\right)^3}\right);$$

(13.77) $$\rho_1 = \frac{E}{1+\nu}\left(\frac{\sqrt{k_1^2+\zeta_1^2}-1+\nu\varepsilon_2}{1-\nu} - \frac{\zeta_1^2}{2\left(\sqrt{k_1^2+\zeta_1^2}\right)^3}\right);$$

(13.78) $$D = \sqrt{[(a+b)(1+\varepsilon_2)\tan\varphi + a\zeta + b\zeta_1]^2 + (R\sin\alpha + k_1 b)^2};$$

(13.79) $$\alpha = \frac{ka}{R}.$$

The equations (13.69) and (13.71) are the equations (12.27) and (13.37) written for the interval $0 \le t \le a$, and the equations (13.70) and (13.72) are the equations (12.27) and (13.37) written for the interval $a < t \le b$. The equations (13.73), (13.74), (13.75) are equivalent to the equations (13.50), (13.52), (13.53). The equation (12.28) is not used here because it is an identity as long as the equation (12.27) holds.

So, we have seven equations to determine seven constants.

All calculations above use the assumption that ε_2 is a given value. If the airbag is not constrained against its deformation along the generatrix, this value can be found from an equation of equilibrium of forces applied to the airbag cross-section:

(13.80) $$Sp = \sigma_2^a ah + \sigma_2^b bh;$$

where S is the area of the cross-section of the hollow filled with gas per one elementary cell; $\sigma_2^a = \sigma_2|_{0\le t\le a}$; $\sigma_2^b = \sigma_2|_{a<t\le a+b}$ are according to the formula (13.67).

We can derive the following by expanding the formula (12.69):

(13.81) $$\frac{pR^2}{2}(\alpha - \cos\alpha\sin\alpha) = pR(a + b\cos\alpha)(1+\varepsilon_2)\nu + Eh(a+b)\varepsilon_2.$$

Thus, in order to determine ε_2, we should add the equation (12.70) to the system (13.69) - (13.75) and solve all these equations as a single system.

For the computation purpose, it is reasonable to use another system equivalent to the equations (13.69) and (13.71):

$$\rho h = \sqrt{p^2 R^2 (1+\varepsilon_2)^2 + \left[T - \frac{Eh\zeta}{2(1+\nu)(k^2+\zeta^2)}\right]^2}\ ; \tag{13.82}$$

$$\frac{\zeta}{k} pR(1+\varepsilon_2) = T - \frac{Eh\zeta}{2(1+\nu)(k^2+\zeta^2)}; \tag{13.83}$$

use an equivalent system instead of the equations (13.70) and (13.72):

$$\rho_1 h = \sqrt{p^2 R^2 (1+\varepsilon_2)^2 \cos^2\alpha + \left[T - \frac{Eh\zeta_1}{2(1+\nu)(k_1^2+\zeta_1^2)}\right]^2}\ ; \tag{13.84}$$

$$\frac{\zeta_1}{k_1} pR(1+\varepsilon_2)\cos\alpha = T - \frac{Eh\zeta_1}{2(1+\nu)(k_1^2+\zeta_1^2)}; \tag{13.85}$$

also, use an equivalent system instead of the equations (13.73) and (13.74):

$$q = \sqrt{p^2 R^2 (1+\varepsilon_2)^2 \cos^2\alpha + T^2}\ ; \tag{13.86}$$

$$(a+b)(1+\varepsilon_2)\tan\varphi + a\zeta + b\zeta_1 = \frac{T(R\sin\alpha + k_1 b)}{pR(1+\varepsilon_2)\cos\alpha}. \tag{13.87}$$

In this system, an unknown value can be expressed via other values using the direct formula (13.86). Thus the system is reduced by one equation.

13.8. Finding unknown constants by a direct method

In order to find the unknown constants R, k, k_1, ζ, ζ_1, ε_2, we can find the point of minimum of the function (12.7) in the space of these unknown constants observing the limitation equality (13.75), instead of solving the system of nonlinear equations (13.69) - (13.75), (12.70).

To do that, we substitute the expressions of x_1, x_2, ε_1, γ from the formulae (13.54), (13.55), (13.64), (13.65) to (12.7) and then take the define integral thus representing W as a function of the desired parameters. A standard procedure of Mathcad-2000 determines the needed constants numerically. Let's do this exercise:

(13.88)

$$W = \frac{Eha}{2(1+\nu)}\left[\frac{\left(\sqrt{k^2+\zeta^2}-1\right)^2 + 2\nu\left(\sqrt{k^2+\zeta^2}-1\right)\varepsilon_2 + \varepsilon_2^2}{1-\nu} + \frac{\zeta^2}{2(k^2+\zeta^2)}\right] +$$

$$+ \frac{Ehb}{2(1+\nu)}\left[\frac{\left(\sqrt{k_1^2+\zeta_1^2}-1\right)^2 + 2\nu\left(\sqrt{k_1^2+\zeta_1^2}-1\right)\varepsilon_2 + \varepsilon_2^2}{1-\nu} + \frac{\zeta_1^2}{2(k_1^2+\zeta_1^2)}\right] - \frac{pkRa}{2}\left(1 - \frac{R}{2ka}\sin\frac{2ka}{R}\right)$$

Note that the accuracy of determining this function's minimum is not always satisfactory. Therefore the further investigation is based on the solution of the system of nonlinear algebraic equations.

13.9. Changing to the real system

In the previous sections we have obtained an exact solution of the problem regarding a simplified infinitely long model No.2. In this model its cylindrical hollows are placed at an angle to the tension force that stretches the airbag.

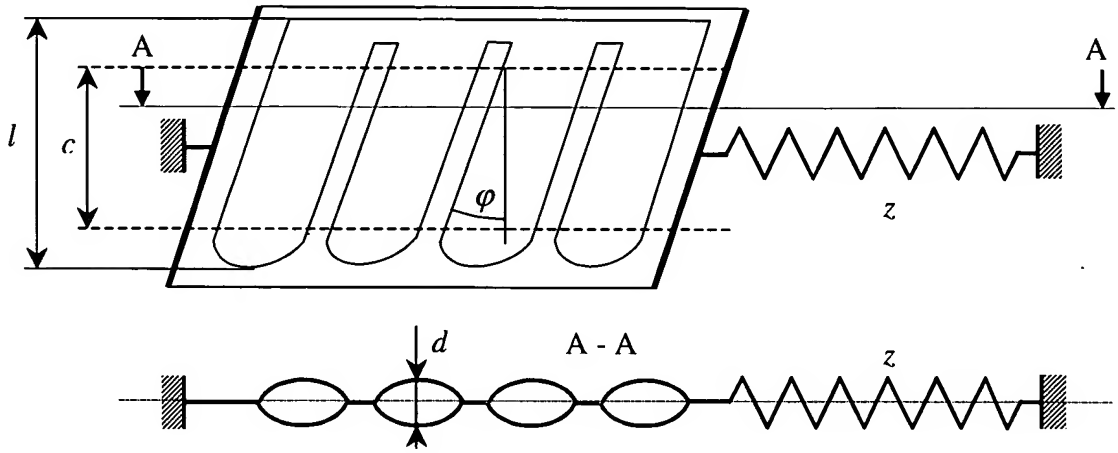

Fig. 13.4. A design model of the airbag

The real system has finite sizes and a finite number of hollows filled with gas. Also, it has additional elastic parts and elements that affect its behavior as a whole.

Fig. 12.3 shows a design model of the airbag. This diagram includes a working area with a certain number of hollows of the effective width c, and an additional elastic part with the compliance z. The inclination of the hollows is described by the angle φ as shown on the figure.

Let the tension force be Q and elongation Δ for this airbag. Referring to data obtained for the elementary cell model, we can determine these values by the formulae:

(13.89) $$Q = 2qc\sqrt{1+\tan^2\varphi};$$

(13.90) $$\Delta = 2\delta n + Qz.$$

13.10. Procedure of analysis

It is recommended to obtain all necessary dependencies for a real airbag as diagrams (graphs). The convenient parameter for the graphs is the elongation of the elementary cell δ. The lower limit of this value is negative: this occurs when the pressure in the hollow tends to zero and there is no tension force applied to the airbag. The lower elongation limit can be expressed by the formula:

(13.91) $$\delta_{min} = (a+b)\left(\sqrt{\xi^2+\tan^2\varphi} - \sqrt{1+\tan^2\varphi}\right);$$

where $\xi = \dfrac{2a+\pi b}{\pi(a+b)}$.

The upper limit can be 0 in most cases.

The source data for the problem are:

h, the thickness of the film;

E, the elasticity modulus of the film;

ν, the Poisson ratio of the film;

a, the half-width of the non-glued stripe (Fig. 12.1);

b, the half-width of the glued stripe (Fig. 12.1);

c, the effective width of the airbag (Fig. 12.3);

n, the number of the inflatable hollows;

p, the pressure in the airbag.

For each value of the parameter δ we should solve the compatible system of seven nonlinear equations (13.75), (12.70) - (13.85), (13.87) with respect to the variables R, ε_2, k, k_1, ζ, ζ_1, T. Then, we can find the stress in the material by the formulae (13.66) - (13.68), the tension force per unit length by the formulae (13.86), the full tension force in the airbag and its full elongation by the formulae (13.89) and (13.90).

Also, we can determine the thickness of the inflated hollow (Fig. 12.3)

(13.92) $$d = 2R(1-\cos\alpha);$$

and the force per unit length that tears the film sheets apart at their glued boundary:

(13.93) $$r = pR(1+\varepsilon_2)\sin\alpha\,.$$

13.11. Dependencies for the real airbag

Here the real airbag will be a side impact head protector for the "Saturn" car [21]. This airbag has four inclined cylindrical hollows in the driver area and one more hollow in the passenger area. The hollows are about 25 cm long and 10.9 cm wide. The glued stripes between them are about 1 cm wide. The material is an impregnated synthetic fabric.

The chapter 12 gives a set of curves built for the following source data: a = 5.45 cm; b = 0.5 cm; n = 5; c = 12 cm; h = 0.02 cm; E = 4000 kgf/cm^2; ν= 0.39; z = 0.2 cm/kgf. Fig. 12.8 duplicates the data here for convenience of comparison.

The fotogrammetry of the airbag (Fig. 11.1) shows that the four principal hollows are placed so that $\tan\varphi$=0.528. Results of calculations done with the same source data and the inclination taken into account are shown on Fig. 13.6.

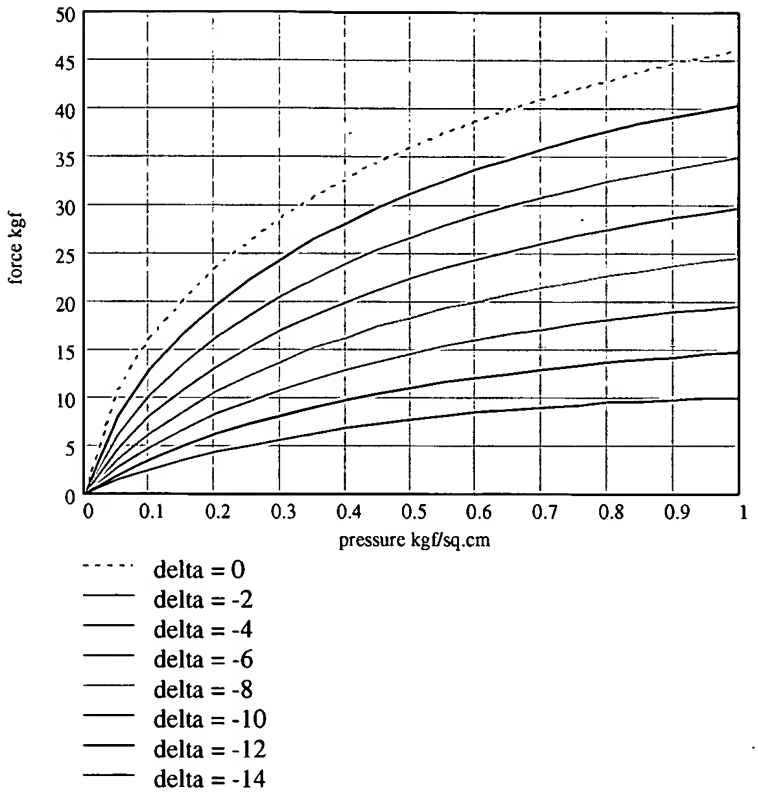

Fig. 13.5. Dependence of the lengthwise tension force in the airbag on the internal pressure and elongation, from chapter 12

The comparison shows that the inclination of the hollows causes the lengthwise tension of the airbag to increase when the airbag shrinks little, and vice versa: it causes the tension to reduce when the airbag's length shrinks much.

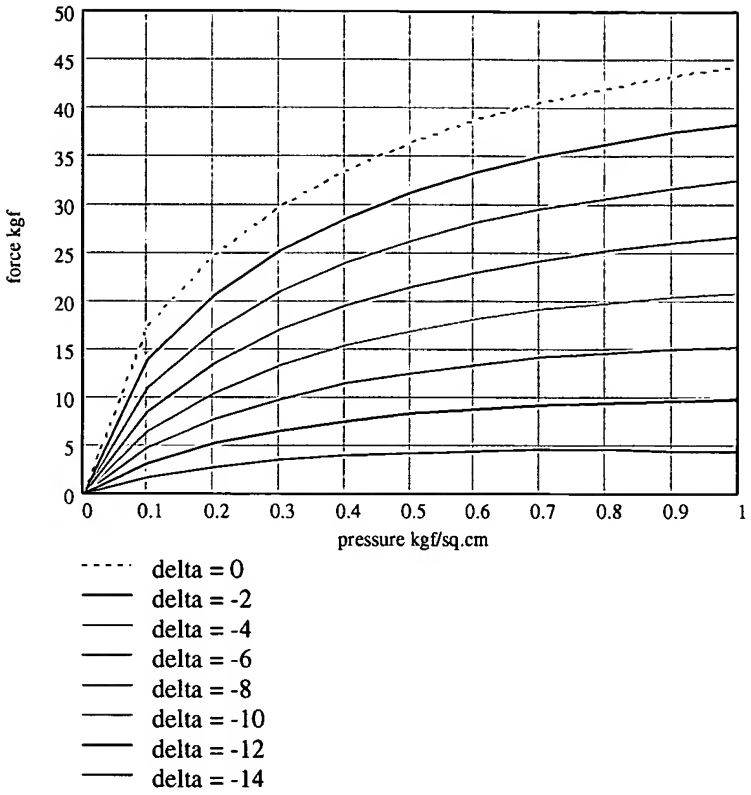

Fig. 13.6. Dependence of the lengthwise tension force on the internal pressure, taking into account the inclination of the hollows

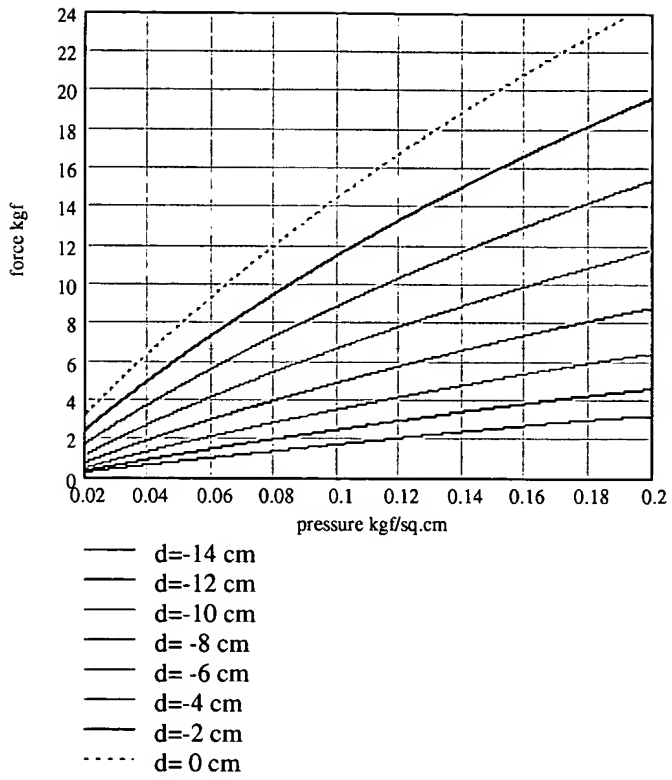

Fig. 13.7. Experimental data from [21]

The model with the inclined hollows shows better correspondence to the reality, comparing to the model with the perpendicular hollows.

Though, any comparison with experimental data is very relative. We don't know for sure the material thickness, nor its mechanical properties. The compliance factor of the system z is also unknown. It would be good to make a comparison between theoretical and experimental data after having measured the material thickness h, elasticity modulus E, Poisson ratio ν, compliance factor z.

As for the effective width of the airbag c, we think it's acceptable to determine it by the formula:

(13.94) $$c = l - 2.4a;$$

where l is the width of the area with the hollows (see Fig. 12.3);

a is the half-width of the hollow (see Fig. 12.1 and Fig. 13.3).

13.12. Effect of inclination of hollows

Let us consider the dependence of the airbag tension force on the inclination angle of the hollows. To do that, we use the source data from Section 13.11, with the inclination angle tangent varied within the limits 0 to 1.0. The analysis has been done for two levels of pressure: low 0.1 kgf/cm^2 and high 1.0 kgf/cm^2.

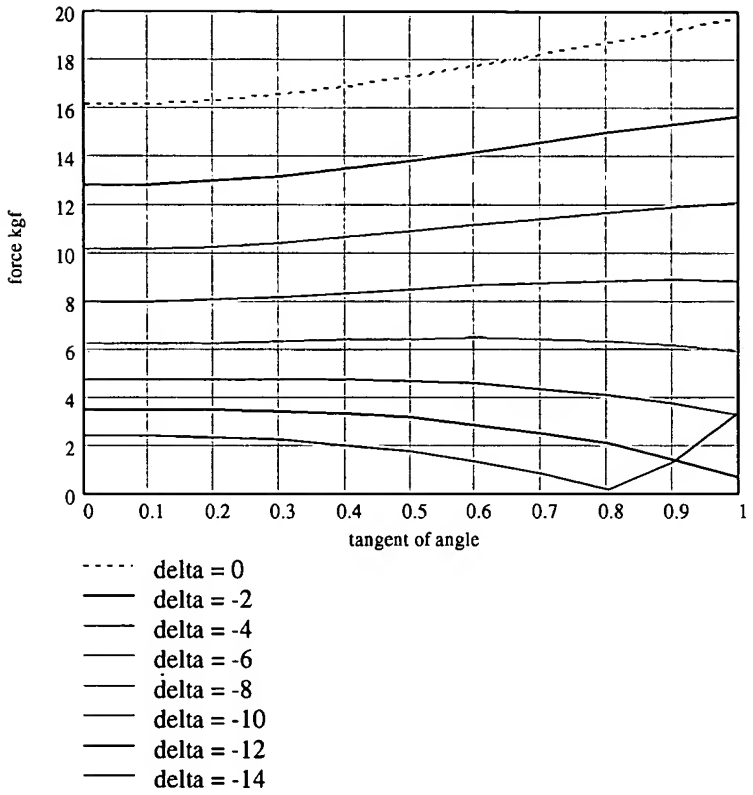

Fig. 13.8. Dependence of the airbag tension force on the inclination of the hollows at the pressure 0.1 kgf/cm^2

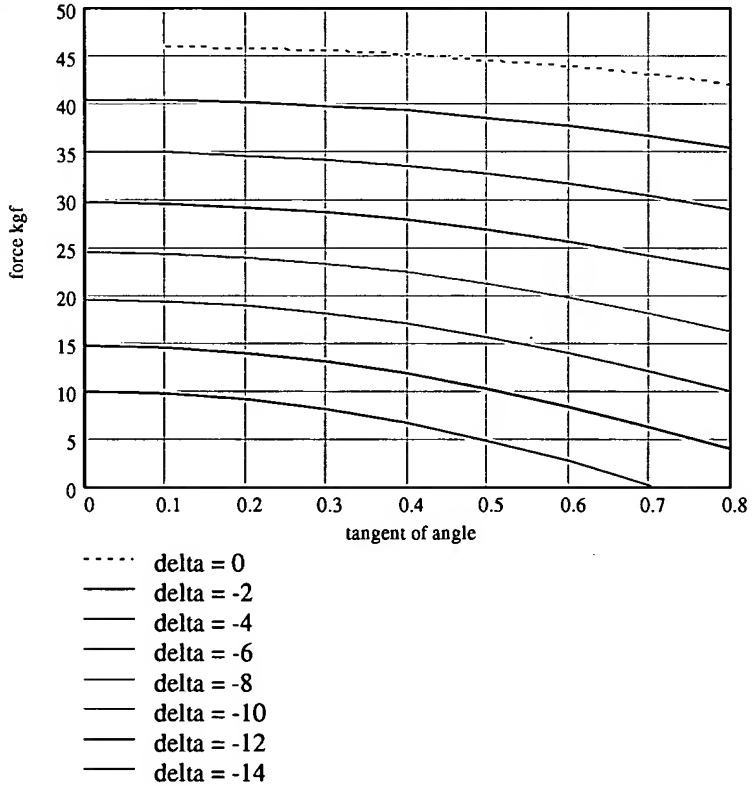

Fig. 13.9. Dependence of the airbag tension force on the inclination of the hollows at the pressure 1 kgf/cm^2

Fig. 13.8 and Fig. 13.9 shows that the inclination of the hollows does not influence dramatically the mechanical behavior of the airbag. The principal tendency is that the airbag becomes more compliant in the lengthwise direction as the inclination angle increases. This tendency is not quite the case at a low gas pressure within the airbag. Thus, the inclination angle of the hollows can be chosen from engineering considerations, without referring to the airbag tension regulation.

14. AXISYMMETRIC PROBLEM OF STRESS CONCENTRATION NEAR A ROUND GLUED AREA

This chapter features a solution of an axisymmetrical problem for a simplest safety airbag made of two round sheets of film connected along their outline and also in a round area in their central parts. The following is to be investigated: the airbag's shape under pressure, stress in the film including the round glued area, stress in the glued seam. Special attention is paid to the linear stress of the glued seam peeling and the peeling angle of the glued pieces of film.

14.1. Design model

The airbag under consideration consists of two round pieces of film of the radius b glued along their exterior contour and within a circle in their common central part of the radius a. The schematic model is shown on Fig. 14.1. This airbag has an annular hollow which is $b - a$ wide in its initial non-deformed state. As the airbag is inflated, the width of this hollow decreases.

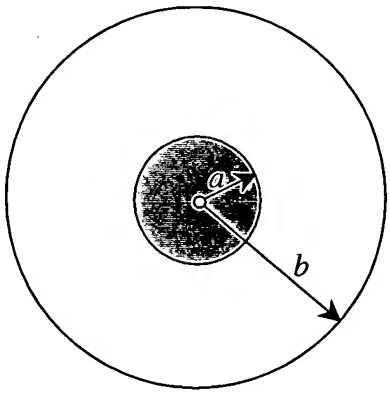

Fig. 14.1. A sketch of the inflatable toric airbag. The glued area is grayed

We assume the film to have the thickness of h, to be made of an isotropic material, and to have the elasticity modulus E and Poisson ratio ν.

The problem is to determine the stress and strain in the film when the hollow is filled with gas under pressure p above ambient.

Let's assume the system may have large deformations and displacements. We assume also that folds are "smeared" (evenly distributed) over the material.

Let the airbag is referred to a cylindrical coordinate system r, θ, z so that the axis of revolution of the airbag be coincident with the z axis. As the airbag is a body of revolution, its shape is completely determined by a fragment of a curve that represents the meridional section of the shell. This curve is shown on Fig. 14.2 schematically.

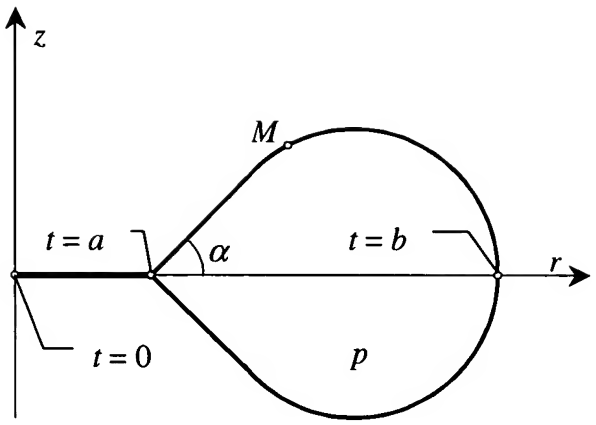

Fig. 14.2. Cross-section of the toric airbag

Let this line be specified parametrically using coordinates $r(t)$, $z(t)$ depending on parameter t. Parameter t is the length of the line that connects the airbag's center and the current point M when the airbag is not deformed.

As the system is dissymmetric with respect to the plane $z = 0$, we will deal with only the lower semi-curve $z \le 0$. Parameter t will then change within the following limits: $0 \le t \le b$.

14.2. Physical relationships

The following conventional physical relationships hold for the material in tension:

$$\sigma_1 = \frac{E}{1-\nu^2}(\varepsilon_1 + \nu\varepsilon_2); \quad (14.1)$$

$$\sigma_2 = \frac{E}{1-\nu^2}(\nu\varepsilon_1 + \varepsilon_2); \quad (14.2)$$

ε_1 is an elastic relative elongation of the material in the meridional direction;

ε_2 is an elastic relative elongation of the material in the circular direction;

σ_1 is a meridional stress;

σ_2 is a circular stress.

14.3. Differential equations

The displacement method is used to solve the problem. Its principal unknowns are $r(t)$ и $z(t)$. As all variables are functions of the only parameter t, its notation will be omitted further below.

The problem posed is similar to that posed and solved in[20] in the part of derivation and solution of the appropriate differential equations. The difference is that there is no pressing die in this problem, and also boundary conditions are different.

Let's give the system of differential equations omitting its derivation.

Table 1. System of differential equations

No folds		Folds
$r' = \frac{N_r(K-\nu\Delta)}{N}$	Case	$r' = \frac{N_r K}{N}$

$z' = \frac{N_0(K - \nu\Delta)}{N}$		$z' = \frac{N_0 K}{N}$
$N_r' = \frac{B\Delta}{t} - \frac{2\pi r p N_0 (K - \nu\Delta)}{N}$		$N_r' = -\frac{2\pi r p N_0 K}{N}$
$N_z' = 0$		$N_z' = 0$

Besides the principal unknown functions r and z, conjugate functions N_r and N_z feature in this system. The following notation has been introduced to simplify the writing:

(14.3) $B=2\pi thE;$

(14.4) $N_0=N_z+\pi pr^2;$

(14.5) $N = \sqrt{N_r^2 + N_0^2}\ ;$

(14.6) $K = 1 + \frac{N}{B};$

(14.7) $\Delta = \frac{r}{t} - 1 + \frac{\nu N}{B}.$

At $\Delta \geq 0$ there are no folds, at $\Delta < 0$ there are radial folds.

In addition to the notation described in [20], the symbol (14.5) has been introduced and r_0 has been replaced by t.

14.4. Boundary conditions

Let's deal with the part of the airbag where the hollow is located: $a \leq t \leq b$.

It is obvious that the z coordinate at the beginning and at the end of the integration interval will be zero.

(14.8) $z(a) = 0;$

(14.9) $z(b) = 0.$

As for the boundary conditions at the point $t = a$, note that at $0 \leq t \leq a$ the uniform tension of the central round area takes place, with the following equalities being true:

(14.10) $\varepsilon_1 = \varepsilon_2 = \varepsilon;$

where ε is an arbitrary constant.

Thus

(14.11) $r = (1+\varepsilon)\, t;$

(14.12) $\sigma_1 = \sigma_2 = \frac{\varepsilon E}{1-\nu}.$

Repeating the considerations from Section "Boundary conditions" of the paper [20], we come to a conclusion that the initial conditions for the unknown functions r and N_r can be expressed via the arbitrary constant ε by the following formulae:

(14.13) $r(a) = a(1+\varepsilon);$

(14.14) $$N_r(a) = \frac{2\pi h E \varepsilon a}{1-\nu}.$$

Also,

(14.15) $$N_r(b) = 0.$$

This is a natural condition for function N_r at the end of the interval.

Function N_z is constant at the whole interval of integration. Its value is another arbitrary constant. Using the Runge – Kutta method for the integration of the system of differential equations, one should specify $z(a) = 0$ and then choose values of constants ε and N_z so that conditions (14.9) and (14.15) hold at the end of the integration interval.

14.5. Formulae for the desirable values

In this chapter we are interested with the shape of the hollow in its inflated state and linear stresses of the glued seam peeling.

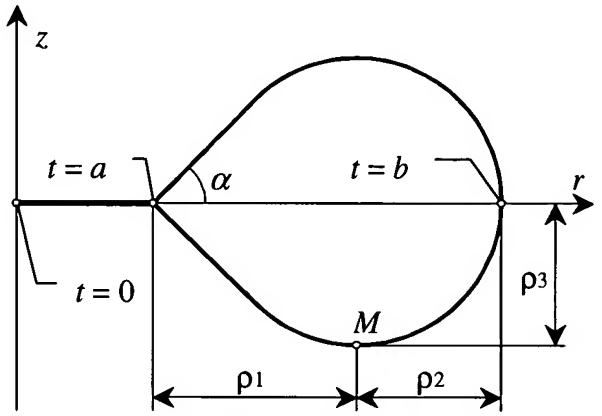

Fig. 14.3. Parameters of the shape

The shape of the hollow can be described sufficiently well by three radii: large radius ρ_1, medium radius ρ_2, small radius ρ_3, and the peeling angle of the glued films α at the boundary of the central glued area (Fig. 14.3). Point M used here for the determination of all three radii corresponds to the ultimate value of the z coordinate.

The radial coordinate of this point is found from the condition of the equality to zero of function N_0 defined by formula (14.4):

(14.16) $$r_M = \sqrt{\frac{-N_z}{\pi p}}.$$

Thus

(14.17) $$\rho_1 = r_M - r(a);$$

(14.18) $$\rho_2 = r(b) - r_M.$$

The small radius can be determined directly:

(14.19) $$\rho_3 = -\min_t z(t).$$

Sine of angle α can be determined by the following formula:

(14.20) $$\sin(\alpha) = -\frac{N_0(a)}{N(a)}.$$

The linear peeling stress at the glued seam of the central area is determined by the formula:

(14.21) $$T_a = -\frac{N_0(a)}{2\pi a};$$

The following formula determines the linear peeling stress of the exterior contour:

(14.22) $$T_b = \frac{N_0(b)}{2\pi b}.$$

The peeling angle at the contour is 90°.

14.6. Dimensionless quantities

Let us assume we are considering a curvilinear hollow that has the following half-width in its flat unstressed state (in plane):

(14.23) $$d = \frac{b-a}{2}$$

and its radius of rounding along the interior edge is a (см. Fig. 14.2).

Let's introduce a dimensionless parameter

(14.24) $$\eta = \frac{d}{a};$$

that describes the relative curvature of the hollow.

Note that $\eta = 0$ for a rectilinear hollow, and $\eta \to \infty$ for a most curved hollow when $a \to 0$.

Let's introduce dimensionless coefficients of shape:

(14.25) $$\theta_1 = \frac{\rho_1}{\rho_0};$$

(14.26) $$\theta_2 = \frac{\rho_2}{\rho_0};$$

(14.27) $$\theta_3 = \frac{\rho_3}{\rho_0};$$

where ρ_0 is the radius of the rectilinear hollow for the case of an inextensible film, calculated by the formula:

(14.28) $$\rho_0 = \frac{2d}{\pi}.$$

Let's introduce stress concentration coefficients:

(14.29) $$k_a = \frac{T_a}{T_0}$$ for the seam of the central round glued area,

(14.30) $$k_b = \frac{T_b}{T_0}$$ for the seam of the exterior contour.

The reference level of the linear stress is assumed to be its value for the rectilinear hollow:

(14.31) $$T_0 = \frac{2pd}{\pi};$$

where p is an internal pressure above ambient in the airbag.

This formula will be precise if the airbag is made of an inextensible film.

Similar derivations are made for the radial stress too.

The stress concentration coefficients are determined in the following way:

(14.32) $$\zeta_0 = \frac{\sigma_1(0)}{\sigma_0}$$ in interior points of the central round glued area,

(14.33) $$\zeta_a = \frac{\sigma_1(a)}{\sigma_0}$$ in the hollow region near the boundary of the central glued area,

(14.34) $$\zeta_b = \frac{\sigma_1(b)}{\sigma_0}$$ in the hollow region near the outer contour;

where $\sigma_1(0)$, $\sigma_1(a)$ and $\sigma_1(b)$ are radial stresses in the film in interior points of the central round glued area, in the hollow region near the boundary of the central glued area, and in the hollow region near the outer contour, respectively.

The reference levels of the radial stresses are assumed to be their values for the case of a rectilinear hollow formed between two sheets of an inextensible film of the thickness h under internal pressure p above ambient:

(14.35) $$\sigma_0 = \frac{2pd}{\pi h}.$$

Stress $\sigma_1(0)$ can be calculated using (14.14) by the formula:

(14.36) $$\sigma_1(0) = \frac{N_r(a)}{2\pi a h}.$$

14.7. Results of calculation

Calculations were made by a program developed in the MathCAD-2000 environment. The calculation used the following source data:

d = 10 cm, h = 0.01 cm, E = 36000 kgf/cm^2, ν = 0.39, p =1 kgf/cm^2.

Values of all dimensionless parameters listed in Section 14.6 were obtained for curvatures of the hollow described by parameter η in the range $-10 \le \eta \le 10$.

11 problems were solved for the following values of parameter η: 10^{-1}; $10^{-0.8}$; $10^{-0.6}$; $10^{-0.4}$; $10^{-0.2}$; 1; $10^{0.2}$; $10^{0.4}$; $10^{0.6}$; $10^{0.8}$; 10.

The results are listed in the table below.

Table 3. Dimensionless parameters calculated using source data
d = 10 cm, h = 0.01 cm, E = 36000 kgf/cm^2, ν = 0.39, p =1 kgf/cm^2.

η	θ_1	θ_2	θ_3	$\sin\alpha$	ζ_0	ζ_a	$\zeta_b=k_b$	k_a
0.100	1.068	1.008	0.992	0.996	0.100	1.109	0.925	1.105

0.158	1.098	1.007	0.982	0.991	0.159	1.170	0.889	1.159
0.251	1.139	1.005	0.969	0.980	0.252	1.269	0.845	1.244
0.398	1.192	1.000	0.952	0.961	0.397	1.431	0.797	1.375
0.631	1.255	0.994	0.931	0.930	0.621	1.693	0.750	1.575
1.000	1.321	0.984	0.908	0.890	0.967	2.117	0.708	1.883
1.585	1.384	0.973	0.886	0.845	1.496	2.795	0.675	2.361
2.512	1.437	0.962	0.867	0.803	2.302	3.866	0.652	3.106
3.981	1.479	0.953	0.853	0.773	3.512	5.536	0.636	4.279
6.310	1.510	0.947	0.843	0.757	5.298	8.104	0.625	6.133
10.000	1.532	0.943	0.837	0.756	7.850	11.998	0.619	9.073

Shapes of the hollow's meridian for minimum, medium and maximum values of the curvature parameter η are shown on Fig. 14.4, Fig. 14.5 and Fig. 14.6. The diagrams outline the fold formation zone by a blue dotted line. As one can see from the diagrams, almost the whole shell except for a narrow region near the central glued area is covered by radial folds and is free from circular stresses.

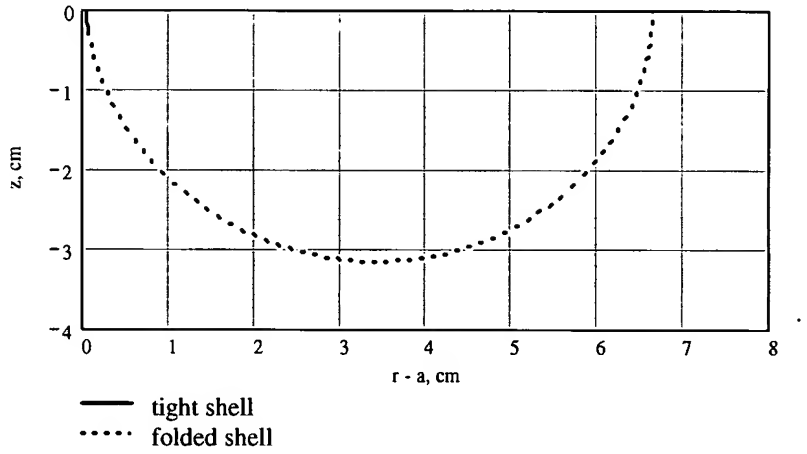

Fig. 14.4. Shape of the meridian of the hollow at $\eta = 0.1$

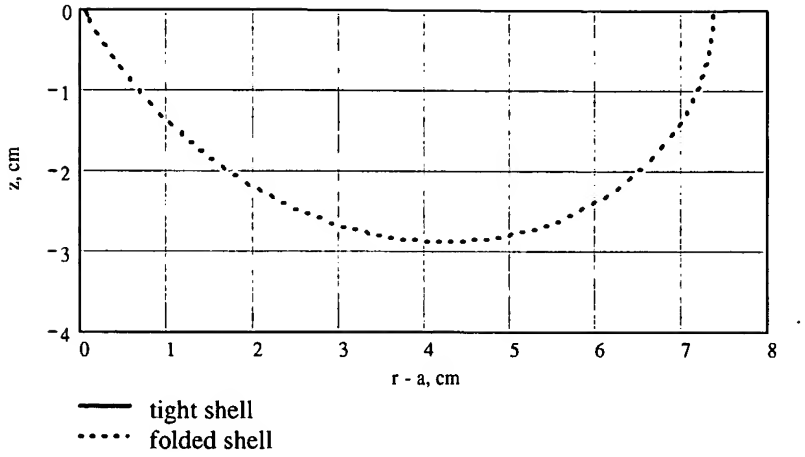

Fig. 14.5. Shape of the meridian of the hollow at $\eta = 1$

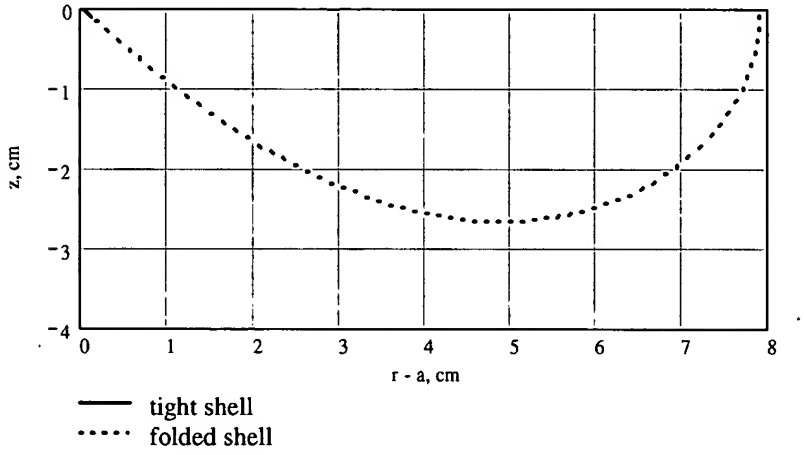

Fig. 14.6. Shape of the meridian of the hollow at $\eta = 10$

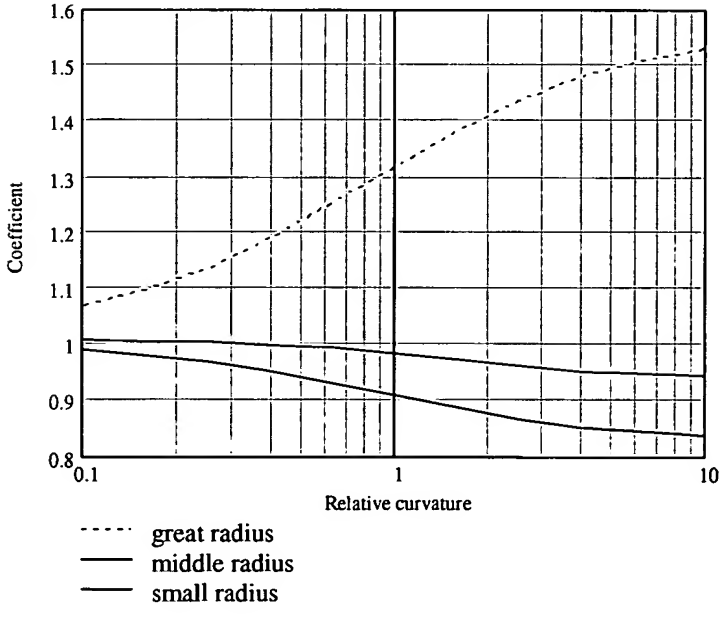

Fig. 14.7. Dimensionless coefficients of shape θ_1, θ_2 and θ_3

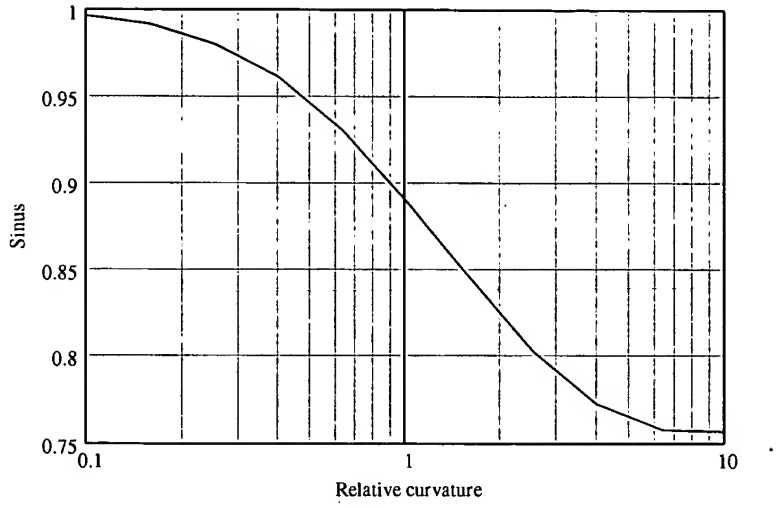

Fig. 14.8. Sine of the peeling angle α of the seam of the central glued area

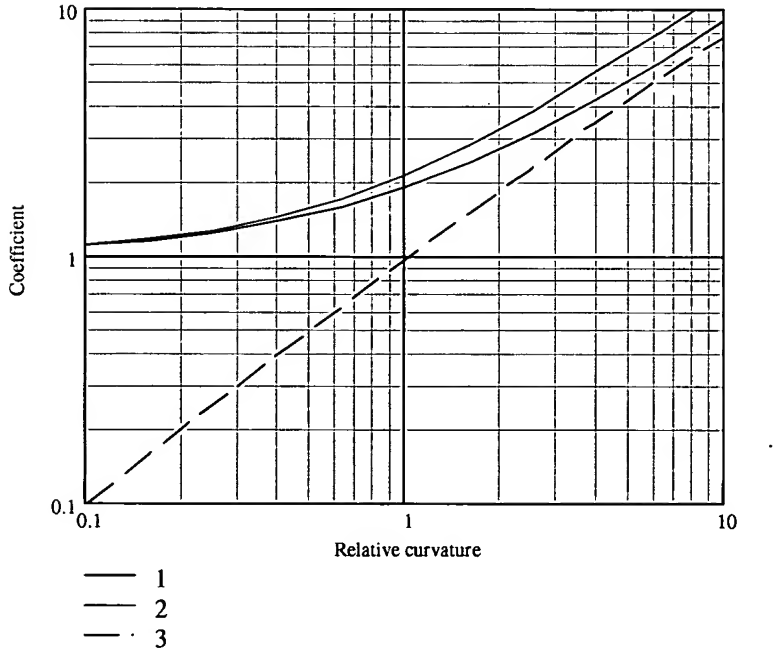

Fig. 14.9. Coefficients of concentration of:
1 – radial stress in the hollow region near the boundary of the glued area;
2 – linear peeling stress at the seam of the central glued area;
3 – radial stress in interior points of the central glued area

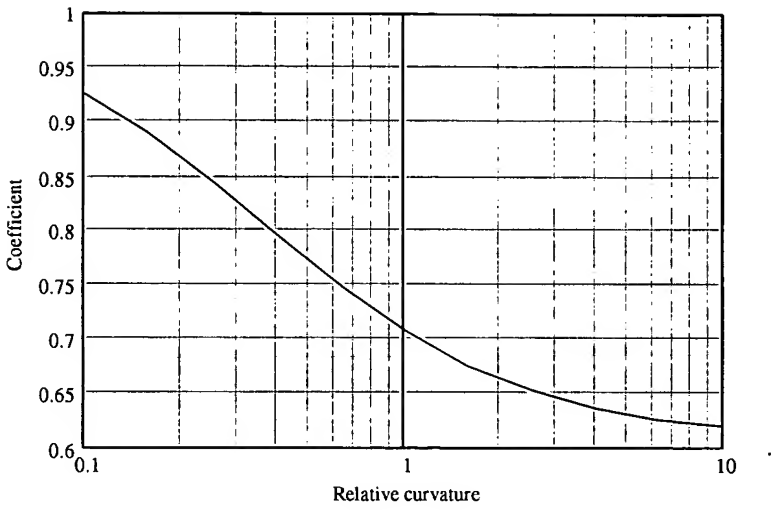

Fig. 14.10. Coefficient of decrease of the radial stress and linear peeling stress in the glued area along the outer contour

15. BIPERIODICAL MODELS OF AIRBAGS WITH ROUND GLUED AREAS

This chapter features the results of the numerical computations of the stress and strain of endlessly stretching biperiodical models of airbags with round glued areas.

The allotment of the linear peeling stress along the glued contour is investigated.

Two types of models are investigated. In the first type model the centers of the round glued areas are located in the nodal points of a triangular grid, and in the second type model they are located in the nodal points of a square grid.

The series of problems are resolved in which the glued area radius relations are varied to the grid spacing within the range 0.1,..,0.3.

The problem turned out to be unexpectedly difficult. There were observed, besides strong nonlinearity, the characteristics of the differential equations system degeneracy in the initial stage of the equations system deformation and degeneracy in the folds-forming stage (due to the degeneracy of the material itself). It was discovered at the last moment that the film deformable surface self-intersection is observed in the obtained solutions. This circumstance put the problem to the category of contact ones.

As the numerical model is extremely unstable, there were taken some measures to stabilize it. The equibiaxial preliminary expansion of the airbag field was used as one of the stabilizing factors, which was gradually diminished in the process of the problem solution. As the other stabilizing factor an additional shell of special material with vanishingly small modulus of elasticity and very high coefficient of the thermal strain was used.

15.1. The main calculated prerequisites

The finite-element method, realized in multiphysical program system ANSYS, version 5.5.1. was used for computations. As the basic finite element the triangular membrane element SHELL41 is used which takes into account big displacements and deformations correctly and takes only tension stress. While working under conditions of negative deformations the element loses its response force in one or two directions imitating folds forming. At the same time the element becomes inwardly variable.

For this inward variability prevention, which leads to the instability of the calculating process a workaround is used. It means that simultaneously with the basic shell of the finite elements the second shell of material with special characteristics is adjusted. This material has vanishingly small modulus of elasticity and very high coefficient of the thermal strain. The negative temperature is assigned for the elements of the second shell with the expectation of the thermal strain to be equal -1.0. An unstrained member of this material under the temperature influence shrinks to the zero size. At the same time low modulus of elasticity lets this element to be deformed almost without strain.

Thus, the conglomerate of two elements – membrane and special – never undergoes compression stress; it is not internally changeable and practically doesn't differ on its characteristics from the element SHELL41, which imitates folds forming.

In order to stabilize the system on the initial stage of deformation when it is nearly flat as well as in the process of its skeleton reconstruction some efforts are made to the system, which causes proportional biaxial pretension. On the last stage of problem solution these efforts gradually reduce and in an ideal case should be reduced to zero.

However, the moment comes when the shell heavily bulges and some parts of it exceed the plane of symmetry. Such deformation conflicts with the physical meaning as it corresponds to the strained surface with self-intersections. It results in the necessity to supplement the problem with the restricted inequations or to work in the rigid contact surface to the system, which coincides with the plane of symmetry. Such problem complication heavily increases (till hours) its solution time and brings additional elements of instability to the process of solution.

In order to get the final problem solution we had to turn to rather rarefied finite elements system.

15.2. Model with glued areas in nodes of a triangular grid

The model being investigated results from two infinitely extending film sheets with the centres in nodes of a triangular grid being glued in round areas. The scheme of the work part for this model is shown on Fig. 15.1.

Grid spacing a, round glued area radius r. Into the hollow between sheets gas is pumped under the pressure p.

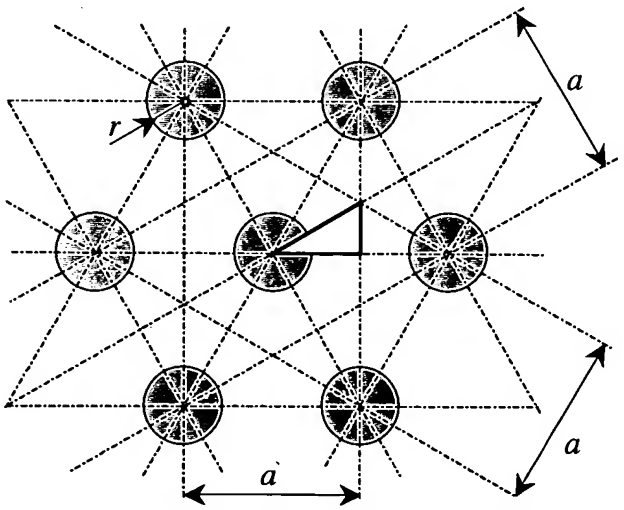

Fig. 15.1. The scheme of the work part for airbag with biperiodical system of round glued areas in the nodes of the triangular grid.

Calculations were made with the following source data:

- Film sheet sickness h= 0.01 cm;

- Modulus of elasticity E= 36000 kgf/cm^2;
- Poisson ratio ν=0.39;
- Grid spacing a= 10 cm;
- Gas pressure above ambient p = 1 atm.

Round glued area radius r was varied.

The problems are solved for radii r: 1.0; 1.5; 2.0; 2.5; 3.0.

Concidering symmetry characteristics present in this problem, it is enough to make a finite-element method solution only for unit cell, which has right triangle form shown on Fig. 15.1 and more detailed on Fig. 15.2.

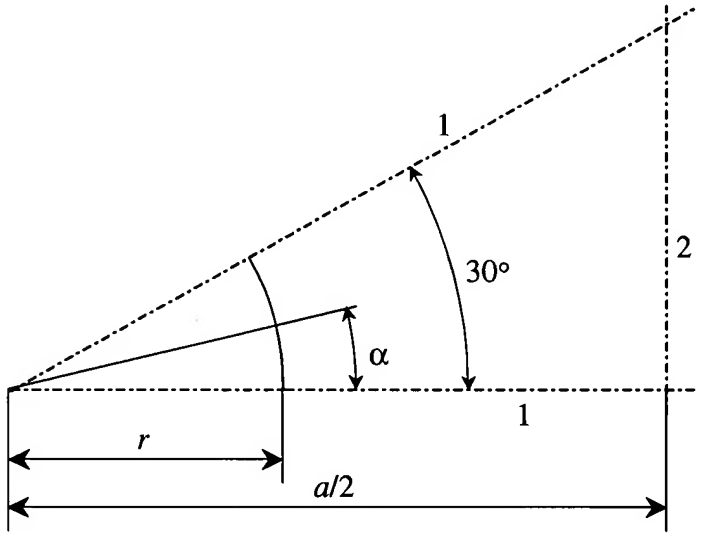

Fig. 15.2. Unit cell scheme .
1 – immovable planes of symmetry, 2 - movable plane of symmetry.

On each side of this triangle mirror symmetry conditions are observed. Concidering missing fixation at infinity, one of the lines (or rather planes) of symmetry must be movable.

Dummy finite elements of vanishingly small rigidity, which serve for gas pressure load transfer to the movable plane of symmetry, are located on the same plane.

Unit cell splitting to finite elements is shown on Fig. 15.3.

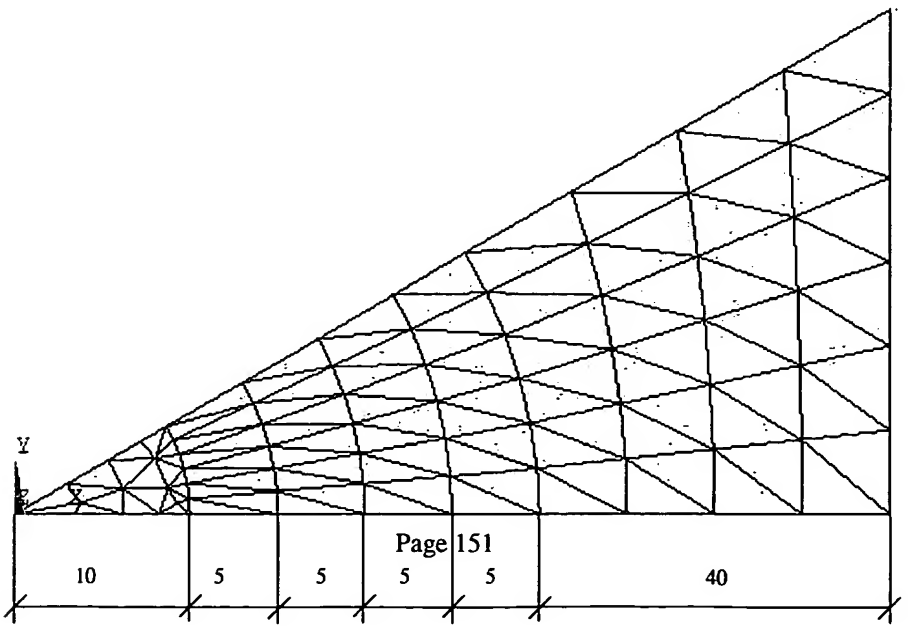

Fig. 15.3. Unit cell splitting to finite elements. Sizes are in millimeters.

Airbags calculations with round glued areas of different radii are made with this splitting. Unit cells strained schemes are given on Fig. 15.5 - Fig. 15.9. Folds, connecting nearest round glued areas, are formed on the surface of airbag at small glued area radii . It can be seen on big finite elements contractions.

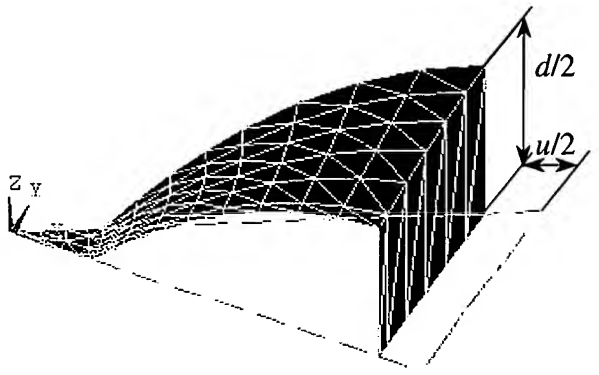

Fig. 15.4. Typical sizes of airbag deformation.

As the gas is pumped, the airbag inflates and its linear dimensions contract.

Let the airbag thickness be indicated as d, and the size, which characterizes linear dimensions contraction as u. Geometrical meaning of these sizes and their connection with unit cell movement is evident from Fig. 15.4.

Airbag thickness ratio d/a and its contraction u/a depending on glued area radius

(15.1) $$\rho = \frac{r}{a}.$$

are listed in the Table 4.

Table 4. Airbag thickness ratio and contraction for the triangular grid case

	$\rho = 0.10$	$\rho = 0.15$	$\rho = 0.20$	$\rho = 0.25$	$\rho = 0.30$
Thickness ratio d/a	0.4323	0.3635	0.2947	0.2285	0.1682
Contraction u/a	0.1026	0.0798	0.0572	0.0372	0.0209

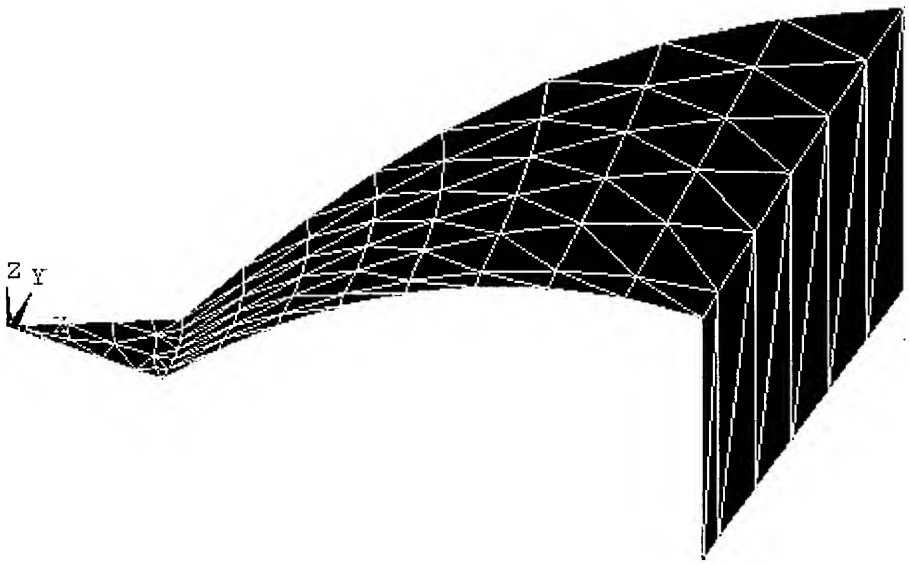

Fig. 15.5.Unit cells strained scheme at glued area radius 1 cm.

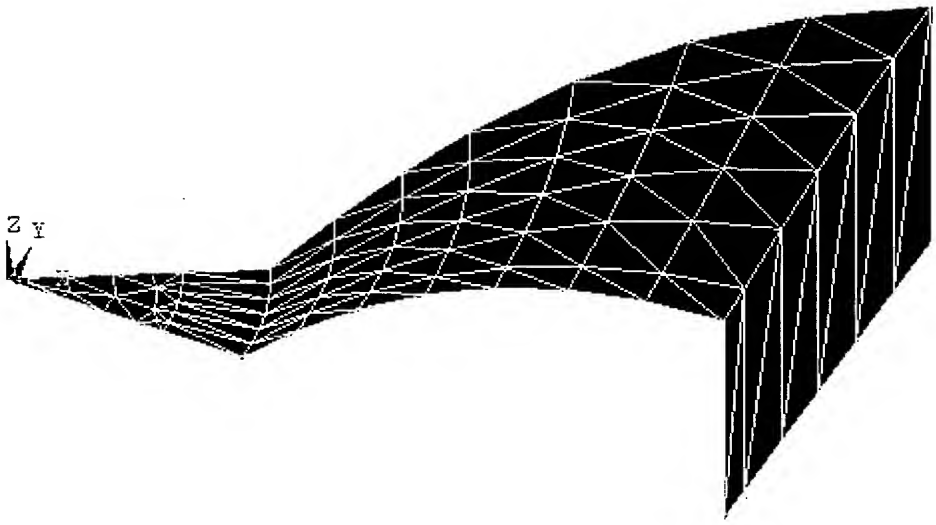

Fig. 15.6. Unit cells strained scheme at glued area radius 1.5 cm.

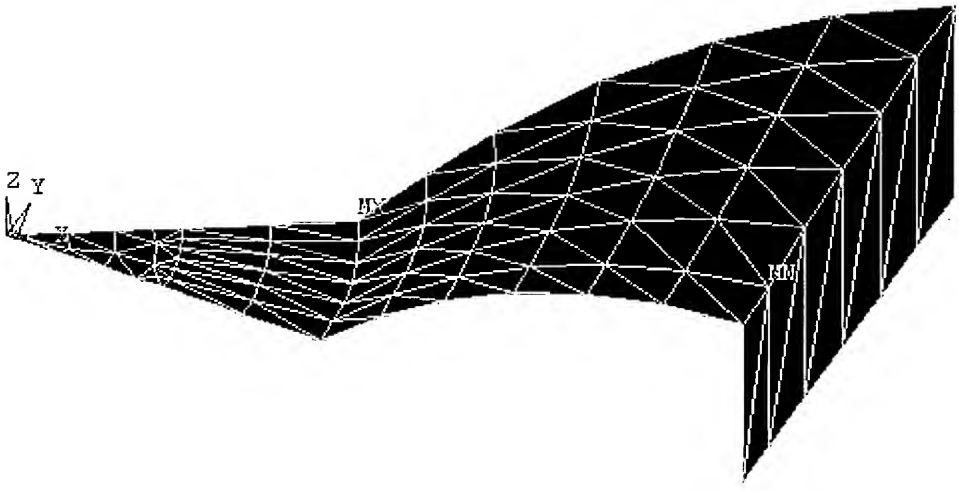

Fig. 15.7. Unit cells strained scheme at glued area radius 2 cm.

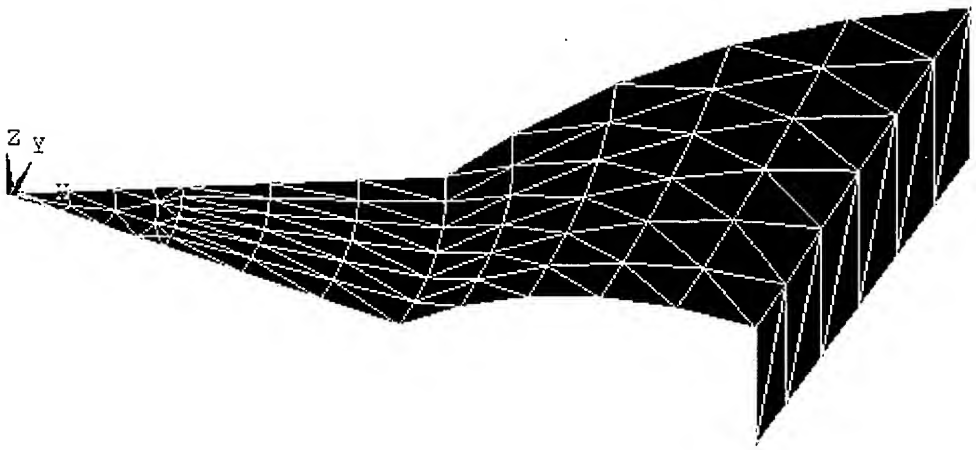

Fig. 15.8. Unit cells strained scheme at glued area radius 2.5 cm.

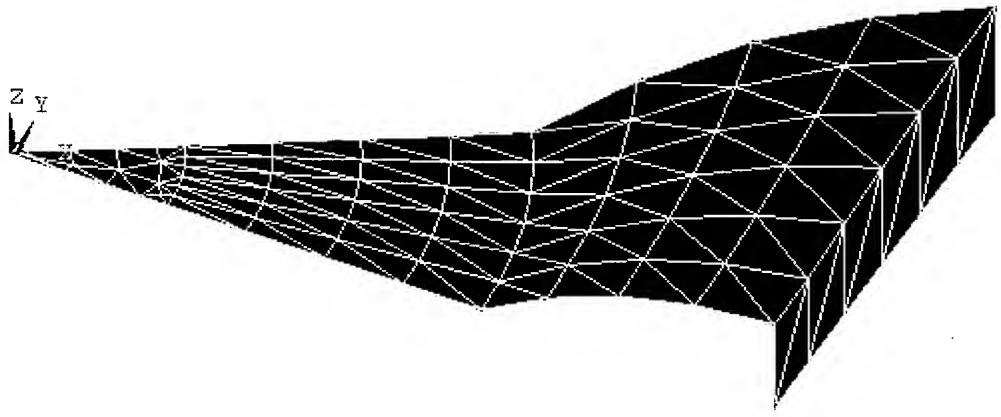

Fig. 15.9. Unit cells strained scheme at glued area radius 3 cm.

Table 5. Linear peeling stress R_{45} for the triangular grid case in kgf/cm.

	ρ = 0.10	ρ = 0.15	ρ = 0.20	ρ = 0.25	ρ = 0.30
α = 0	10.082	7.557	4.846	3.362	2.628
α = 5	2.576	1.782	1.308	1.581	1.374
α = 10	10.436	5.386	4.439	3.124	2.557
α = 15	12.747	8.443	5.586	4.132	3.179
α = 20	14.397	9.442	6.724	4.879	3.553
α = 25	15.086	10.070	7.200	5.181	3.738
α = 30	11.792	8.508	6.509	4.927	3.113

Linear peeling stress is tabulated depending on the angle α (see Fig. 15.2) and relative glued area radius ρ.

The same data are depicted graphically on Fig. 15.10.

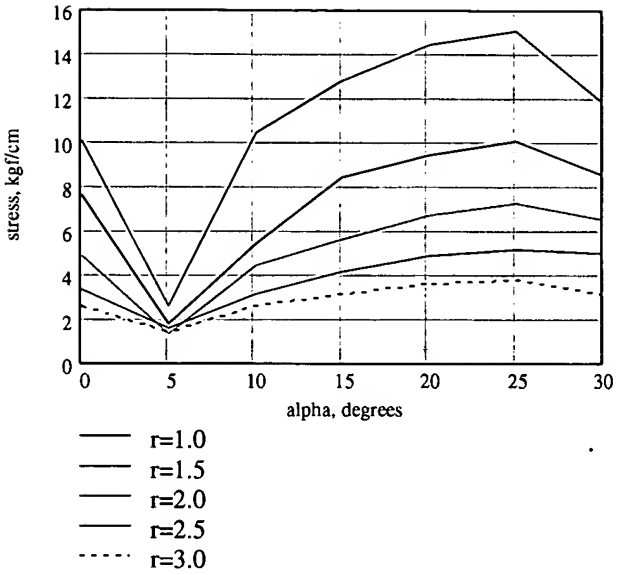

Fig. 15.10. Linear peeling stress R_{30} for the triangular grid case.

Linear peeling stress concentration coefficients k, which had been obtained by numerical method, are given in Table 6 . As a normalizing divisor an averaged linear peeling stress is taken, which can be calculated by the following formula:

(15.2) $$R^0_{30} = \frac{p}{2\pi r}\left(\frac{3a^2 \tan 30°}{2} - \pi r^2\right).$$

Table 6.Linear peeling stress concentration coefficients k_{30} for the triangular grid case .

	ρ = 0.10	ρ = 0.15	ρ = 0.20	ρ = 0.25	ρ = 0.30
α = 0	0.759	0.896	0.822	0.789	0.849
α = 5	0.194	0.211	0.222	0.371	0.444
α = 10	0.786	0.638	0.753	0.733	0.826
α = 15	0.96	1.001	0.948	0.969	1.027
α = 20	1.084	1.119	1.141	1.144	1.148
α = 25	1.136	1.193	1.222	1.215	1.208
α = 30	0.888	1.008	1.105	1.156	1.006

In order to get a real value of the linear peeling stress R_{30}, concentration coefficient from Table 6 must be multiplied by the normalizing divisor calculated by formula (15.2):

(15.3) $$R_{30} = k_{30} R^0_{30}.$$

15.3. Model with glued areas in nodes of a square grid

Calculations for the model with round glued areas in nodes of a square grid are made similarly to the previous case.

The scheme of the work part for this model is shown on Fig. 15.11.

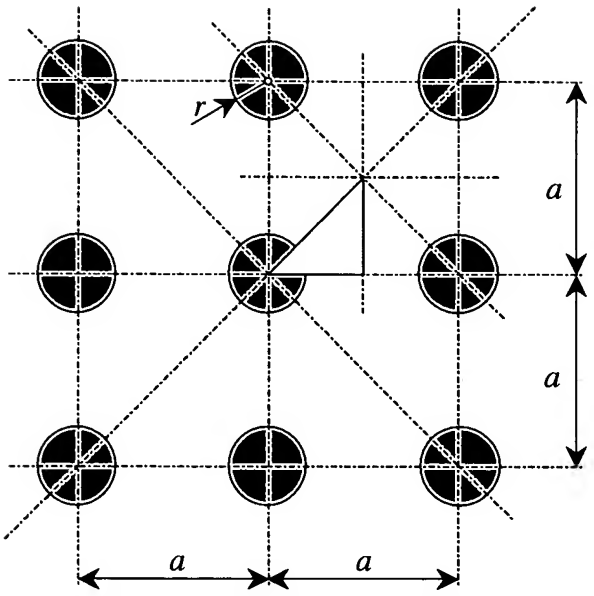

Fig. 15.11.The scheme of the work part for airbag with biperiodical system of round glued areas in the nodes of a square grid.

As in the previous case, grid spacing a, round glued area radius r. Into the hollow between sheets gas is pumped under the pressure p.

Calculations were made with the following source data:

- Film sheet sickness h= 0.01 cm;
- Modulus of elasticity E= 36000 kgf/cm^2;
- Poisson ratio ν=0.39;
- Grid spacing a= 10 cm;
- Gas pressure above ambient p = 1 atm.

Round glued area radius r was varied.

The problems are solved for radii r: 1.0; 1.5; 2.0; 2.5; 3.0 cm.

The form and sizes of the unit cell are shown on Fig. 15.12.

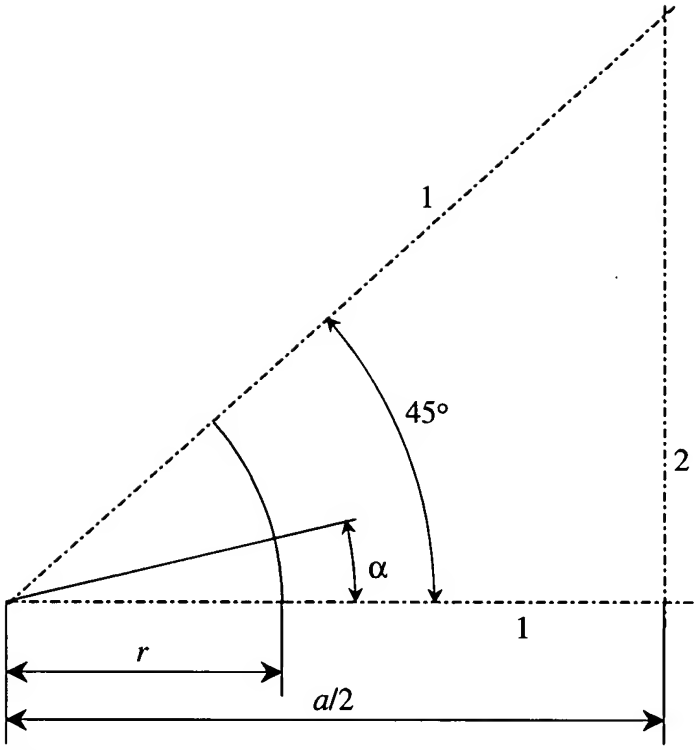

Fig. 15.12. Unit cell scheme .

1 – immovable planes of symmetry, 2 - movable plane of symmetry.

Unit cell splitting to finite elements is accepted the same for all problems.

It is shown on Fig. 15.13.

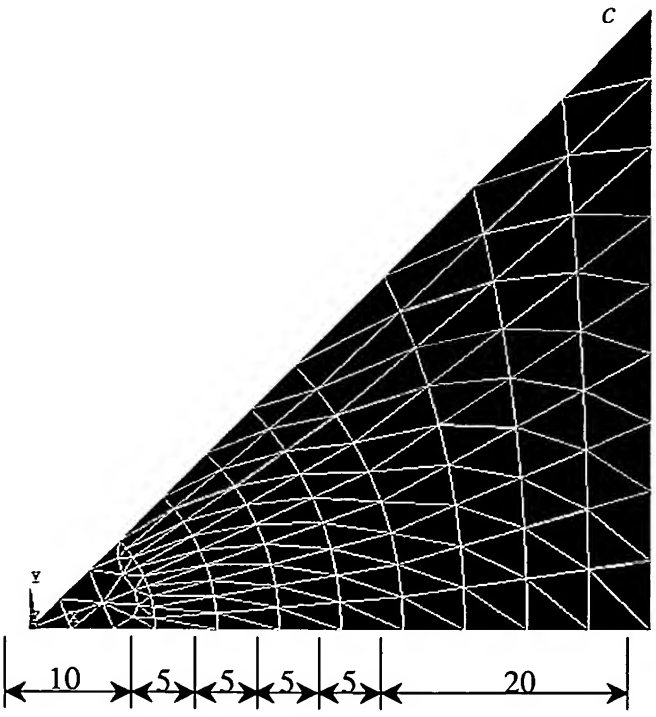

Fig. 15.13. Unit cell splitting to finite elements. Sizes are in millimeters.

Airbags calculations with round glued areas of different radii are made with this splitting. Unit cells strained schemes are given on Fig. 15.14 - Fig. 15.18. Deep folds, connecting nearest round glued areas, are formed on the surface of airbag at small glued area radii . It can be seen on the pictures.
. At big glued area radii the surface of the airbag remains practically smooth.

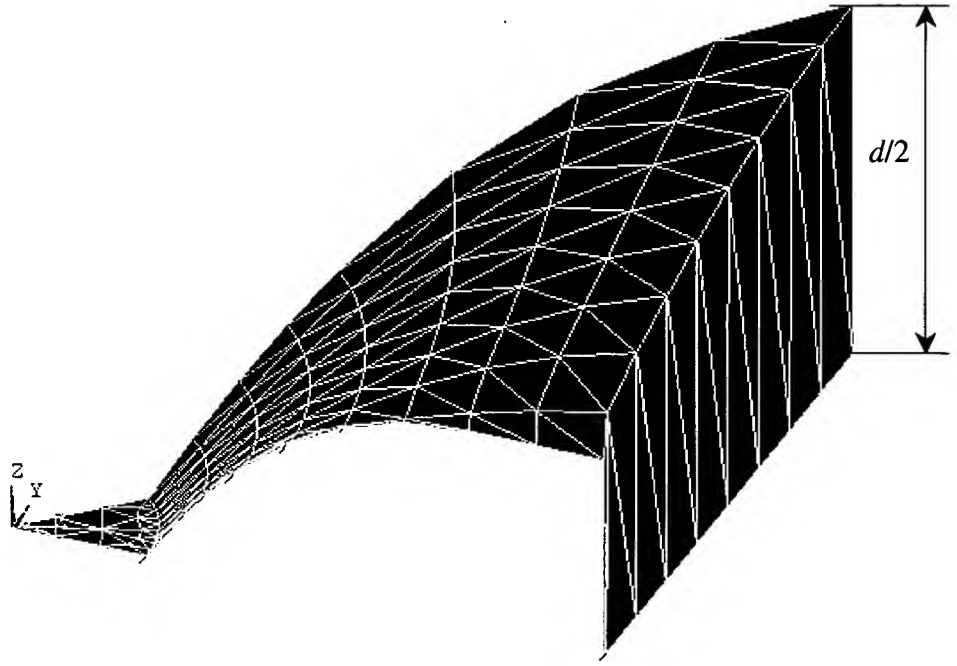

Fig. 15.14. Unit cells strained scheme at glued area radius 1 cm.

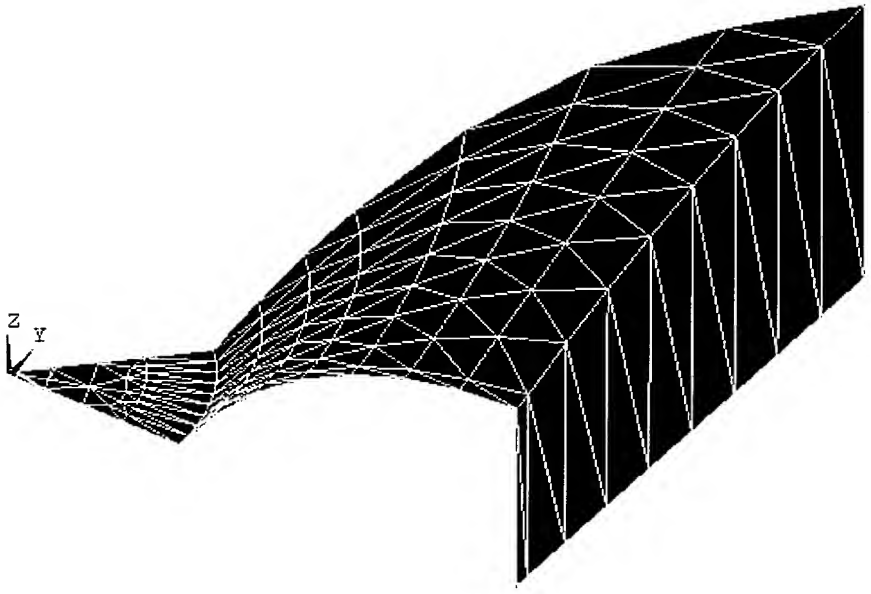

Fig. 15.15.Unit cells strained scheme at glued area radius 1.5 cm.

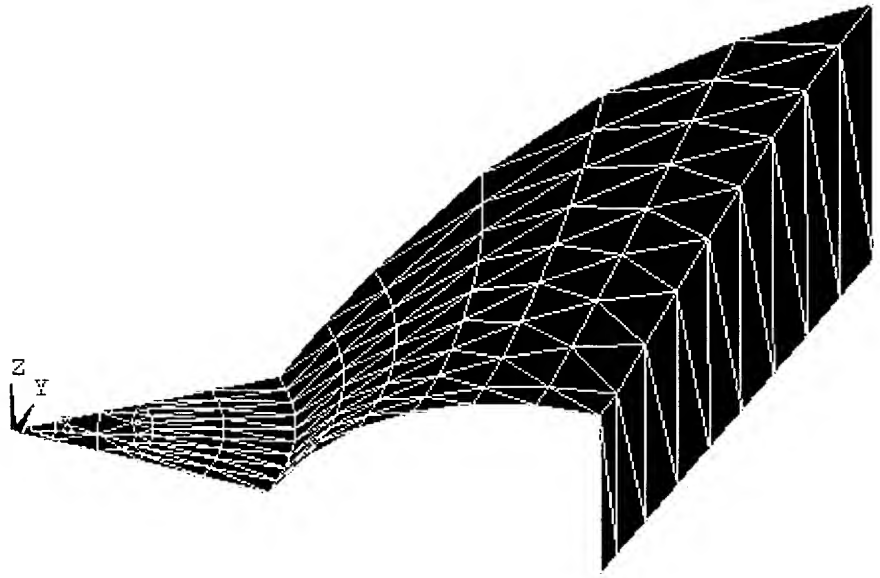

Fig. 15.16. Unit cells strained scheme at glued area radius 2 cm.

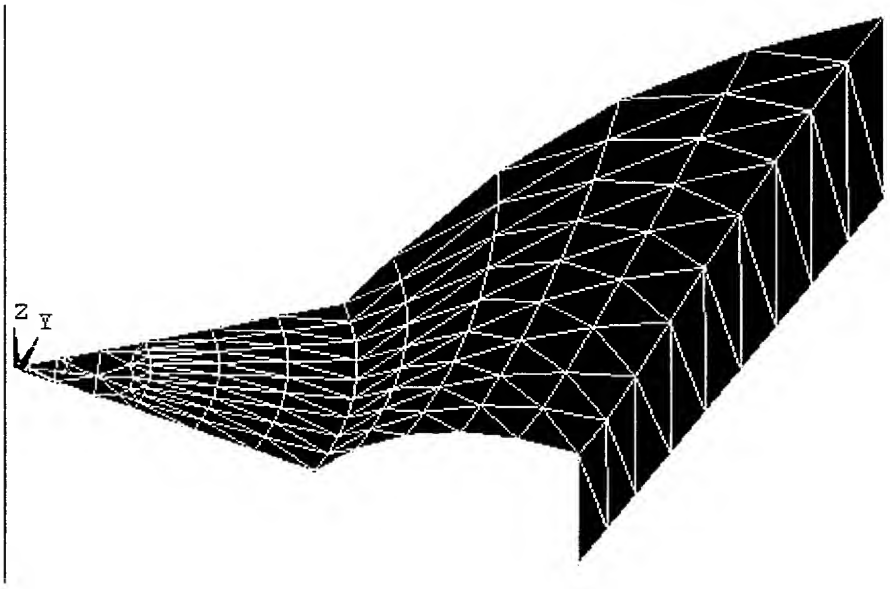

Fig. 15.17.

Unit cells strained scheme at glued area radius 2.5 cm.

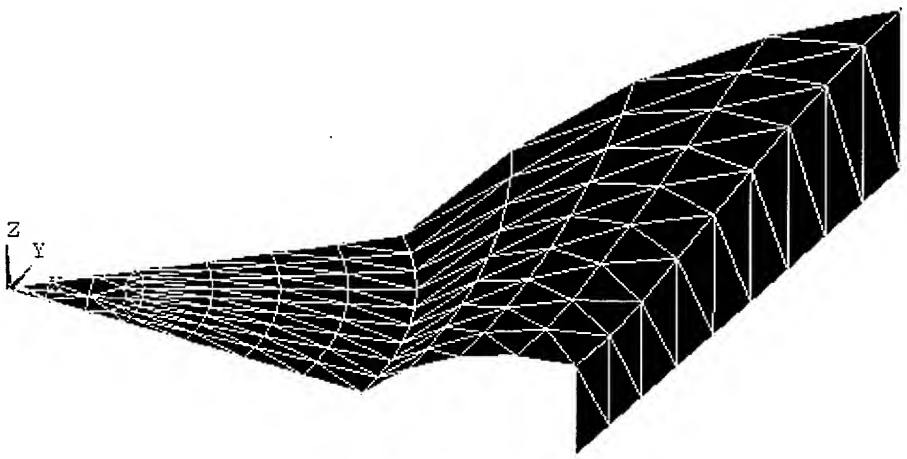

Fig. 15.18. Unit cells strained scheme at glued area radius 3 cm

As the gas is pumped, the airbag inflates and its linear dimensions contract.

These deformations are evaluated quantitatively by the relative airbag thickness *d/a* and its contraction *u/a*, which is uniform in all directions (see Fig. 15.4).

Table 5. Airbag thickness ratio and contraction

	ρ = 0.10	ρ = 0.15	ρ = 0.20	ρ = 0.25	ρ = 0.30
Thickness ratio	0.5566	0.5027	0.4253	0.3486	0.2750
Contraction	0.1178	0.1054	0.0798	0,0565	0.0360

Table 7. Linear peeling stress R_{45} for the square grid case in kgf/cm.

	ρ = 0.10	ρ = 0.15	ρ = 0.20	ρ = 0.25	ρ = 0.30
α = 0	12.381	8.410	5.617	3.860	2.688
α = 5	-0.360	-0.992	-0.153	0.828	1.180
α = 10	4.274	2.764	2.235	2.130	1.544
α = 15	6.493	3.581	2.822	2.411	1.751
α = 20	9.888	5.835	4.185	2.885	2.331
α = 25	13.438	9.619	6.602	4.682	3.703
α = 30	17.429	12.283	8.826	6.485	4.785
α = 35	18.942	14.015	9.871	7.125	5.343
α = 40	18.481	13.574	10.135	7.541	5.650
α = 45	16.591	12.277	9.244	6.917	5.511

The same data are shown graphically on Fig. 15.19.

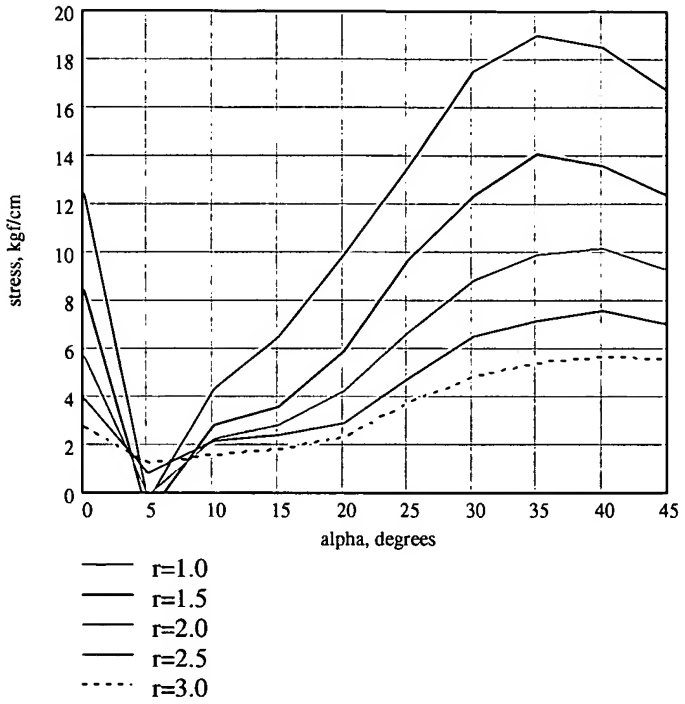

Fig. 15.19. Linear peeling stress R_{45} for the square grid case .

Linear peeling stress concentration coefficients k_{45}, , which had been obtained by numerical method are given in Table 8 .

As a normalizing divisor an averaged linear peeling stress is taken which can be calculated by the following formula:

(15.4) $$R^{a}{}_{45} = \frac{p}{2\pi r}\left(a^2 - \pi r^2\right)$$

Table 8. Linear peeling stress concentration coefficients k_{45} for the square grid case .

	ρ = 0.10	ρ = 0.15	ρ = 0.20	ρ = 0.25	ρ = 0.30
α = 0	0.803	0.853	0.807	0.755	0.706
α = 5	-0.023	-0.101	-0.022	0.162	0.310
α = 10	0.277	0.280	0.321	0.416	0.406
α = 15	0.421	0.363	0.406	0.471	0.460
α = 20	0.641	0.592	0.601	0.564	0.613
α = 25	0.872	0.976	0.949	0.915	0.973
α = 30	1.131	1.246	1.269	1.268	1.257
α = 35	1.229	1.421	1.419	1.393	1.404
α = 40	1.199	1.377	1.457	1.474	1.485
α = 45	1.076	1.245	1.329	1.352	1.448

In order to get a real value of the linear peeling stress R_{45}, concentration coefficient from Table 8 must be multiplied by the normalizing divisor calculated by formula: (15.4):

(15.5) $R_{45} = k_{45}R^0_{45}$.

It is necessary to note that the problem to be solved is ill-conditioned regarding its physical nature. Obviously, full system energy has many local minimums and iterative process finds one of them occasionally. That explains the evident scatter of readings, given in tables and diagrams.

16. AIRBAG WITH NARROW CHANNELS BETWEEN HOLLOWS

This chapter discusses results of a numerical analysis of the stress and strain distribution in periodical models of airbags having narrow channels between their adjacent hollows.

Principal properties of the shape of an inflated airbag and the distribution of the linear peeling stress along the glued contour have been studied.

16.1. Key assumptions of the analysis

The analysis used a finite element method implemented in a multi-physical computational software ANSYS, version 5.5.1. The main finite element used was a triangular membrane element SHELL41 that allows for large displacements and strains correctly and resists to tension only.

16.2. A model of an airbag having channels between its adjacent hollows

A plane schematic of a few cells of the model is shown in Fig. 16.1. As can be seen from the figure, the model in question is made of two infinitely extending strips of film $2(a+b)$ wide glued in the shaded areas. The radius of the glued area is r, the width of the channel is $2z$. The glued area and the whole system possess a translation symmetry with spacing $2c$.

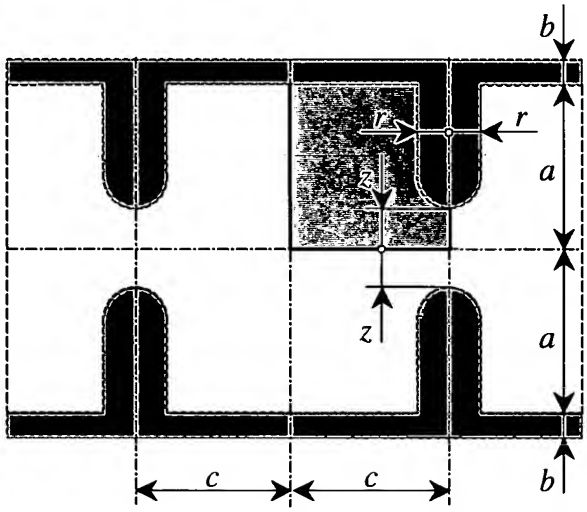

Fig. 16.1. A schematic of cells of the periodic model of an airbag with air channels between adjacent hollows.

A gas under pressure p is pumped to the hollow between the two film sheets.

The following source data were used for the analysis:

- Film sheet thickness h= 0.01 cm;
- Elasticity modulus E= 36000 kg/cm^2;
- Poisson ratio ν=0.39;
- Gauge pressure of the gas p = 1 atmosphere.

- Fixed geometric sizes: a= 5 cm; b=0 cm; r=1 cm.

Sizes c and z were subject to variation.

The problems were solved with c equal to 3; 5; 7; 9 cm at z = 1 cm and with z equal to 0.5; 1.0; 1.5; 2.0 cm at c = 5 cm.

The value of b was assumed to be zero as one that had little effect on the result of the analysis.

Due to the properties of symmetry possessed by the shape, it suffices to perform the finite element analysis only for an elementary cell of the rectangular shape shown in Fig. 16.1and in Fig. 16.2 more detail.

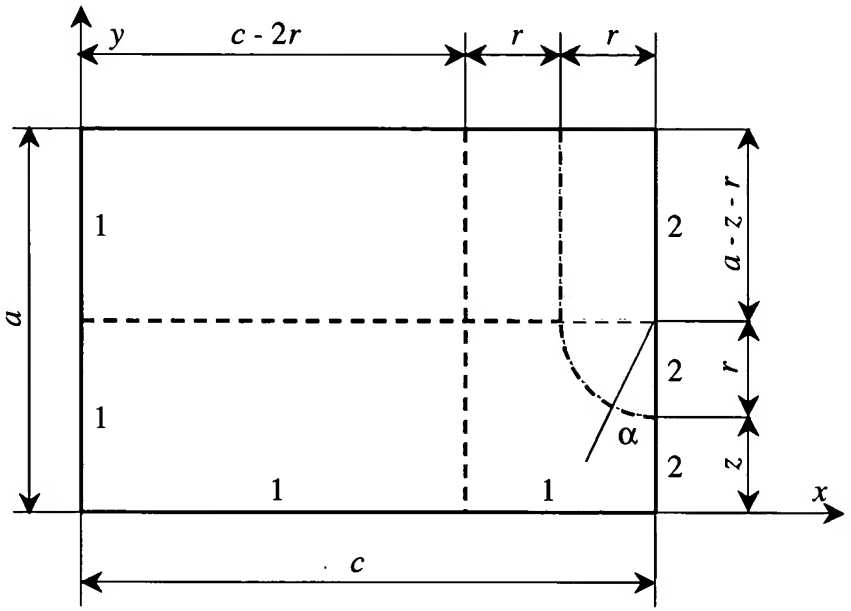

Fig. 16.2. A schematic of an elementary cell.
(1) fixed planes of symmetry, (2) moving plane of symmetry

Conditions of bilateral symmetry hold at three sides of this rectangle. As there is no fixation in the infinity, one of the symmetry planes must be capable of moving. The arrangement of the symmetry planes is shown in Fig. 16.2.

The division of the elementary cell into finite elements is shown in Fig. 16.3.

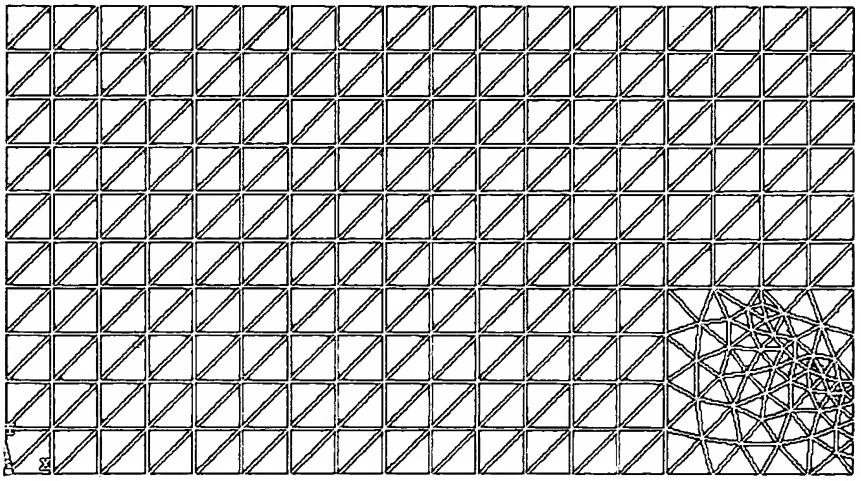

Fig. 16.3. A division of an elementary cell into finite elements.
a = 5 cm; c = 9 cm; r = 1 cm; z = 1 cm.

16.3. Dependence of sizes of the airbag and the peeling stress at the boundary of the glued area on the length of the hollow

Given below are results of solution of a series of problems where the length of the hollow was a variable value. Fig. 16.4 to Fig. 16.7 show deformed shapes of the elementary cell and give principal source data used in the analysis.

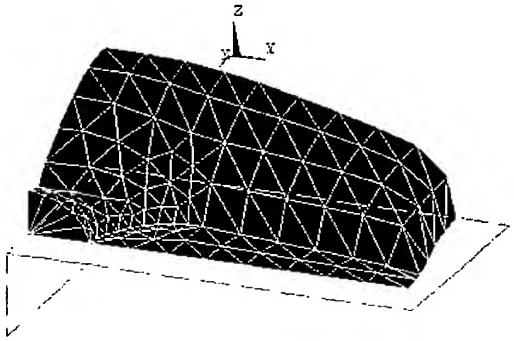

Fig. 16.4. A deformed shape of the elementary cell at $a = 5$ cm; $c = 3$ cm; $r = 1$ cm; $z = 1$ cm.

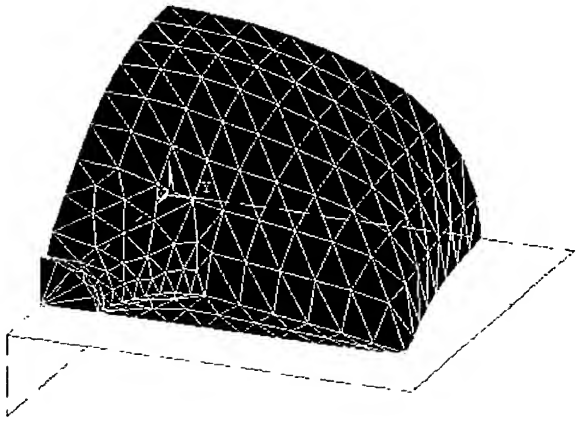

Fig. 16.5. A deformed shape of the elementary cell at $a = 5$ cm; $c = 5$ cm; $r = 1$ cm; $z = 1$ cm.

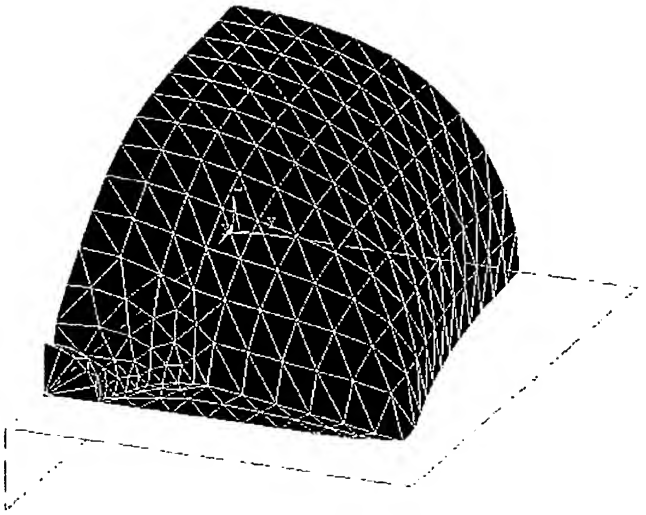

Fig. 16.6. A deformed shape of the elementary cell at $a = 5$ cm; $c = 7$ cm; $r = 1$ cm; $z = 1$ cm.

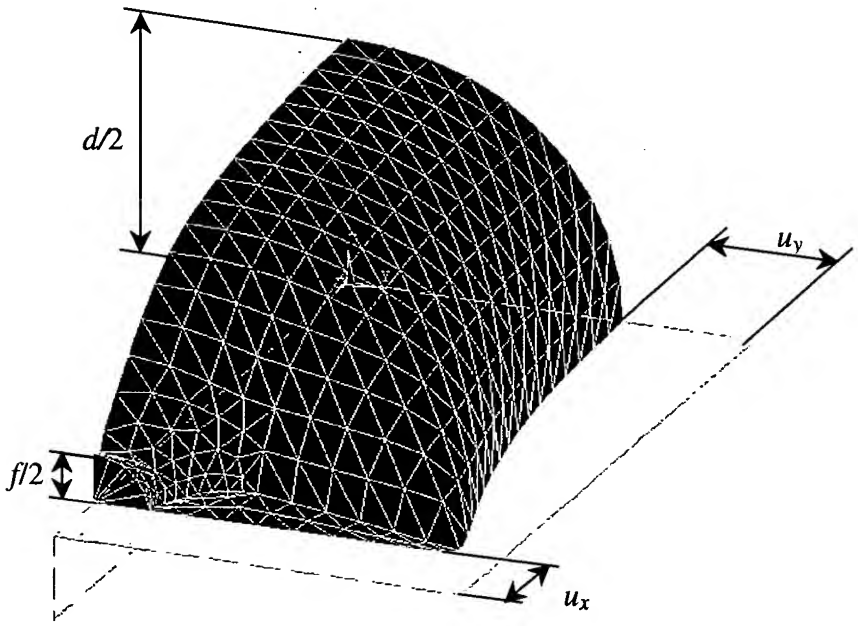

Fig. 16.7. A deformed shape of the elementary cell at $a = 5$ cm; $c = 9$ cm; $r = 1$ cm; $z = 1$ cm.

These schematics show that folds are formed in the areas of the channels. The folds appear also in the glued region, which results in this region narrowing in the direction of the hollow's corner.

The geometric dimensions of the protective airbag in its inflated state have been studied: thickness d, the channel's height f, contractions u_x and u_y. These are shown in Fig. 16.7.

Values of these dimensions are given in Table 4.

Table 9. Geometric dimensions of the protective airbag in its inflated state

	$c = 3$ cm	$c = 5$ cm	$c = 7$ cm	$c = 9$ cm
Airbag thickness d	2.9282	4.6068	5.4414	5.9452
Channel height f	1.0790	1.1826	1.2652	1.2082

Contraction in x direction	0.6579	1.0583	1.1843	1.1921
Contraction in y direction	0.6530	1.1295	1.4567	1.6153

Fig. 16.8 shows dependencies of the airbag thickness d and the channel height f on the c dimension.

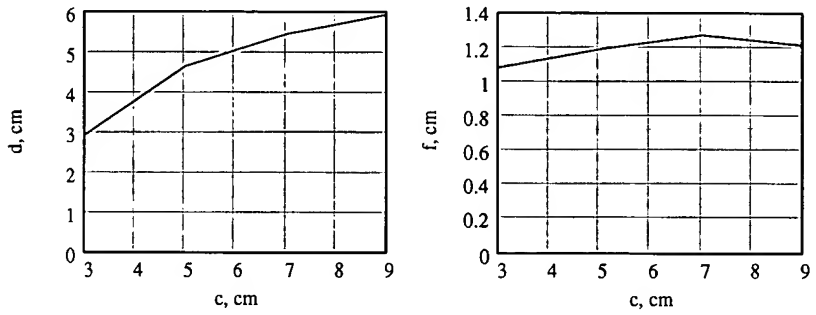

Fig. 16.8. Dependence of the airbag thickness d and the channel height f on the c size

The thickness of the airbag grows as the hollow length increases, tending to the value $20/\pi = 6.366$. The channel height tends to the value $4/\pi = 1.273$. Some instability in the behavior of this quantity can be noticed. The explanation for this is an instability of the fold formation.

Fig. 16.9 shows diagrams of relative contractions of the airbag in the directions x and y.

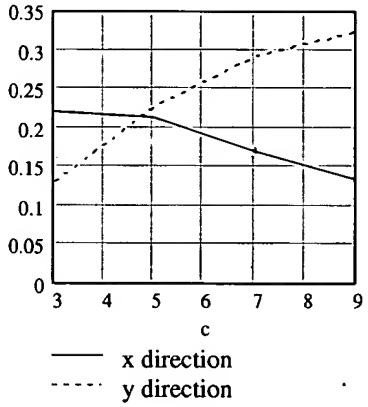

Fig. 16.9. Relative contractions of the airbag

The maximum peeling stress can be detected in the semi-circular glued area. This is tabulated vs. angle α (see Fig. 16.2) and size c in Table 10.

Table 10. Linear peeling stress in the semi-circular glued area, kgf/cm.

	$c = 3$ cm	$c = 5$ cm	$c = 7$ cm	$c = 9$ cm
$\alpha = 0$	0.4585	0.4481	0.5788	0.6602
$\alpha = 10$	0.6166	0.6642	0.5736	0.6447
$\alpha = 20$	0.5496	0.5633	0.6269	0.4201
$\alpha = 30$	0.5026	0.6006	0.3301	0.6149

$\alpha = 40$	0.4797	0.8533	0.2201	0.2688
$\alpha = 50$	2.3324	2.9152	2.9536	3.6338
$\alpha = 60$	6.9014	7.2006	10.1490	8.9788
$\alpha = 70$	6.7891	11.7564	9.5840	8.1324
$\alpha = 80$	8.0871	8.7404	10.6711	14.9662
$\alpha = 90$	1.2990	2.0780	2.0958	1.6554

The same data are shown graphically in Fig. 16.10.

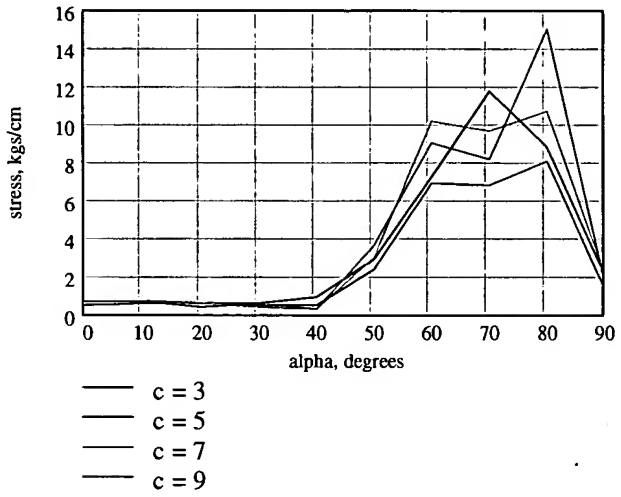

Fig. 16.10. Linear peeling stress in the semi-circular glued area

As can be seen on the diagrams, at angles $60° \le \alpha \le 80°$ a noticeable stress concentration appears. The spread of the values can be explained by the contiguity of the folded region.

16.4. Dependence of the airbag dimensions and the peeling stress at the boundary of the glued area on the channel width

Given below are results of solution of a series of problems where the variable quantity is the channel width z. Fig. 16.5 to Fig. 16.14 show the deformed shapes of the elementary cell and give principal source data used in the analysis.

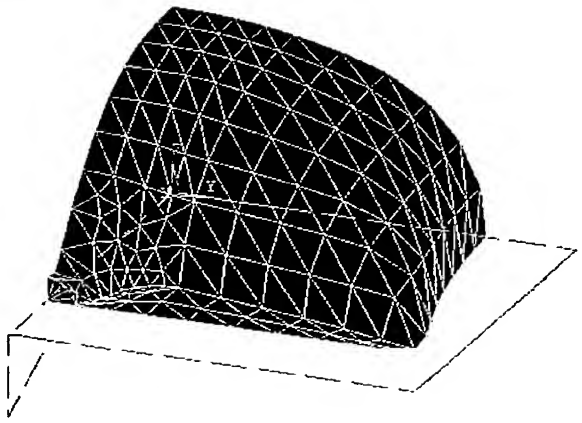

Fig. 16.11. A deformed shape of the elementary cell at $a = 5$ cm; $c = 5$ cm; $r = 1$ cm; $z = 0.5$ cm.

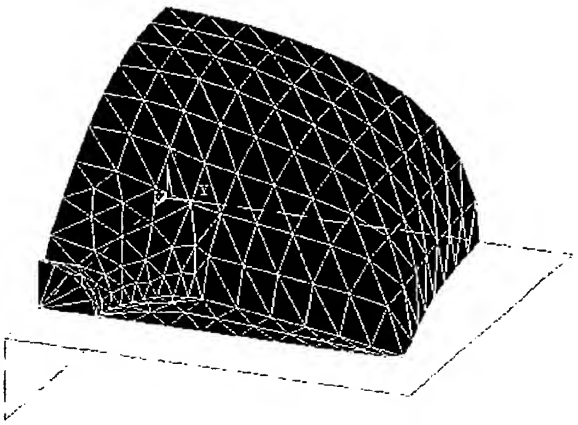

Fig. 16.12. A deformed shape of the elementary cell at $a = 5$ cm; $c = 5$ cm; $r = 1$ cm; $z = 1$ cm.

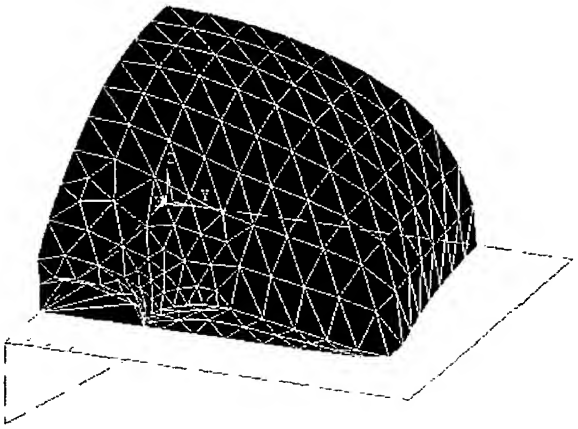

Fig. 16.13. A deformed shape of the elementary cell at $a = 5$ cm; $c = 5$ cm; $r = 1$ cm; $z = 1.5$ cm.

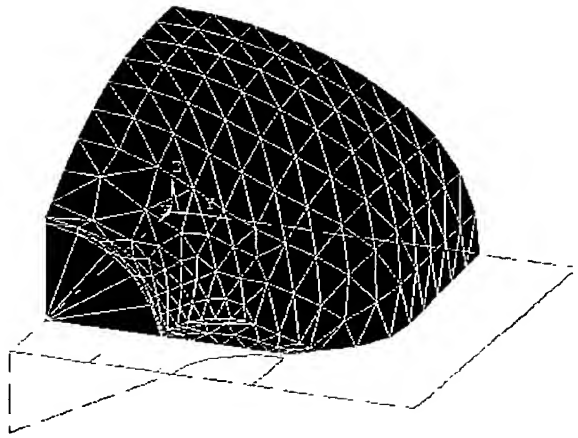

Fig. 16.14. A deformed shape of the elementary cell at $a = 5$ cm; $c = 5$ cm; $r = 1$ cm; $z = 2$ cm.

The geometric dimensions of the protective airbag in its inflated state have been studied: thickness d, the channel's height f, contractions u_x and u_y. These are shown in Fig. 16.7.

Values of these geometric dimensions are given in Table 11.

Table 11. Geometric dimensions of the protective airbag in its inflated state

	z = 0.5 cm	z = 1.0 cm	z = 1.5 cm	z = 2.0 cm
Airbag thickness d	4.5284	4.6068	4.7850	4.9924
Channel height f	0.5882	1.1826	1.3356	2.3680
Contraction in x direction	1.1514	1.0583	1.0705	1.0822
Contraction in y direction	1.1232	1.1295	1.1711	1.1988

Fig. 16.15 shows the dependence of the airbag thickness d and the channel height f on size z.

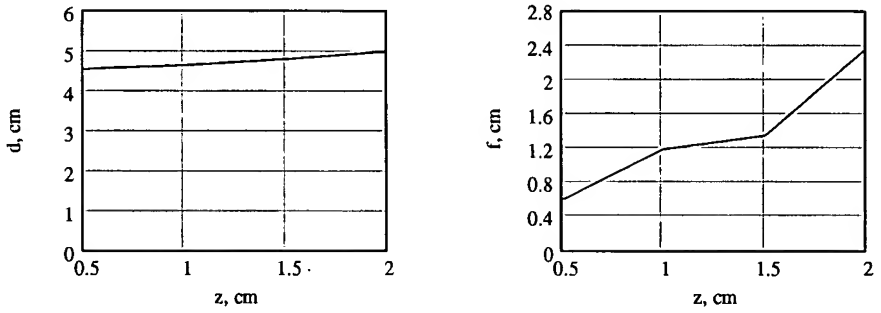

Fig. 16.15. Dependence of the airbag thickness d and the height of the channel f on size z

The thickness of the airbag increases a bit as the channel becomes wider. The height of the channel grows as its width increases. In the diagram of Fig. 16.15 one can see a non-smooth variation of the value of f. The explanation for this is that it is the channel's vicinity where the folds arise, and the central point of the channel can be sometimes at the top of a fold and sometimes at the bottom of a concave.

Fig. 16.16 shows diagrams of the relative contraction of the airbag in the direction of x and y.

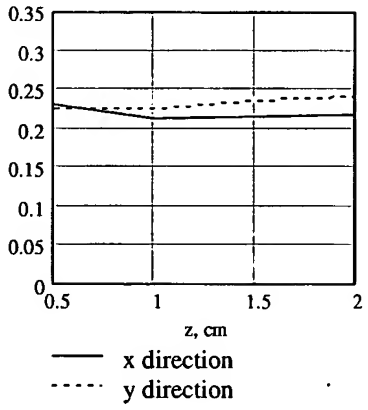

Fig. 16.16. Relative contraction of the airbag

These contraction values depend little on the width of the channel.

The maximum linear peeling stress can be observed in the semi-circular glued area. This is tabulated vs. angle α (see Fig. 16.2) and size z in Table 12.

Table 12. Linear peeling stress in the semi-circular glued area, in kgf/cm.

	$z = 0.5$ cm	$z = 1$ cm	$z = 1.5$ cm	$z = 2$ cm
$\alpha = 0$	0.3163	0.4481	0.2327	1.4292
$\alpha = 10$	0.3840	0.6642	0.4252	2.1043
$\alpha = 20$	0.3100	0.5635	0.6430	2.9817
$\alpha = 30$	0.1501	0.6006	0.9163	3.1759
$\alpha = 40$	0.0791	0.8533	1.1897	5.1840
$\alpha = 50$	1.0590	2.9146	8.1668	8.3181
$\alpha = 60$	4.0550	7.2006	7.6596	7.7622
$\alpha = 70$	6.9547	11.7564	8.6510	8.1868
$\alpha = 80$	12.1089	8.7404	13.5679	6.6607
$\alpha = 90$	1.7862	2.0780	0.3443	1.0787

The same data are presented graphically in Fig. 16.17.

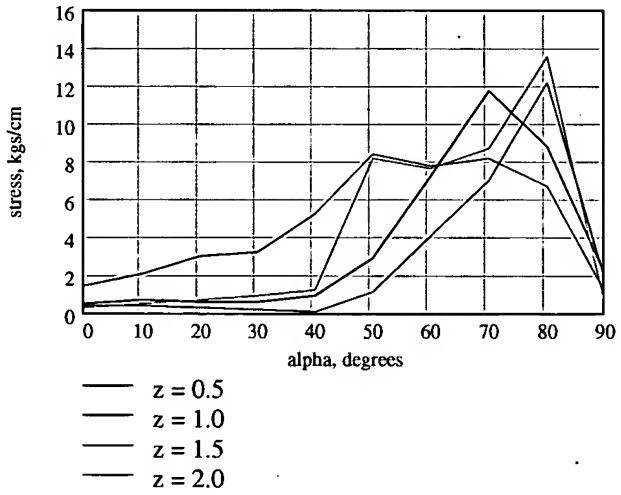

Fig. 16.17. Linear peeling stress in the semi-circular glued area

As one can see on the diagrams, at angles $50° \leq \alpha \leq 80°$ a substantial stress concentration appears. The spread of the values is even greater than that in Fig. 16.17. It can be explained by the contiguity of the folded area.

The analysis enables us to have only a qualitative idea of the magnitude of the peeling stress. This stress reaches the values of 8 to 15 kgf/cm^2.

17. AIRBAG HAVING A LONG GAS-FEEDING HOLLOW

This chapter presents results of a numerical analysis of the stress/strain distribution in periodical models of airbags having long hollows for the purpose of gas feeding.

The objects of investigation include qualitative properties of the shape of an inflated airbag and a distribution of the linear peeling stress in the seam of the elliptic adhesive joint. The effect of stress concentration in an area of a maximum curvature of the ellipse has been studied in detail.

17.1. Analytical tools employed

The analysis was performed using the finite element method as implemented in the multi-physical software system ANSYS, version 5.5.1. The principal finite element used was a triangular membrane element SHELL41 that allowed for large displacements/strains and resisted to tension only.

17.2. Models of adjoining and intersecting hollows

The airbags implement a popular design solution in which a long hollow commonly used to feed the gas is adjoined by a few shorter hollows perpendicularly or at another angle. There are areas of stress concentration in places where the hollows join one another.

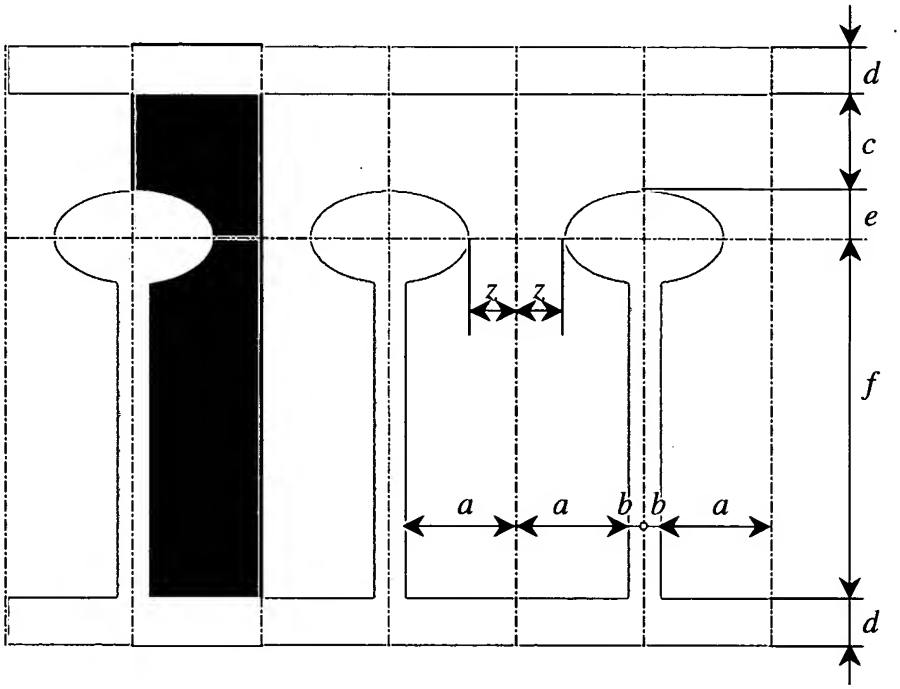

Fig. 17.1. An airbag model with a long gas-feeding hollow

A simplified model of this design and its elementary cell are shown in Fig. 17.1.

Same investigations can be performed with a bi-periodical model shown in Fig. 17.2. In this case the elementary cell is smaller in size and can be covered by a denser mesh of finite elements. This model possesses an advantageous difference from the previous one: in its deformed shape it maintains a translation symmetry [19] while that model loses this kind of symmetry when deformed. The quantities in question are affected by the model type only a little bit.

The model shown in Fig. 17.2 was chosen for the serial analysis.

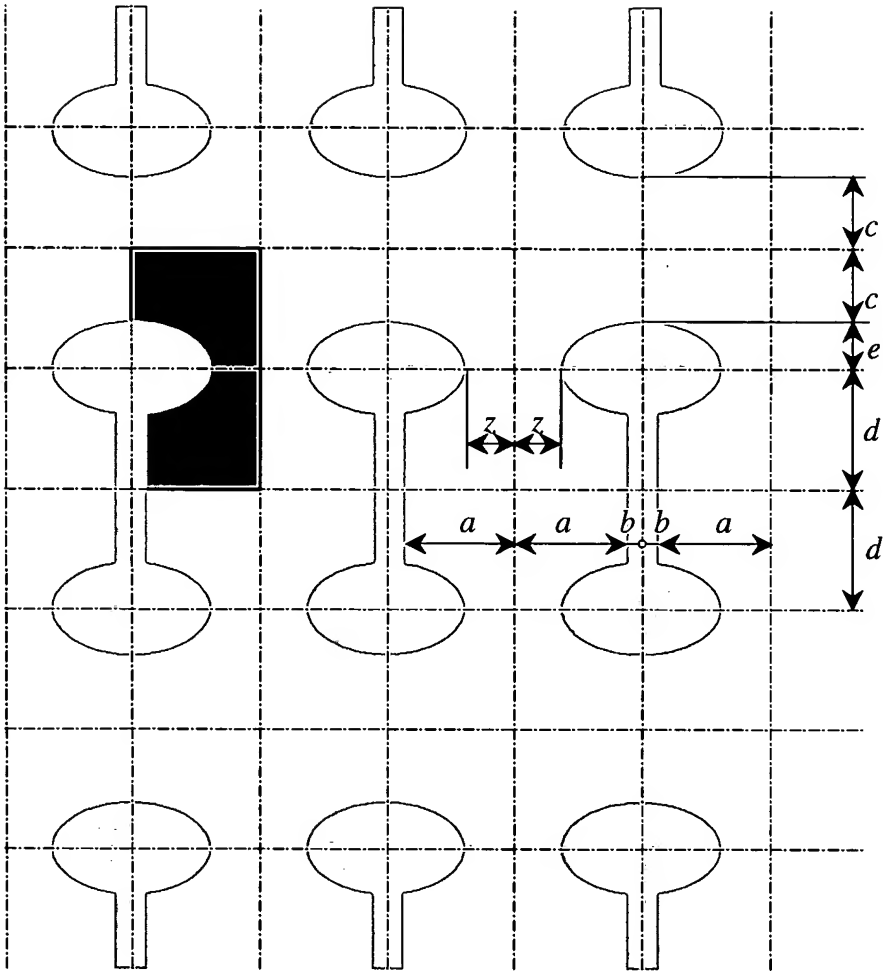

Fig. 17.2. An airbag model with a long gas-feeding hollow and a smaller elementary cell

17.3. Description of the series of problems solved

The design model includes an elliptic adhesive joint. The ratio of the ellipse's semi-axes influences the distribution of the peeling stress at the boundary of the adhesive joint. The more extended the ellipse is, the greater is the stress concentration in the place of a maximum curvature of its boundary.

It is exactly this phenomenon that this chapter deals with. A series of problems was solved at a constant size of the semi-major axis (3 cm) and a variable size of its semi-minor axis e. The analysis was performed at e = 1.00 cm; 1.25 cm; 1.50 cm; 1.75 cm; 2.00 cm. The other parameters are the same in all problems:

- the film sheet thickness h= 0.01 cm;
- elasticity modulus E= 3600 kg/cm^2;
- Poisson ratio ν=0.39;
- half-width of the main hollow a= 5 cm;
- half-width of the distributive hollow c= 3 cm;
- half-width of the channel z= 3 cm;
- semi-major axis of the ellipse 3 cm;
- length of the elementary cell 15 cm;
- gas pressure above ambient p = 1 atmosphere.

All these quantities are shown in a detailed pattern drawing of the elementary cell presented in Fig. 17.3.

The choice of a lower elasticity modulus E= 3600 kg/cm^2 should be emphasized. Numerous attempts undertaken by the author to obtain a stable solution for a stiff material with its elasticity modulus E = 36000 kg/cm^2 had no success. In all cases folds were formed causing a saw-tooth distribution of the peeling stress along the contour of the adhesive joint. The shape of the folds was determined apparently by the method of meshing into finite elements rather than the physical sense of the problem. Having understood this, the author lowered ten times the stiffness of the material thus obtaining smooth shapes of the bag in its inflated state and smooth curves of the peeling stress distribution along the adhesive joint. It made possible to analyze the results of the calculation. There should be no big error caused by the lower stiffness of the material because in both cases the peeling stress is integrally balanced by nearly the same gas pressure.

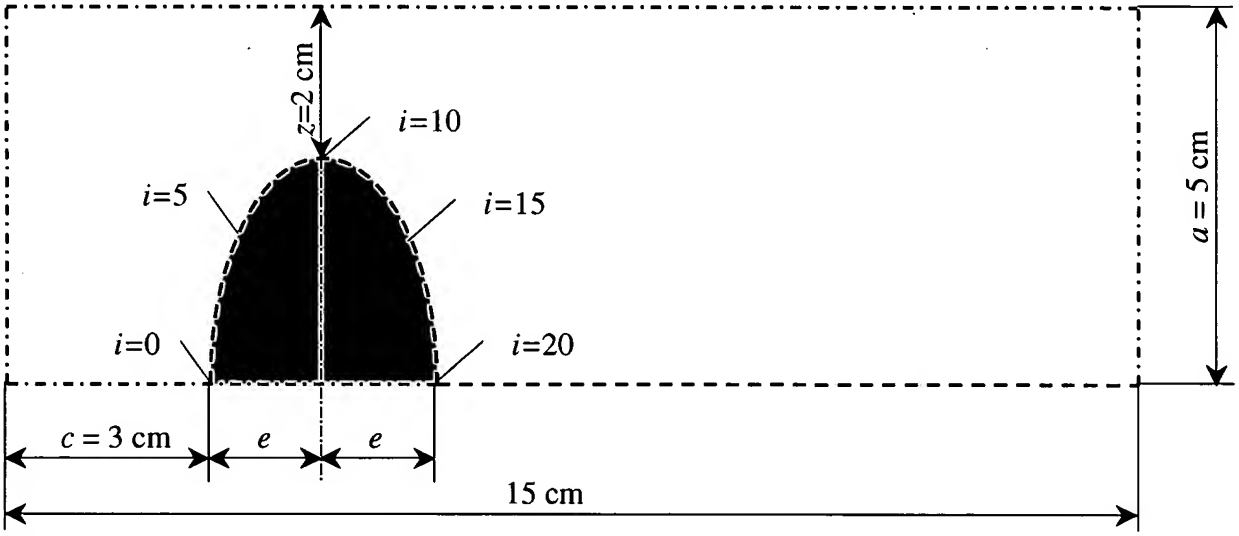

Fig. 17.3. A schematic of the elementary cell. The dashed line shows the boundary of the adhesive joint that resists to the peeling stress. Also, the principle of the point numbering at the elliptic joint boundary is shown

17.4. Results of the solution

All five problems have been solved successfully.

Fig. 17.4 to Fig. 17.8 show deformed shapes of the elementary cell at different values of e.

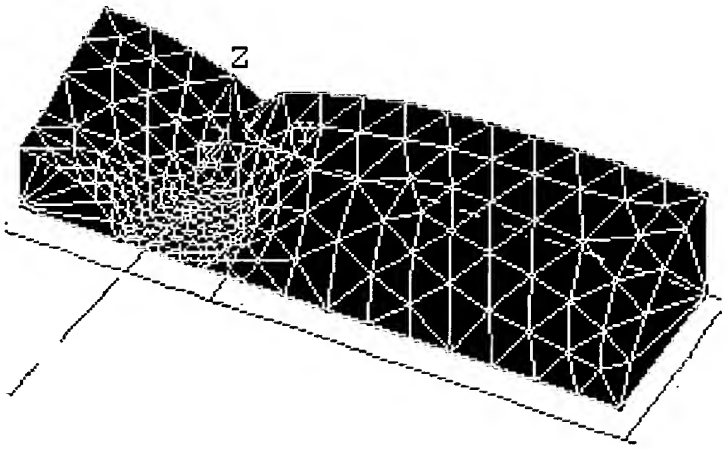

Fig. 17.4. A deformed shape of the elementary cell at $e = 1.00$ cm

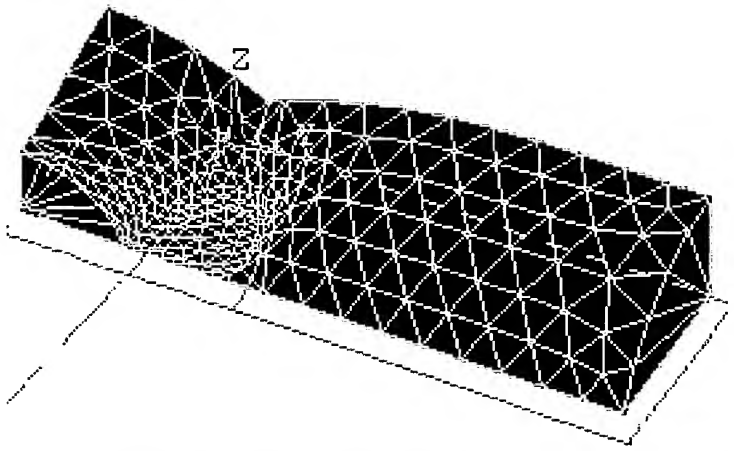

Fig. 17.5. A deformed shape of the elementary cell at $e = 1.25$ cm

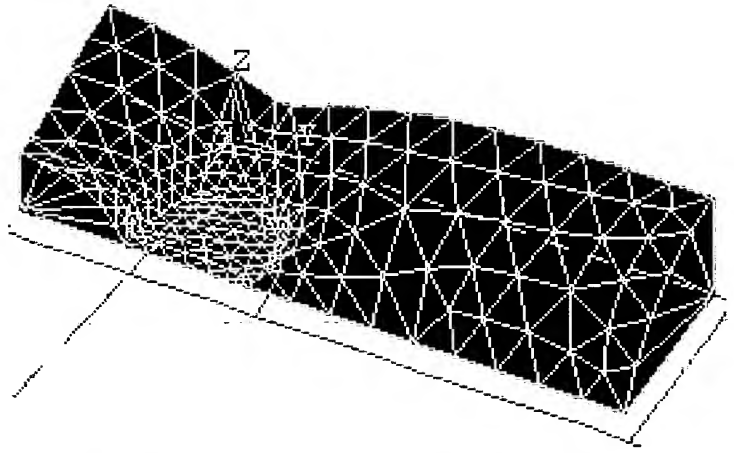

Fig. 17.6. A deformed shape of the elementary cell at $e = 1.50$ cm

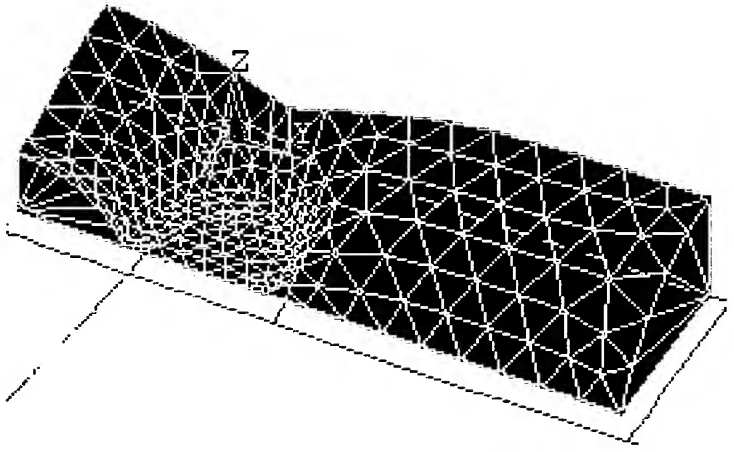

Fig. 17.7. A deformed shape of the elementary cell at $e = 1.75$ cm

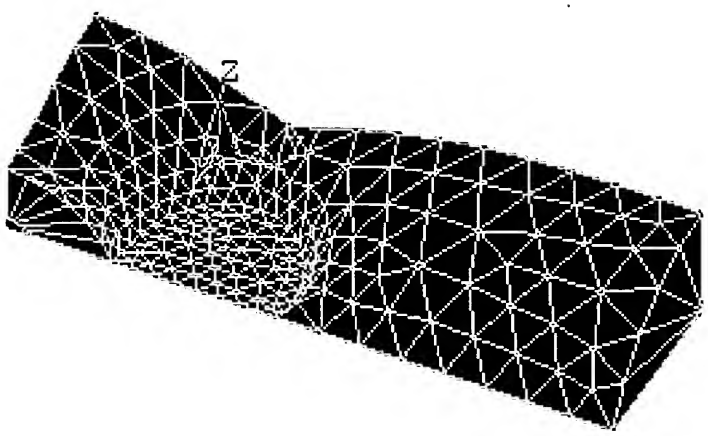

Fig. 17.8. A deformed shape of the elementary cell at e = 2.00 cm

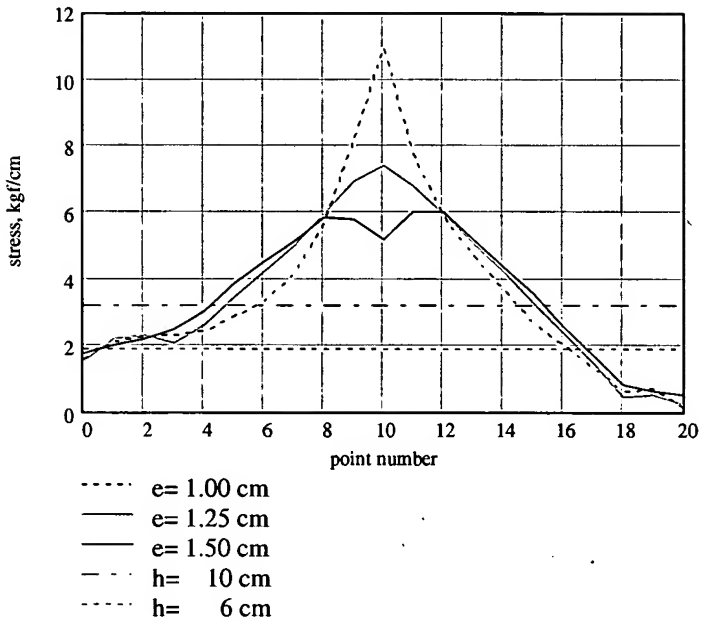

Fig. 17.9. A distribution of the peeling stress along the boundary of the elliptic adhesive joint in more extended ellipses

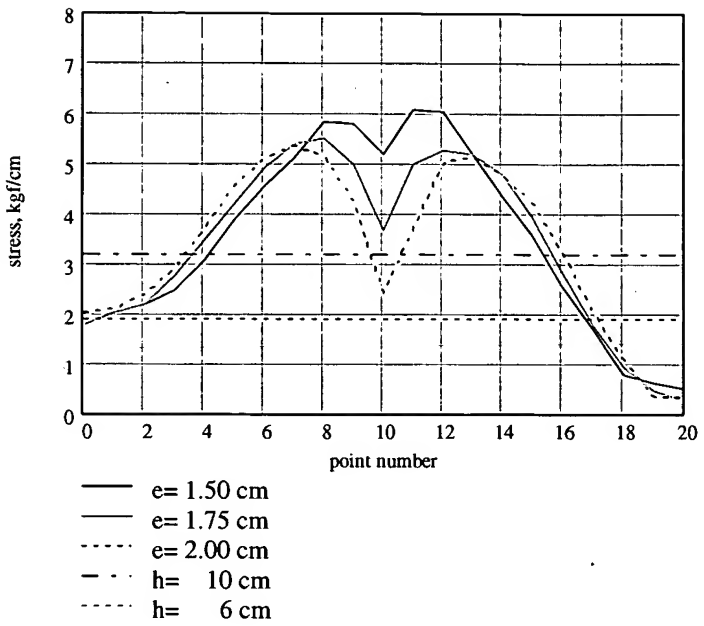

Fig. 17.10. A distribution of the peeling stress along the boundary of the elliptic adhesive joint in less extended ellipses

Also, the peeling stress at the boundary of the elliptic adhesive joint has been determined by this analysis. The boundary was divided into 20 segments of an equal length. End points of the segments are numbered from 0 to 20 as shown in Fig. 17.3.

The peeling stress is calculated in these points and represented as plots in Fig.9 and Fig.10.

The same diagrams show the level of the peeling stress for two idealized cases as horizontal lines. The first one of those (h = 10 cm) conforms to the case of an infinite cylindrical hollow glued out of two strips 10 cm wide (the main hollow), the second case (h = 6 cm) corresponds to the case of an infinite cylindrical hollow glued out of two strips 6 cm wide (the gas distributing hollow).

As the plots demonstrate, the level of the stress in the intersecting hollows is always higher than that in the idealized case of non-intersecting hollows of the same size. The more extended the elliptic joint, the higher the peeling stress at its boundary. As the length of the semi-minor axis of the ellipse increases, the peeling stress at the vertex of the ellipse falls. This dependence is shown as a plot in Fig. 17.11.

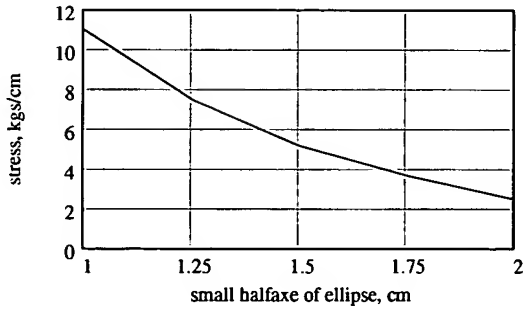

Fig. 17.11. Peeling stress at the ellipse's vertex (i = 10) v. its semi-minor axis

At the beginning ($e \leq 1.25$ см) the peeling stress at the vertex of the ellipse exceeds that in nearby points. Then ($e \geq 1.50$ cm), the peeling stress at the vertex becomes less than that in the nearby points. Apparently, the rational size of the semi-minor axis of the ellipse in the presented series of problems should be 1.40 cm or so, when the stress at the ellipse's vertex becomes level with that in points located near the vertex.

18. REFERENCES

[16]. G.A.Korn, T.M.Korn. Mathematical Handbook for Scientists and Engineers. Second, enlarged and revised edition. McGraw-Hill Book Company. New York, San Francisco, Toronto, London, Sydney, 1968.

[17]. K.Washizu. Variational methods in elasticity and plasticity, Third edition, Pergamon Press, Oxford, New York, Toronto, Sydney, Paris, Frankfurt, 1982.

[18]. Pontryaghin L.S., Boltyansky V.G., Gamkrelidze R.V., Mischenko E.F. Mathematical theory of optimal processes. Moscow, *Nauka* Publishers, 1969. (*In Russian*)

[19]. Buryshkin M.L., Gordeyev V.N. Efficient methods and computation programs for analysis of symmetric structures. Kiev, *Budivelnyk* Publishers, 1984. (*In Russian*)

[20]. Appendix 1. Investigation of axisymmetric film airbags.

[21]. Appendix 3. Experimental studies of a side impact inflatable head protector.